Cape Peninsula
University of Technology

KINETIC ENERGY RECOVERY AND CONTROL OF WIND TURBINE GENERATORS FOR GRID FREQUENCY SUPPORT

by

AKSHER BHOWON

Thesis submitted in fulfilment of the requirements for the degree

Master of Engineering in Electrical Engineering

in the Faculty of Engineering and the Built Environment

at the Cape Peninsula University of Technology

Supervisor: Prof Khaled Aboalez

Co-supervisor: Dr Marco Adonis

Bellville

March 2023

DECLARATION

I, Aksher Bhowon, declare that the contents of this thesis represent my own unaided work, and that the thesis/dissertation has not previously been submitted for academic examination towards any qualification. Furthermore, it represents my own opinions and not necessarily those of the Cape Peninsula University of Technology.

aBhowon

07-03-2023

Signed **Date**

ABSTRACT

The nominal frequency of the national grid is 50 Hz. A deviation around this nominal point indicates an imbalance between supply and demand. There is an acceptable range by which the frequency may deviate to protect the grid integrity and all the connected devices. Large synchronous generators provide an inherent inertial response to frequency deviations due to their large rotating mass that is coupled to the grid via an electro-mechanical interaction between the rotor and stator. Wind energy conversion systems (WECS) have become increasingly important as a contribution to grid frequency support, to maintain power at the nominal frequency and mitigate power failures or supply shortages against demand. However, variable speed wind turbine (VSWT) generators are decoupled from the network by power electronic converters and therefore do not respond naturally to a system frequency change. As the finite nature of non-renewable energy resources are realised and climate change concerns become more prevalent, the need to shift to more sustainable forms of energy such as the adoption of renewable energy has seen an increase. A systematic literature review methodology was used and aimed to investigate the control methods used by WECS, more specifically variable speed wind turbines (VSWT), in supporting grid frequency as well as, the limitations of such methods. The Emulated Inertial Response was the primary means of providing frequency support identified by literature within a period of 2015 – mid 2022. Following the systematic literature review, a mathematical model of a doubly-fed induction generator (DFIG) and a frequency support controller was developed to provide an emulated inertial response and modelled using MATLAB/Simulink. The results showed that the frequency support controller provided adequate frequency support by raising the frequency nadir following a disturbance, even in the cases of consecutive disturbances.

ACKNOWLEDGEMENTS

I wish to thank:

- Prof. K M Aboalez, my supervisor and Dr. M Adonis, my co-supervisor. Their motivation, guidance, and advice has been invaluable during the journey of completing this thesis. I would like to especially thank them for their patience throughout this journey especially as deadlines slipped and understanding the difficulty of trying to balance between being a part-time student and a full-time employee.
- Dr. T Jones, and Dr. I K Peddle for their willingness to assist with study leave and encouraging me to pursue this degree.
- My colleagues and friends, thank you for the motivation and the interest that you have shown toward me completing this degree.

TABLE OF CONTENTS

LIST OF FIGURES

LIST OF TABLES

ABBREVIATIONS AND SYMBOLS

Abbreviations and Acronyms

AC	Alternating current
DC	Direct current
DFIG	Doubly-fed induction generator
EV	Electric vehicle
FSWT	Fixed speed wind turbine
GSC	Grid-side converter
Hz	Hertz
IEEE	Institute of Electrical and Electronics Engineers
IGBT	Insulated-gate bipolar transistor
LFO	Low-frequency oscillation
MPC	Model predictive control
MPPT	Maximum power point tracking
MVA	Mega volt-ampere
MW	Megawatt
PCC	Point of common coupling
PLL	Phase-locked loop
PMSG	Permanent magnet synchronous generator
POC	Point of connection
pu	Per unit
PWM	Pulse width modulation
REF	Reference
RES	Renewable energy source
ROCOF	Rate of change of frequency
RPM	Revolutions per minute
RPP	Renewable power producer
RSC	Rotor-side converter
SG	Synchronous generator
STATCOM	Static synchronous compensator
SVC	Static VAR compensators
V2G	Vehicle to grid
VAR	Volt ampere reactive
VSM	Virtual synchronous machine
VSWT	Variable speed wind turbine
WPP	Wind power plant
WTG	Wind turbine generator

Symbols

D	Damping Constant
E_k	Kinetic Energy
f	Frequency
H	Inertia Constant
i	Instantaneous Current
J	Moment of Inertia

K_p	Proportional Gain
K_i	Integral Gain
K_s	Shaft Stiffness
L	Inductance
P	Power
Q	Reactive Power
R_p	Droop Gain
T_{em}	Electromagnetic Torque
T_m	Mechanical Torque
v	Instantaneous Voltage
V	Voltage

Greek Letters

β	Pitch Angle
ψ	Flux Linkage
λ	Tip Speed Ratio
ρ	Density of Air
θ	Tortional Twist
ω	Angular Speed

CHAPTER 1: Introduction

1.1. Research Background

The nominal frequency of the transmission network in South Africa is 50 Hz (National Energy Regulator of South Africa, 2010). The frequency of a transmission network or grid is maintained at its nominal value by the balance between generation and consumption. In other words, a generator is required to either increase or decrease the active power produced in reaction to deviations around the nominal system frequency (Anaya-Lara et al., 2009). A significant deviation in the frequency of the transmission network may lead to instability in the system or damage to connected devices (Ma & Li, 2013). The Grid Connection Code for Renewable Power Producers (RPPs) in South Africa states that in the event of frequency deviations in the national transmission network, RPPs shall be designed to be capable to provide a power-frequency response to stabilise the network frequency (Eskom Transmission Division, 2014).

Conventional rotating synchronous generators that are committed to the grid add rotational inertia to the grid due to their large rotating masses that are coupled to the grid via an electro-mechanical interaction between the rotor and stator (Ulbig et al., 2014). This allows the SG to exchange (both absorb and release) its kinetic energy with the grid proportional to the rate of change of frequency (ROCOF) (Ulbig et al., 2014). This inertial response limits the ROCOF (Boyle et al., 2018) and results in slower frequency dynamics which allows for a greater response time to react to events such as a loss of generation, loss of line or a sudden increase in load (Ulbig et al., 2014). Conversely, power electronic interfaced variable speed wind turbines do not inherently provide rotating inertia to the grid (Ulbig et al., 2014).

The lack of an inherent internal response lowers the effective system inertia and results in quicker grid frequency dynamics with the decline of rotating inertia and can lead to situations where traditional frequency controllers become too slow, relative to the disturbance, to limit large frequency deviations (Ulbig et al., 2014). This is a problem prevalent in isolated systems or systems with high wind power penetration. When a frequency drop occurs in such a system, the system can experience a large rate of change of frequency and frequency nadir.

Burning fossil fuels in conventional power plants to generate electricity produce pollutants as by-products that lead to serious environmental problems such as acid rain and global warming (Dreidy et al., 2017a). There has been a notable increase in installed wind turbine generating capacity from 94 GW in 2007 to 539 GW in 2017, globally (Aberg et al., 2018). In South Africa alone the installed wind turbine generating capacity has increased from 790 MW 2015 to 1468 MW 2017 (DoE, 2018). As a country that has signed the Paris Climate Accord (and still an active member in November 2022), an agreement that endorses a limit of a 1,5 degree increase in global temperature, South Africa may be turning to renewable energy sources such as, but not limited to, WTGs, to decrease the dependency of the power system on fossil fuels

(Dreidy et al., 2017a). With climate change, and the global community realising the finite nature of natural resources, the use of renewable energy sources such as wind will increase. It is of importance to address the stability and power quality concerns that arise.

1.2. Significance of Research

The prospect of climate change and the increasing demand for energy has placed a demand on clean or renewable energy sources. Energy from the wind is typically harnessed by variable speed wind turbines (VSWTs). VSWTs are not directly coupled to the grid via an electro-mechanical interaction and thus effectively reduce the grid's effective system inertia for each unit connected. A low system inertia reduces the stability of the grid's frequency.

Countries with high wind power penetration are thus faced with the challenge to use wind turbines to emulate an inertial response which is inherent to large rotating steam driven turbines to ensure their grid's frequency stability. In South Africa, the national grid code stipulates that wind turbines are required to be able to support the grid frequency if called upon during the primary regulation phase.

Grid frequency stability is of importance to electricity supply commissions and transmission network operators such as Eskom in South Africa. This creates a need for VSWT manufacturers to develop control system solutions for their VSWTs that better address the problem of grid frequency support. The results of this thesis will not only be useful for the development of wind energy conversion systems (WECS) but to assist with the stability of the transmission grid's frequency stability.

1.3. Research Problem

The rotating mass within variable speed wind turbines are decoupled from the grid by their power converters and do not provide an inherent inertial response to frequency events on the grid. This reduces the effective system inertia of the grid which is of concern for frequency stability of the grid. This concern further asserted by the unpredictable nature of renewable energy sources which can cause an appreciable imbalance between supply and demand. This in turn will cause frequency to deviate from the nominal frequency considerably. Enough deviation from the nominal grid frequency can lead to load shedding and ultimately grid collapse.

VSWTs are required by the Grid Connection Code for Renewable power plants (RPPs) in South Africa, to be able to provide amongst other things primary frequency regulation (Eskom Transmission Division, 2014). Without the active participation of VSWT's in frequency regulation, the task of frequency regulation is left to conventional steam turbine driven

generators. However, with the increase in renewable energy sources there may not be enough energy in reserve from conventional steam driven turbine generators alone to regulate the grid frequency.

1.4. Research Methodology

This research will be centred around the topic of frequency support in large scale power systems. MATLAB/Simulink is a preferred simulation environment to model dynamic time varying systems. The method of investigation will be mathematical modelling in MATLAB/Simulink and the sampling method will be experimental results gathered by simulations. The research will be approached in the following manner:

1. To investigate the systems used by VSWTs, in supporting grid frequency as well as, the limitations of such methods a systematic literature review of works published within the period of 2015-2022 will be conducted.
2. A mathematical model of a doubly-fed induction generator (DFIG) is formulated and benchmarked against work published in an accredited journal to validate the accuracy of the model.
3. After the DFIG model has been successfully verified, a proposed supplementary frequency support controller is introduced to the rotor-side converter (RSC) of the verified DFIG model. This will provide an accurate baseline with which any improvement can be compared to. A block diagram of the proposed system overview is shown in Figure 1.1.

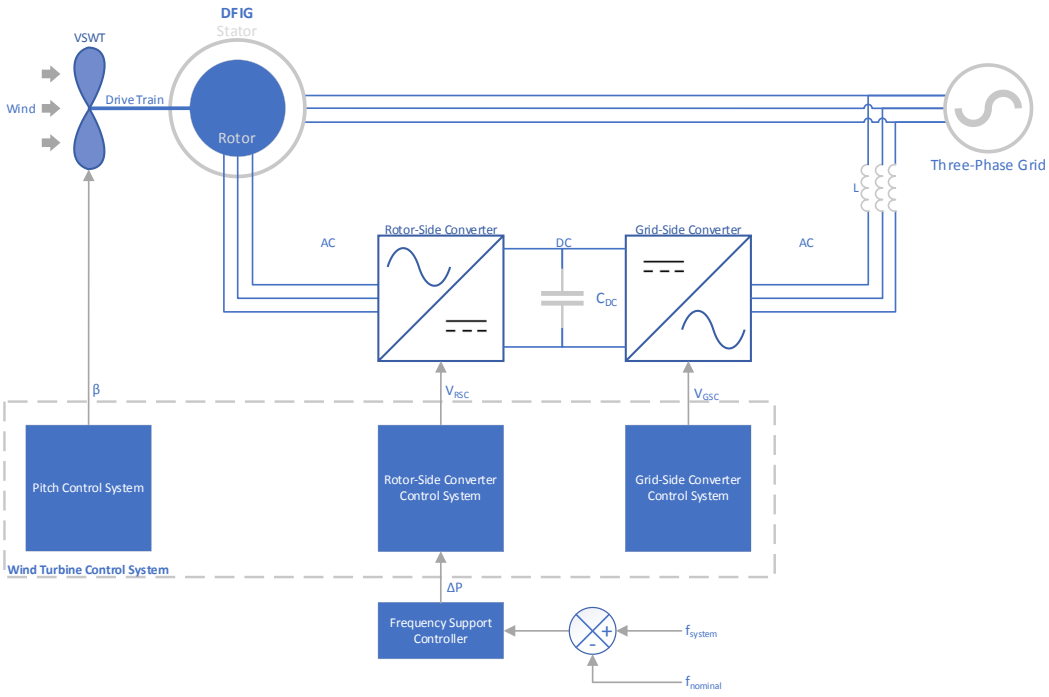

Figure 1.1: DFIG with proposed frequency support controller

4. The results obtained through various case studies of the DFIG model with frequency support capabilities is compared to the results obtained to the DFIG model without such capabilities. An analysis and discussion of the results will be performed.

The secondary and tertiary research objectives (detailed in points 2 and 3 above) will be met by mathematical modelling in MATLAB/Simulink and experimental results will be gathered by off-line simulations. The benchmark DFIG model and the DFIG model with frequency support will remain the same throughout all case studies performed. Furthermore, this research will not require an ethics clearance as it is simulation based and no data is gathered.

1.5. Scope and Limitations

This study will evaluate the need for and importance of frequency control/regulation. This study is based on the kinetic energy recovery of DFIG wind turbines to contribute to grid frequency regulation and will only consider DFIG wind turbine generators. A comparative analysis will be conducted between DFIG wind turbines with and without frequency support capabilities to identify any improvements to the grid frequency. While this study may implement and model a wind turbine model, control system design, power converters, it will not cover a detailed design of such systems. Furthermore, this thesis is written from the perspective of large-scale power systems but will not include other power quality related issues.

1.6. Thesis Structure

This thesis is structured as follows – Chapter 2 presents a systematic literature review relating to the grid frequency support of variable speed wind turbine generators to support. A mathematical model of a DFIG and the supplementary frequency controller is presented in Chapter 3, while a description of the computer modelling, benchmarking, simulation results and discussion of results is presented in Chapter 4. Lastly, Chapter 5 concludes this study and presents recommendations for future research.

A list of publications, their publication statuses as well as their abstracts has been included in Appendix A.

1.7. Summary

Large synchronous generators provide an inherent inertial response to frequency deviations due to their large rotating mass that is coupled to the grid via an electro-mechanical interaction between the rotor and stator. This response acts to overcome the immediate imbalance between supply and demand of the network. Conversely, the rotating mass within variable speed wind turbines are decoupled from the grid by their back-to-back power converters and

do not provide an inherent inertial response to frequency events on the grid. This reduces the effective system inertia of the grid as wind penetration increases which leads to an increase in the speed of the grid's dynamics and is of concern for the frequency stability of the grid.

With climate change, and the global community realising the finite nature of natural resources, the use of renewable energy sources such as wind will increase. Furthermore, grid codes such as the Grid Connection Code for Renewable Power Plants (Eskom Transmission Division, 2014), have requirements for wind turbine generators to provide grid-frequency support. It is important to address the frequency stability concerns that arise. This research offers a means to recovering kinetic energy from the rotating mass of the rotor of a doubly-fed induction generator to support the frequency of the transmission network. The results of this thesis shall be obtained by computer simulations in MATLAB/Simulink.

CHAPTER 2: Systematic Literature Review

2.1. Introduction

The transmission network, commonly referred to as the grid, is the high-voltage system that interconnects and transfers electrical energy from the generation network of power plants to the distribution network. The nominal frequency of the transmission network in South Africa is 50 Hz (National Energy Regulator of South Africa, 2010). The frequency of a transmission network or grid is maintained at its nominal value by the balance between generation and consumption. In other words, a generator is required to either increase or decrease the active power produced in reaction to deviations around the nominal system frequency (Anaya-Lara et al., 2009). A significant deviation in the frequency of the transmission network may lead to the instability of the system or damage to connected devices (Ma & Li, 2013). More specific to the topic of this paper, a deviation too far below the nominal frequency can cause generation units to fall out-of-step and cause of out-of-step protection relays to disconnect the generator units from the grid. This will place further demand on the remaining generators and will potentially lead to grid collapse if this frequency event does continue.

Conventional rotating synchronous generators that are committed to the grid add rotational inertia to the grid. This is due to their large rotating masses that are coupled to the grid via an electro-mechanical interaction between the rotor and stator (Ulbig et al., 2014). This electro-mechanical interaction enables the synchronous generator to exchange (both absorb and release) its kinetic energy with the grid, proportional to the rate of change of frequency (ROCOF) (Boyle et al., 2018). This is known as an inertial response and is described by the swing equation (Okedu, 2017). It acts to overcome the immediate imbalance between supply and demand of the network. The generator, at the instant of the disturbance, will convert the kinetic energy of the rotor to electrical energy, limiting the rate of change of frequency and frequency nadir as the rotor slows down in the process. In power systems, a loss of generators, load shedding or a 3-5% load change is considered a large disturbance (Fang et al., 2018a). Following the inertial response, the generator's governor will adjust the setpoint and bring the machine up to speed again within a period in the order of seconds thus, providing primary frequency regulation. Secondary frequency regulation mechanisms, such as generation redispatch and automatic generation control, occur within an order of tens of seconds to minutes.

Conversely, variable speed wind turbines with back-to-back power electronic converters provide no inertia to the power system since, the power electronic converters decouple the rotating mass of the variable speed wind turbine (VSWT) from the grid (Ulbig et al., 2014). Consequently, the effective inertia of the power system begins to decline with the increase in wind power penetration. VSWTs therefore, do not naturally respond to a system frequency change. The operation of a VSWT is governed by its MPPT (Maximum Power Point Tracking)

algorithm so to extract the maximum possible power from the wind to convert to electrical power (Oshnoei et al., 2018). The decline of rotating inertia leads to an increase in speed of grid frequency dynamics and may lead to situations where traditional frequency controllers become too slow, relative to the disturbance, to limit large frequency deviations. The problem of low grid inertia is more prevalent in isolated systems or systems with high wind power penetration. When a frequency drop occurs in such a system, the system can experience a large ROCOF and frequency nadir. This concern is further asserted by the stochastic nature of wind energy which can cause an appreciable imbalance between supply and demand (Sáez et al., 2008). This is of concern to the frequency stability of such electrical networks.

To overcome the challenges associated with frequency stability, wind turbine generators (WTGs) need to implement frequency control systems to allow them to partake in the regulation of the power system frequency (Dreidy et al., 2017b). Modern technologies and new control systems aid the feasibility for wind power plants (WPPs) to achieve this. Escalated by the finite nature of fossil fuels, in conjunction with climate change, the reliance on such renewable energy systems is increasing globally. More specifically, South Africa's installed wind turbine generating capacity has increased from 790 MW 2015 to 1468 MW 2017 (DoE, 2018). As a country that has signed the Paris Climate Accord (and still an active member at the time of writing), an agreement that endorses a limit of a 1.5 °C increase in global temperature, South Africa may be turning to renewable energy sources such as, but not limited to, WTGs, to decrease the dependency of the power system on fossil fuels (Dreidy et al., 2017b). It is of importance to address the frequency stability concerns that may arise with an increase in wind power penetration.

This systematic literature review aims to evaluate the recent work, 2015-2022, of wind energy conversion systems for grid frequency support. More specifically, to review the methods in which this is achieved as well as provide an analytical view based on the frequency of research papers published annually pertaining to this field. Thereafter, a conclusion can be formulated to determine whether wind energy conversion systems for grid frequency support have gained interest and relevance.

Structured as follows – section 2.2 sets out the methodology used to conduct this study. The research questions are formulated in section 2.3 and the search process is described in section 2.4. This is followed by the data collection and analysis in section 2.5. Thereafter the findings are presented in section 2.6. Based on the findings, section 2.7 identifies areas to be considered for future works within this field. Finally, section 2.8 concludes the systematic literature review.

2.2. Methodology

A research methodology is the practical framework used to identify, select, process, and analyse information within a research study (University of the Witwatersrand, 2022). In the context of a research paper, this section allows the reader to critically evaluate the study's validity and reliability (University of the Witwatersrand, 2022).

Specifically, this review adopts the basic systematic literature review methodology, as described by Kitchenham (Kitchenham et al., 2010). This method of review is often used in medicine. However, this has been extended to other fields such as software engineering, economics and education, due to its success in evidence-based approaches (Torreglosa et al., 2016). The following actions were followed when conducting the research for this study:

1. The formulation of research questions
2. Search process
3. Inclusion criteria
4. Exclusion criteria
5. Quality assessment
6. Data collection
7. Data analysis

2.3. Research Questions

As stipulated by the methodology, the first process involves the formulation of research questions from which the basis and focus of the study is determined. The research questions are rooted in identifying solutions and limitations to VSWTs providing grid frequency support. The two research questions investigated in this study include:

RQ1: What control methods are VSWTs using to support the grid frequency?

RQ2: What are the limitations of VSWTs in supporting the grid frequency?

2.4. Search Process

The search process included the manual entry of simple search strings based on title, keywords, and abstract. Given the relevance of IEEE to this research topic, IEEE Xplore Digital Library was the primary library used, whilst ScienceDirect and Wiley Online Library were included to supplement the search process.

The inclusion and exclusion criteria for this study are criteria used to refine the search. The inclusion criteria included all papers relevant to the keywords searched and period set by this study, 2015-2022.

Conversely all papers outside this period were excluded. The exclusion criteria further excluded papers which were not written in English and/or were unpublished, including conference papers, reviews, and case studies. In addition, duplicate papers and/or those not relevant to the topic were excluded. Furthermore, papers related to frequency support but not in the context of wind energy conversion systems or wind turbine generators were excluded. Table 2.1 summarizes the search criteria and filters applied to each of the digital libraries searched.

Table 2.1: Search criteria applied

Digital Library	Search String	Search Filters
IEEE Xplore Digital Library	WECS Grid Frequency support	Journals 2015-2022
	Wind turbine Frequency support	Journals 2015-2022
	Variable speed wind turbine frequency support	Journals 2015-2022
ScienceDirect (Elsevier)	WECS Grid Frequency support	Article Engineering 2015-2022
	Wind turbine frequency support	Article Engineering 2015-2022
	Variable speed wind turbine frequency support	Article Engineering 2015-2022
Wiley Online Library	WECS Grid Frequency support	Journals Energy Electrical & Electronics Engineering 2015-2022
	Wind turbine Frequency support	Journals Energy Electrical & Electronics Engineering 2015-2022
	Variable speed wind turbine frequency support	Journals Energy Electrical & Electronics Engineering 2015-2022

A secondary screening was applied, where to each paper that satisfied the keywords used during the search to determine if it addressed the research questions. Those papers that did not, were also excluded. Based on the refinement and screening criteria, a sum of 56 papers

were included in this review. A summary of the number of articles included from each publication is included in Table 2.2 below:

Table 2.2: Article sources and number of articles found

Article Source	Number of Journal Articles
ScienceDirect (Elsevier)	9
IEEE Xplore Digital Library	42
Wiley Online Library	5
Total	56

2.5. Data Collection and Analysis

A consistent data collection and analysis process for each of the 56 papers was applied, with respect to the research questions posed. In this way, the data collected was classified and categorised based on the control methods used by VSWTs to support grid frequency and further evaluated by their limitations thereof.

2.6. Results

The following section discusses the results of the literature review conducted in supporting the two research questions posed by this paper. The results associated to each research question are sub-categorized and each paper's contribution discussed thereunder.

2.6.1 RQ1: How are VSWTs supporting the grid frequency?

Wind energy conversion systems differ from conventional synchronous generators since they do not have an inertial response to naturally suppress frequency disturbances by, exchanging the kinetic energy of the rotor with the grid. The rate at which the grid frequency will change in an imbalance between supply and demand, is related to system inertia (Miao et al., 2015). As the number of wind turbine generators connected to the grid increase, the effective system inertia will decrease and by extension, grid frequency dynamics will increase. Literature surveyed suggests that it is indeed possible for VSWTs to provide grid frequency support through either an inertial response or partake in the grid frequency regulation. This research question (RQ1) is aimed at investigating the various methods and implementations of WECS supporting the grid frequency.

Recent literature surveyed identified three prevailing methods of supporting the grid frequency. These include VSWTs which operate in a de-loaded state, implement an embedded energy storage and those which emulate an inertial response. Systems which emulate an inertial

response either rely on the kinetic energy of the rotor or the electrostatic energy stored within the DC-Link capacitor of the VSWT WTG itself. These classifications are illustrated by a hierarchical diagram in Figure 2.1. The surveyed literature is classified by these three prevailing methods.

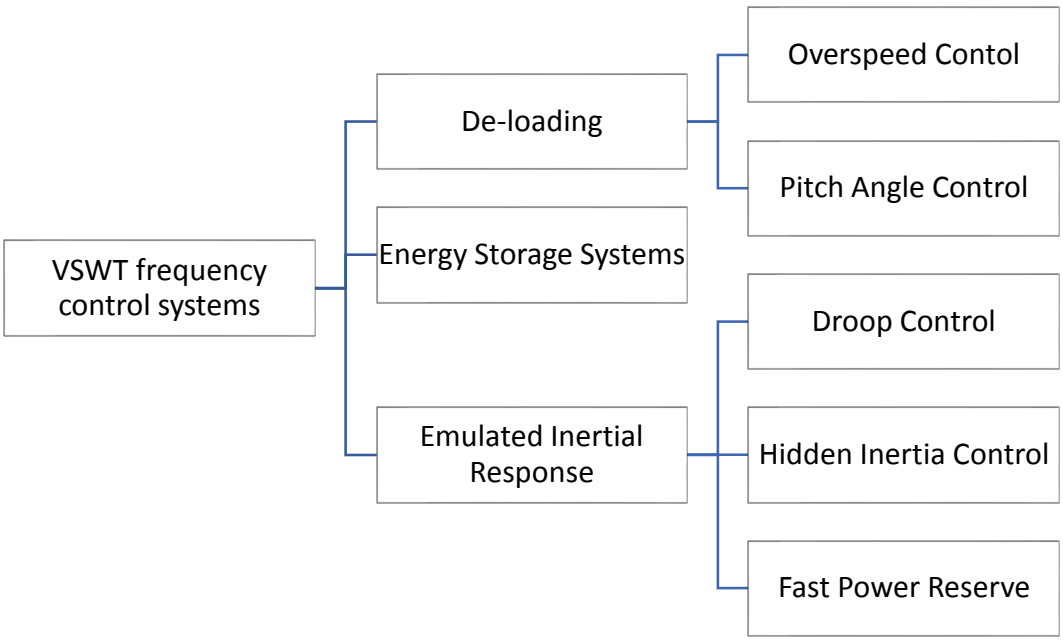

Figure 2.1: General classification of VSWTs frequency control systems (Fernández-Bustamante et al., 2021)

2.6.1.1 De-loading

Wind turbines operate along an MPPT curve to extract the maximum energy from the wind. However, operating along this MPPT curve leaves no additional power reserve for frequency support (Lin & Wu, 2021). To provide additional power reserve for frequency support, a de-loading control system can be implemented. A de-loading control system operates a WTG in a suboptimal point, where the WTG deviates from the MPPT curve to provide additional active power for grid frequency support functions (Fernández-Guillamón et al., 2021). There are two different methods to implement de-loading namely, overspeed control and pitch angle control (Lin & Wu, 2021).

The paper (Attya & Dominguez-Garcia, 2018) evaluates pitch de-loading, kinetic energy recovery, and WTG over-speeding, that enable WTGs to provide short term frequency support, from an electrical and mechanical perspective. The authors found that WTG over-speeding showed a faster response to a frequency event, accompanied by a higher initial power surge. While pitch de-loading provided a more sustainable support followed by a smoother recovery. WTG over-speeding could have implications on the mechanical stability of the WTG however,

wasted less energy when compared to pitch de-loading. An important aspect of kinetic energy recovery is that it does not deviate from the MPPT curve at normal operation. However, the system is most likely to suffer a second frequency dip as the rotors of the WTGs recover to the nominal rotor speed. The simulation environment used was MATLAB/Simulink.

The paper (Ye et al., 2016) presents an analytical model for short-term grid frequency report to evaluate the contribution of inertial and droop responses from a wind farm. The available mechanical power of a VSWT was approximated by a second order polynomial which quantified the kinetic energy and wind power reserve over a wide range of operating points. Since the VSWT operating characteristics and conditions were now quantified, the frequency controller gains could be adjusted accordingly, thereby ensuring stable performance of the wind farm during frequency transients. To stimulate the frequency response of a wind farm during wind power fluctuations, a modified system frequency response model which considered the inertial and droop responses was developed. The efficacy of the model was verified by comparisons of the results with those obtained empirically.

Two virtual inertia control schemes, an equation based and an adaptive fuzzy logic-based scheme, are proposed in (Pradhan et al., 2018). The proposed control schemes dynamically modulate the gains of the inertia control schemes based on system events to improve the primary frequency response of the WECS. The efficacy of the proposed schemes was validated in MATLAB/Simulink while additional hardware-in-the-loop simulations on the OPAL-RT real time simulator platform were presented to further substantiate the proposed schemes. It was concluded that the adaptive fuzzy logic-based scheme provided better frequency regulation when compared to the dynamic-equation based scheme.

The paper (Wang & Tomsovic, 2018), proposes an active power control scheme which enables DFIGs (Doubly Fed Induction Generators) to partake in grid frequency support. Herein, a power surge-based co-ordination strategy provides an inertial response while a power reserve control method assists with primary frequency control. The DFIG is therefore designed to provide both inertial and primary frequency support by adjusting the reserve amount whilst considering under- and over frequency events. The effectiveness of this proposed control scheme was validated through case studies on a 181-bus WECC system with 50 % wind penetration. The paper concludes by stating that future work will see the inclusion of secondary frequency control within the control scheme which will make use of a co-ordinated strategy between DFIGs and conventional synchronous generators.

A droop control scheme for WTGs that uses rotor speed control for frequency support is proposed in (Boyle et al., 2021). The proposed control scheme does not add frequency-droop control signals to the WTG's power reference, but instead relies on the method of power tracking by adjusting the wind turbine's power tracking curve for primary frequency regulation. The efficacy of the proposed control scheme was validated through simulations in DIgSILENT

Power Factory on a modified IEEE 39-bus power system. The results showed that the proposed scheme produces a linear frequency droop response independent of the power tracking method used. This is an improvement over conventional frequency-droop controllers whose frequency regulating responses are dependent on the method of power tracking used.

In (Tessaro & de Oliveira, 2020), the authors propose an optimisation function which determines the operating point of de-loaded WTGs to reduce the magnitude of speed deviation and settling time caused by the inertial response and participation in frequency control. The optimisation function was integrated into a combined inertial and frequency control strategy for Type-4 (fully rated power converter) WTGs, based on the concept of a virtual synchronous generator. The paper presents an analysis of the impact of the inertial response and frequency control on the dynamics of VSWTs. The results showed that the kinetic energy and mechanical energy variations in the WTG depend on its operating point. The control strategy and optimisation process were evaluated by nonlinear time-domain simulations using the ODE23tb solver in MATLAB. The validation of the optimisation function included wind speed and load variations.

In (Fu et al., 2017), an integrated controller to provide both an inertial response and primary frequency regulation is proposed. More specifically, this includes a de-loaded pitch control system is proposed alongside an optimised MPPT controller to reserve capacity for frequency regulation and, provide an inertial response while under de-loaded operation. The de-loading controller can estimate the proper pitch angle or regulate the tip ratio to attain the required de-loading. Under de-loading option, the MPPT controller will switch from the MPPT curve to a virtual inertial control curve depending on the frequency variation. In this way, the WTG may provide frequency support to the grid by shifting its active power reference.

The authors in (Yan & Saha, 2015) present a method which estimates the grid frequency response as a result of a generator tripping. This method applies to both, conventional synchronous machines, and wind turbine generations for grid frequency support. In this way, system operators can continuously evaluate the inertia and headroom produced and adjust the amount of WTG inertial and active power control required for reliable system operation accordingly. The authors' full model proposed was validated by simulation on PSS/E. As concluded by the authors, determining the optimal amount of WTG inertia and active power support from conventional synchronous generators, will be the focus of their future work.

The authors in (Bianchi & Dominguez-Garcia, 2016) present a co-ordinated, distributed control scheme which allows offshore wind power plants (WPPs), connected through an HVDC system, to support the primary frequency control efforts of the AC grids on land. The control scheme is designed to account for AC areas and WPPs which may be operated by different operators. In addition, the control scheme considered the limited power reserve of the wind turbine generators in the WPPs and will adjust accordingly to maintain a suitable frequency

regulation. In the case of a substantial change in the power demand, the control scheme will permit all stations to share their power reserves so that the frequency in the AC areas converge close to the nominal frequency. Slight changes to the power demand result in the control scheme restoring the frequency in the AC areas to the nominal frequency value. This control scheme was validated through transient simulations in a modified version of the Cigré DC grid benchmark which included a five-terminal HVDC grid, comprised of two WPPs and three AC networks. MATLAB/SimPowerSystem was the simulation environment used in this paper.

A dynamic de-loading control scheme for a DFIG to provide additional active power for grid frequency support is proposed in (Ouyang et al., 2021). The proposed control scheme co-ordinates the rotor acceleration control and pitch angle control while considering the frequency regulation demands of the grid and the prediction error of wind power. This control scheme was simulated in MATLAB. The results show that despite a small amount of wind abandonment, this control scheme can provide frequency support to the grid and mitigate the secondary frequency drop following frequency regulation.

A summary of the papers classified as de-loading control, grouped by research area is shown in Figure 2.3.

Table 2.3: Publications in de-loading control for VSWTs

Research Area	Reference	Year of Publication
Overspeed Control	(Boyle et al., 2021)	2021
	(Attya & Dominguez-Garcia, 2018)	2018
	(Wang & Tomsovic, 2018)	2018
	(Pradhan et al., 2018)	2017
	(Ye et al., 2016)	2016
Pitch Angle Control	(Ouyang et al., 2021)	2021
	(Tessaro & de Oliveira, 2020)	2020
	(Fu et al., 2017)	2017
	(Bianchi & Dominguez-Garcia, 2016)	2016
	(Yan & Saha, 2015)	2015

2.6.1.2 Energy Storage Systems

Energy storage systems can partake in frequency regulation and work with WTGs to improve the system inertia or augment the frequency response of WTGs (Lin & Wu, 2021). Specifically, in the context of frequency regulation, energy storage systems can mitigate the secondary frequency drop of WTGs during the rotor recovery phase of the WTG (Lin & Wu, 2021).

The authors in (Miao et al., 2015) propose a strategy which provides better performance of temporary frequency support as well as, addresses the problem of system frequency oscillation and a secondary frequency drop. The solution is based on a co-ordinated control of

WTGs in conjunction with an energy storage system (ESS). The proposed strategy was simulated on PSCAD/EMTDC to verify its effectiveness. The authors concluded that a secondary frequency drop may be avoided by an ESS rated to only 10% of the WTG.

A specified time consensus (STC) control for ESS assisted DFIG WTGs to assist in frequency regulation is proposed in (Xiong, Yang, He, et al., 2022). The efficacy of the proposed control scheme is validated by simulations conducted in MATLAB/Simulink. The results showed that the proposed strategy can provide a smooth power output of the WTG and improve the frequency regulation capability.

The paper (Choi et al., 2016) presents a hybrid operation strategy for a WECS using ESS, for grid frequency support. This operating strategy provided a reserve power margin by de-loaded operation in addition to, relying on the kinetic energy of the rotor. The ESS is used concurrently with the kinetic energy discharge to provide additional energy to the grid during a frequency deviation. Furthermore, the ESS is used to maintain the power balance between generation and consumption thereby, mitigating the stochastic nature of wind. The effectiveness of the proposed hybrid operation strategy was verified using PSCAD/EMTDC.

In (Attya & Hartkopf, 2015), an algorithm is proposed to integrate hydro-electric pumped storage (HEPS) station with WECS, provide grid frequency support. This strategy embeds the idea that excess energy from the WECS is stored in a HEPS, providing energy during frequency drops. The major benefit being that the WTG will always follow its MPPT curve since, no frequency support methods are applied to the WTG allowing for deviation. This ensures that the maximum energy will always be extracted from the wind. The major HEPS aspects of this system were estimated while, case studies examined the impact of the algorithm on frequency recovery at 40% wind power penetration. The simulation environment used was MATLAB/Simulink.

A co-operative control strategy of a WECS and compressed air energy storage for frequency regulation is proposed in (Abouzeid et al., 2021). The effectiveness of the proposed co-ordinated control strategy was evaluated under various scenarios and load profiles using MATLAB/Simulink simulations.

The authors in (Zhao-xia et al., 2019), present an embedded solution that uses a hierarchal controller on a microgrid comprising of wind turbines and battery units. In this way, the solution provides a co-ordinated frequency support to a weak grid by adjusting the active power flow through the tie-line in accordance with grid frequency requirements. To deal with the interactions between the impedance of the weak grid and output impedance of the microgrid, a stability analysis model was developed. This proposed approach was validated through simulation using MATLAB/SimPowerSystem toolbox.

The paper (Tan et al., 2019) proposed a multilevel embedded ESS consisting of super-capacitors and lead-acid batteries inside a PMSG (Permanent magnet synchronous generator) to provide frequency support. The super-capacitors are used to emulate an inertial response while the lead-acid batteries are used to provide the primary frequency response. The secondary frequency response is provided by the mechanical power reserved in the wind turbine by using a suboptimal MPPT strategy. In addition, a supplementary control strategy is proposed, which makes use of the super-capacitors and lead-acid batteries to provide a primary and secondary frequency response, respectively. Simulations were performed using MATLAB/SimPowerSystem and laboratory tests were conducted to validate the effectiveness of the proposed control strategy. By utilising the complimentary characteristics of lead-acid batteries and super-capacitors, the solution eliminates frequent cycling of the lead-acid batteries while also relieving mechanical stress from WECS due to abrupt electromagnetic changes when partaking in frequency regulation.

An inertial response control scheme with a super-capacitor ESS is proposed in (Yan et al., 2020). The inertial response is designed using the generator torque limits. The energy released from the ESS is used to augment the active power deficit during the recovery process of the turbine rotor. In addition, a damping controller is added to the inertial control to suppress mechanical oscillations in the shaft and tower of the turbine during frequency support. The mechanical system of the wind turbine generator was modelled and simulated using FAST by the NREL whilst, the electrical system of the wind turbine generator was developed in MATLAB/Simulink. The simulation results show that the proposed method can improve the frequency nadir, mitigate the secondary frequency dip, and reduce the magnitude in the mechanical subsystem.

To mitigate the impact of the wake effect in grid frequency support, the paper (Xiong, Yang, Huang, et al., 2022), proposes an optimal ESS allocation (OEA) scheme for DFIG based wind turbines. To realise the OEA scheme, wind turbines are placed in a cluster, considering their received wind speed. Each wind turbine within a cluster will share the same ESS. The OEA scheme tries to optimise the coherency of all the clusters' frequency support margins so that all wind turbines maintain the same frequency stability. In the OEA scheme, the ESSs do not directly provide frequency support services to the grid, rather, it serves to improve the wind turbine's frequency support capability and the system security. In this implementation, the required capacity of the ESS need not be so large as in the case of when ESSs are directly providing frequency support thereby reducing the level of investment needed to deploy an ESS. The effectiveness of the OEA is verified by simulation studies conducted on a modified 29-bus Hydro-Quebec transmission system with one DFIG wind farm.

A summary of the papers classified as ESS is shown in Table 2.4.

Table 2.4: Publications in energy storage systems for VSWTs

Research Area	Reference	Year of Publication
Energy Storage Systems	(Xiong, Yang, Huang, et al., 2022)	2022
	(Xiong, Yang, He, et al., 2022)	2021
	(Abouzeid et al., 2021)	2021
	(Yan et al., 2020)	2020
	(Zhao-xia et al., 2019)	2019
	(Tan et al., 2019)	2019
	(Choi et al., 2016)	2016
	(Miao et al., 2015)	2015
	(Attya & Hartkopf, 2015)	2015

2.6.1.3 Emulated Inertial Response

The energy contained within a WTG system can be used when the frequency deviation exceeds the allowable frequency range (Fernández-Bustamante et al., 2021). Droop control provides additional power in proportion to the frequency deviation (Lin & Wu, 2021). When a wind turbine operates at its maximum power, the additional power required is obtained from the kinetic energy of the rotating mass (Fernández-Bustamante et al., 2021). Like droop control, hidden inertia emulation also releases kinetic energy from the wind turbine generator, but the inertial response is instead based on the response of traditional synchronous generators (Fernández-Bustamante et al., 2021). Kinetic energy from the wind turbine can also be released by the fast power reserve controller which acts on the rotor speed signal (Fernández-Bustamante et al., 2021).

To improve the primary frequency response of wind power plants, the authors in (Mahish & Pradhan, 2020) propose a distributed synchronised control technique. The droop control uses an optimum power share ratio and the frequency of each WPP at the point of common coupling (PCC) to calculate the droop. The control technique finds the optimum power share ratio through an interactive algorithm. The synchronised droop characteristic of the WPPs are functions of the frequency variation at the PCC and are inversely proportional to the respective power share ratios. The droop is therefore changed with the frequency variation followed by the load-generation imbalance due to the disturbance. The synchronised droop varies differently with increasing communications delay between nodes which mitigates the effects of the communications delay on the proposed method. The effectiveness of the proposed control technique was tested on a WPP integrated 39-bus New England system and simulated in PSCAD/EMTDC. The simulation results showed that the primary frequency response of the proposed control technique was better than that of the distributed Newton method. However, the performance of the distributed synchronised droop control, deteriorates if for a false data injection attack on the communications system.

The paper (Adeuyi et al., 2017) presents a communication-free alternative co-ordinated control scheme that prioritises frequency versus active power droop fitted onshore VSCs. This scheme aims to transfer the wind turbine recovery power to undisturbed AC grids and allow for the correct control operation of multi-terminal high voltage direct current (MTDC) system during multiple power imbalances on different AC grids. The control scheme presented in the paper is compared with another co-ordinated control scheme which uses frequency versus DC voltage droop and the MTDC frequency support capability when wind farms to not provide extra power is also evaluated using a 4-terminal HVDC system. The results presented in this paper showed that during a single power imbalance in one AC grid, the fast frequency response from MTDC-connected wind farms limited the RoCoF on disturbed AC grids and transferred additional active power from another AC system contained the system frequency deviation. The MTDC-connected windfarms were equipped with both the alternative co-ordinated control and the co-ordinated control scheme. However, the co-ordinated control scheme was shown to have larger power oscillations when compared to the alternative co-ordinated control scheme under certain conditions. A 3-terminal HVDC system was used to test the effectiveness of the co-ordinated control scheme and alternative co-ordinated control scheme, both of which were modelled in using PSCAD and experimental results were obtained using the RTDS tool of RSCAD. While the MTDC frequency support capability when find farms do not provide extra power was verified using a 4-terminal system and modelled using MATLAB/Simulink.

In (Ashouri-Zadeh et al., 2016), a control scheme is proposed for DFIG based wind turbines for improved transient response and participation in grid frequency support. The proposed control scheme consists of a main controller with two auxiliary controllers. The main controller is a fuzzy-based controller whose parameters are optimised using the genetic algorithm to achieve an optimal transient response. The two auxiliary controllers, frequency deviation and wind speed oscillation controllers, enable the DFIG to provide frequency to the grid and mitigate the impacts of wind speed fluctuations on the WTG output power by using the kinetic energy of the WTG. The performance of the controllers is highly dependent on the operating point of the WECS. Simulations were performed considering various scenarios to prove that the proposed control scheme can enhance the power system's frequency performance after disturbances.

The authors in (Toulabi, Bahrami, et al., 2017) developed a nonlinear dynamic model for the DFIG's output power integrated into a dynamic model of the power grid. In addition to this, a state feedback controller is proposed by considering if DFIGs participate in grid frequency regulation or not. The stability of the entire system is considered using the input-to-state stability theory. The controller was embedded in the DFIG's detailed model and simulations were done to evaluate its performance. In comparison to a conventional controller presented

in the paper, the proposed controller delivered more output power during grid frequency support and a negated transient recovery period were some of the advantages of the proposed controller.

A fast frequency support scheme for wind turbine systems to raise the frequency nadir close to the settling frequency and eliminate the secondary frequency dip is proposed in (Zhao et al., 2020). The frequency support scheme uses the kinetic energy of the wind turbine to raise the frequency nadir close to the settling frequency. In addition to raising the frequency nadir, an adaptive gain function of the real-time rotor speed and wind power penetration level is proposed to provide frequency nadir improvements under various wind speed and wind penetration levels. The last aspect of the proposed frequency support scheme is a new speed recovery strategy to mitigate the secondary frequency deviation associated with the rotor recovering its speed. The speed recovery strategy of the proposed frequency support scheme will not require the wind turbine to recover to the MPPT operating point during the primary frequency support phase. This allows the release of kinetic energy to be large, and no secondary frequency deviation will occur as no energy is extracted from the grid to recover the rotor speed. The three aspects of the proposed frequency support scheme have been implemented together, and the performance and stability of the wind turbines has been verified by comparisons of simulation results using the two-area power system for a DFIG based wind turbines and an IEEE 39-bus power system for PMSG based wind turbines. The simulations were done using RTDS and Dymola.

In (Wang et al., 2015), an active power control method for VSWTs to enhance the inertial response and damping capability during transient events is proposed. The control method implements an optimised power point tracking controller, which shifts the wind turbine operating point from the MPPT curve to the virtual inertia control curves in relation to the frequency deviation. This allows the wind turbine to use its kinetic energy to provide grid frequency support. In addition to frequency support, the authors also theoretically evaluate the effects of the virtual inertia curves on damping power oscillations. When compared with a supplementary derivative control, the proposed optimised power point tracking control method avoids an interaction between the inertial response and the MPPT controller. The optimised power point tracking control method can also contribute to the power system damping and provides a smoother recovery of the rotor speed. The control method was prototyped on a three-machine system comprising of two synchronous generators and a PMSG WTG with a wind penetration level of 31 % to validate the proposed method.

The authors in (Zhang et al., 2016) propose a control strategy that shifts the MPPT curve of the WTG to a virtual inertial control curve in relation to the frequency deviation so to recover the kinetic energy of the wind turbine to provide grid frequency support. When compared to a PD based inertial controller, the proposed virtual inertia control scheme provides a rapid

response in the event of a sudden change in power and a smoother recovery to the MPPT operation. Comparative studies of the network frequency responses with and without the proposed virtual inertial control curves following a sudden system load and wind power change. The simulations for the comparative studies were run using MATLAB/Simulink. The simulation results showed that the proposed control scheme can provide a rapid dynamic frequency support to the grid with reduction to frequency variations during fluctuations in both load and generation.

In (Ghosh et al., 2016), a control strategy for primary and inertial responses for high wind integrated power systems is proposed. The proposed method couples the pitch and power control loops and provides control at both sub- and super synchronous operation. This method can be used for either a WTG or can be used to dispatch an entire wind farm for a primary frequency response and avoid individual turbine control. The proposed control scheme was evaluated on a 39-bus dynamic IEEE New England test system with 39 buses and 10 generators. Two aggregated windfarms were placed at bus 38 and bus 32. The dynamic models of the turbine and converter dynamics were modelled in DIgSILENT Power Factory.

The authors in (Lee et al., 2016) propose an inertial control scheme for a DFIG based wind power plant. The proposed scheme aims to improve the frequency nadir and stable operation of the DFIG, especially when wind speed decreases during inertial control, by using adaptive gains set to be proportional to the kinetic energy stored in the DFIG and the gains decrease with the declining kinetic energy. The results presented in the paper indicate that the proposed scheme improves the frequency nadir and prevents over-deceleration under certain wind and system conditions. The performance of the proposed adaptive gain scheme was verified through the simulations of case studies using EMTP-RV.

The paper (Li, Xu & Wong, 2017) proposes two novel control strategies that enable an inertial response from PMSG wind turbines during transient events. The first strategy aims to provide inertia to the system by simultaneously using the energy of the DC-link capacitor and kinetic energy of the wind turbine rotor. While the second strategy aims to provide inertia to the system by first using the energy of the DC-link capacitor and then the kinetic energy of the rotor in a cascading control scheme. The two control strategies were validated using a case study of one PSMG based wind turbine subject to sudden load variations and then compared. Subject to the same disturbance event, it is shown that both control strategies can provide similar performance in stabilising the system frequency permitting that the control parameters are set correctly in advance. However, the cascaded control scheme characterises itself by enabling a better energy harvest during a frequency disturbance. The simulation environment used in (Li, Xu & Wong, 2017) was not mentioned.

A non-linear system model of a VSWTs may experience large deviations from its operating point during times of frequency support when linear control techniques are used. In (Toulabi,

Dobakhshari, et al., 2017), a novel non-linear controller to enable an inertial response from a VSWT is presented. A regular controller based on the input-output feedback linearisation approach was first designed, and then replaced by the proposed controller where the output power of the wind turbine is expressed in terms of state variables and its Taylor series expansion used in the design of the control system. The proposed controller was embedded in the detailed model of the VSWT in MATLAB/Simulink and the various effects of different controller parameters were investigated. It is also emphasized that an appropriate co-ordination between conventional generating units and VSWTs equipped with the proposed controller results in a negligible transient recovery period. In addition to this, the behaviour of the controller was also investigated in the presence of fluctuating wind power input and is shown to provide a smoother frequency response. The advantages of the proposed controller over that of conventional PI control was also verified.

A co-ordinated control strategy to provide system inertial support for an offshore windfarm that is connected via an HVDC transmission line to an onshore main grid is discussed in (Li, Xu, Ostergaard, et al., 2017). The authors compare two proposed strategies. One where the energy of the HVDC capacitors and the kinetic energy of the wind turbine are used simultaneously to provide inertial support without the installation of remote communication between the two terminals of the HVDC transmission line, while the other strategy employs a sequential release of energy starting with the HVDC capacitors and then using the kinetic energy of the wind turbine with the aid of communication between the onshore and offshore grids. A detailed design and case study of the two control strategies has been conducted to compare and demonstrate the effectiveness of the control strategies in DIgSILENT Power Factory. It was shown from the test system that when subject to the same disturbance event, both strategies exhibit similar performance in stabilizing the system frequency permitting that the control parameters are set correctly in advance. However, the cascaded control scheme has been shown to have better wind energy harvest during a frequency disturbance event. The impact of the time delay introduced by the communication of the two converters in the cascaded control scheme, may have some limited impact on the control system performance and overall system stability.

A distributed virtual inertia scheme is proposed in (Fang et al., 2018b) which can be implemented by grid-side connected power converters without any modification to the system hardware. The virtual inertia provided to the grid uses the energy stored in the DC-link capacitors of the grid-side connected power converters and by regulating the DC-link voltages in proportion to the grid frequency, the DC-link capacitors are aggregated into a large equivalent capacitor. The limitations of the virtual inertia along with the design parameters such as DC-link capacitance, DC-link voltage and maximum DC-link voltage deviation were identified in this paper. The concept was verified by MATLAB/Simulink simulations and

additional experimental results were also obtained to verify the efficacy of the proposed concept. The proposed concept indicates an improvement in both the reduction in frequency deviation and an improvement in the RoCoF.

In (Zhang et al., 2017), the system frequency dynamics during inertia emulation and primary frequency support from wind turbine generators is studied and a mode switching scheme of a wind turbine generator for frequency support is proposed. A proposed concept, a region of safety, which is the initial set of safe trajectories are used to determine switching instances. The barrier certificate methodology was used to derive a new algorithm to enlarge the region of safety for a given desired safe limits and worst-case disturbance scenarios which lead to finding the critical switching instants and a safe recovery procedure. Furthermore, the inertial response and load-damping effects are derived in the respective time frames of both an inertial and primary frequency responses, respectively. The paper (Zhang et al., 2017), presents theoretical results under critical cases.

The paper (Azizipanah-Abarghooee et al., 2020), proposes a torque limit-based method to emulate an inertial response. The efficacy of two torque limit-based methods is investigated through a power system with varying degrees of wind penetration levels in DIgSILENT PowerFactory 2018. The first torque limit-based method considers a definite ramp rate for the inertial power of the wind turbines, while the second torque limit-based method varies the key parameters to obtain a linear relation between its characteristics and the operating point of the VSWT. It was shown that the second torque limit-based method places lower stress on the mechanical parts of the wind turbine, particularly at low rotor speeds, compared to the first torque limit-based method. While the results also show a more stable system operation due to the emulated inertia, the results do however also reveal a deteriorated frequency nadir for both torque limit-based methods while the degree of wind penetration is high due to the incoordination of the VSWT inertial response and the governor response of fossil-fuelled generating units. To mitigate this, it is suggested the inertial power of the VSWT is multiplied by a frequency dependant gain.

Based on a frequency response model derived in (Chen et al., 2021), an estimation method to calculate the virtual moment of inertia provided by a DFIG-based wind farm is proposed. By using the Routh approximation method, an expression for the virtual moment of inertia for the grid connected DFIG system is derived. To augment the availability of the expression, an estimation method based on the matrix pencil method and least squared algorithm for estimating the virtual moment of inertia provided by the wind farm is proposed. The effectiveness of the prosed method and derived expression are tested on a DFIG grid-connected system and a modified IEEE 30-bus system in MATLAB/Simulink. Based on the results, the derived expression of the virtual moment of inertia directly expresses the inertial behaviour of a VSWT with additional frequency control and that the estimation can efficiently

calculate the virtual moment of inertia provided by the wind farm, regardless of VSWTs are involved in the frequency regulation of the grid or not. The ability to distinguish between which VSWTs are involved or not has value in power systems with high wind power penetration since it avoids the complex processing of parametric derivation and frequency response integration.

The frequency nadir and RoCoF are two metrics that temporary grid frequency support schemes strive to improve. The paper (Lao et al., 2021), proposes a rotor-speed based inertia control scheme aimed at improving the performance of the system's frequency regulation. Several case studies were performed, by varying wind spend conditions and wind power penetration levels, to investigate the performance of the proposed control scheme. The proposed control scheme was tested on a 7-machine power system, with an aggregated wind farm on MATLAB/Simulink. The results showed that the proposed scheme contributes to reducing the frequency nadir and RoCoF. In addition, the rotor-speed based inertia control scheme is decoupled from the system frequency which in turn, decouples the inertial response speed from the inertia response amplitude, allowing an appropriate response to be realised, ensuring the stable operation of the WTG and system.

In (Peng et al., 2020), a frequency support scheme for DFIG wind turbines that implements a two-stage switching control scheme is proposed. The first stage of the control scheme uses a variable proportion coefficient designed to emulate an inertial response from the DFIG wind turbine while the second stage of the control scheme uses a fuzzy logic control scheme is used to determine the variable proportion coefficient to both quickly restore the DFIG wind turbine to MPPT operation and avoid a secondary frequency dip to the system. The proposed control scheme was simulated in MATLAB/Simulink and case studies performed on a WSCC 9-bus and IEEE 39-bus power system to verify the effectiveness of the proposed control scheme. The results showed that the proposed control scheme can provide a satisfactory performance for frequency support despite varying operating conductions. The paper concludes by stating that in future work, the feasibility of implementing the control scheme in large-scale power systems with integrated wind turbines will be verified by hardware-in-the-loop simulation.

A time-variable droop control method for WTGs to provide grid frequency support is proposed in (Garmroodi et al., 2018). In the proposed method, a positive droop characteristic provides frequency support and is followed by a period of negative droop to restore the kinetic energy of the rotor. The proposed method is simulated in DIgSILENT Power Factory, and the performance of the proposed control method is studied when subjected to various operating conditions. The results show that the frequency nadir can be improved while WTGs regain their kinetic energy and continue MPPT operation.

An adaptive droop control scheme for DFIGs to provide frequency support is proposed in (Yang et al., 2022). The initial value of the adaptive droop gain is determined in accordance with the wind speed and decreases with time. The efficacy of the proposed control scheme was

simulated on a modified IEEE 14-bus system in EMTP-RV. The results showed that the proposed method prevents a DFIG from stalling and reduces the second frequency drop during the rotor recovery phase.

A RoCoF droop control strategy to mitigate the problems of frequency deviation and high RoCoF is proposed in (Binbing et al., 2020). In response to a high-frequency event, power is contributed to the grid from the reserve margin stored in the DC-link capacitor to mitigate the RoCoF. Once a new steady state has been reached, the reserve energy expended from the DC-link capacitor is recovered. An experimental comparison between the proposed RoCoF droop control strategy and conventional droop control strategy is done on the RT-LAB platform. The results of the comparison show that the by adjusting control parameters such as increasing the droop coefficient or decreasing the bandwidth, a larger virtual inertia can be obtained than that attributed by the capacitor alone.

The paper (Guo et al., 2020), proposes a strategy to co-ordinate the use of the kinetic energy of a VSWT and the energy stored in the DC-link capacitor from a VSC-HVDC connected offshore wind farm too provide grid frequency support. The minimum rotor speed limit for the VSWT is determined by the rate of change of the mechanical power with rotor speed, which reduces the reduction in mechanical power caused by the low rotor speed. While the capacitor energy of the VSC-HVDC is used to contribute to the frequency nadir when the output power of the VSWT is less than the initial value. A detailed selection process of the controller parameters to improve the efficacy of the frequency control strategy is discussed and the proposed strategy was verified using a power system model in MATLAB/Simulink. The simulation results show that the proposed strategy can significantly reduce the grid frequency variation and maintain frequency stability in grids with high penetration of renewable energy.

In (Jiang et al., 2022), a time-sharing frequency co-ordinated control scheme is proposed. The implementation of the proposed scheme uses a frequency dead-band to co-ordinate the priority of the rotor virtual inertia control, DC-link virtual inertia control and a new adaptive frequency droop control. In the proposed control scheme, the electrostatic energy stored within the DC-link capacitor is always used first for frequency support while the kinetic energy of the rotor is only used once the energy stored within the DC-link capacitor has been depleted. The performance of the proposed control scheme is simulated and studied in PSCAD/EMTDC. The results of the paper (Jiang et al., 2022), indicate that the time-sharing frequency co-ordinated control scheme has better performance in wind energy harvesting and system stability when compared to either traditional cascaded control or co-ordinated control strategies. In addition, the proposed scheme can also effectively avoid power oscillations.

In (Zeng et al., 2019), a co-ordinated control strategy for PMSG-based VSWTs to provide frequency support services is proposed. An inertial response is emulated by using the energy stored in the DC-link capacitor. However, since the available energy is relatively small, it is

supplemented by a virtual capacitor control strategy which uses the rotor-side converter to provide a virtual capacitance that is larger than the actual DC-link capacitance by using the wind turbine's kinetic energy in a similar way to the inertial response of a synchronous generator. Lastly, a power-frequency droop control is used to simulate the primary frequency control of a synchronous generator. The efficacy of the proposed control strategy was verified by simulation results in PSCAD/EMTDC and indicate that the RoCoF is mitigated, and the frequency nadir improved by adopting the proposed co-ordinated control strategy.

The authors in (Khajehoddin et al., 2019) presents a control approach based on the VSM concept. The approach presented in (Khajehoddin et al., 2019), called an enhanced virtual synchronous machine (eVSM) uses the existing inertia of the DC-link component and does not emulate the rotating inertia based on an assumption of unlimited energy. The eVSM concept aims to reduce the need of a large DC-link component or battery storage while providing the same inertial response of an equivalent synchronous machines.

The paper (Xiong et al., 2021), proposes a two-level combined control strategy for offshore wind farms to provide frequency support for an onshore system. On the wind turbine level, each wind turbine implements inertial and droop control with adaptive coefficients, which allow wind turbines with high rotor speeds to release more kinetic energy, while working at MPPT mode. To mitigate the second frequency dip that occurs after frequency support, the wind turbines are divided into clusters based on their rotor speed and a step start-up control scheme is implemented for the wind turbine clusters to provide frequency support sequentially. The sequential frequency support allows one cluster to provide frequency support, while another recovers their rotor speed. At the system level, a communication-free allocation control strategy is proposed using the local frequency signal of on shore voltage source converter stations to share the active power among the onshore stations. Case studies were conducted on a 3-area 4-terminal voltage source converter-based multi-terminal high-voltage direct current offshore windfarm, in MATLAB/Simulink, to determine effectiveness of the two-level combined control strategy. The simulation results show the efficacy of the proposed control scheme under various scenarios. The paper concludes by stating that future work will consider optimising the number of clusters and consider asynchronous interconnection to the onshore system.

The authors in (Kabsha & Rather, 2020) propose a control strategy for offshore HVDC connected windfarms to provide an inertial response and primary frequency support. The proposed control strategy uses the HVDC converters to map the onshore frequency variation into a voltage variation in the offshore grid. The authors have identified various limitations of conventional frequency support strategies from offshore connected windfarms including large frequency deviations and high RoCoF in the offshore gird. In contrast, the proposed control strategy achieves the frequency requirements of the regional grid code without stressing the

offshore grid as the frequency deviations and RoCoF are kept low. The proposed control strategy was tested on two test systems, one built entirely in the DIgSILENT PowerFactory environment and the other on an IEEE 39-bus system. However, the proposed control strategy relies on using existing local communication systems to monitor the HVDC link voltage to distinguish between internal disturbances of the offshore AC grid and disturbances that arise due to a frequency disturbance of the main onshore AC grid. The authors are developing an adaptive control strategy with minimal reliance on local communication systems that can discern between internal and external disturbances.

The paper (Martinez Sanz et al., 2015), expands on a communication-less approach previously proposed in literature for offshore wind turbines connected though a DC grid to multiple onshore AC grids. To extend this concept, the authors instead adopt a strategy where the onshore frequency variations are communicated to the offshore converters by using the fibre optic link embedded within the sub-sea DC cables. In the paper, a case study on a 4-terminal DC grid connecting an offshore wind farm and two onshore AC systems illustrates the inertial support from the offshore wind farms with the proposed strategy. An aggregated model of the WTGs within the windfarm was used in the simulations and the parameters were obtained from a simulation model in DIgSILENT Power Factory. It is shown that the proposed weighted frequency scheme strategy can improve the transient frequency deviation in AC grids experiencing an under-frequency event.

The authors of (Ma et al., 2018) propose a clustering-based co-ordinated control scheme for large scale wind farms to provide frequency support. The proposed control scheme considers the distributed layout of WTGs and the wake effects inside the wind farm. WTGs are grouped by their wind profiles and dispatches the same control commands to the same group. This effectively realises a group of WTGs as one single WTG reduces the control variables and complexity of the optimization problem. Simulations were conducted in MATLAB/Simulink to verify the effectiveness of the proposed control strategy.

A hierarchical non-linear model predictive control (MPC) for frequency support is proposed in (Li & Ye, 2021). The proposed hierarchical non-linear MPC reduces the computational burden of the central controller when compared to a centralised non-linear MPC. The efficacy, efficiency, and robustness of the proposed hierarchical non-linear MPC is validated by numerical simulations in MATLAB/Simulink. The results show that the non-linear MPC can reduce the computation time by as much as 50 % when compared to centralised non-linear MPC. This makes the proposed MPC method more favourable for large-scale wind farms implementations by avoiding the requirement of higher performance computation facilities.

In (Yang et al., 2020), a short-term frequency support method for a DFIG is proposed to improve the frequency nadir using less kinetic energy and accelerate the rotor speed recovery while negating a second frequency drop. The proposed method increases the output power of

the DFIG by adding a time-varying incremental power, to the power reference for the MPPT function and then recovers the rotor speed along with the MPPT curve. The simulation results indicate that the proposed method can provide an improvement to the frequency nadir while using less of the DFIG's kinetic energy in various scenarios. However, due to the stochastic nature of wind the frequency support capacity of DFIGs might be unable to meet the instantaneous system frequency requirements and may be required to operate with ESSs to augment the frequency support capability. The authors conclude by stating that in future work, a co-ordinated frequency control scheme between DFIGs and ESSs for frequency control will be studied in power systems with high wind power penetration.

The authors of (Yang et al., 2020), present a short-term frequency support method for doubly fed induction generators (DFIGs) to improve the frequency the nadir of the system using less kinetic energy and negate the second frequency drop caused by the rotor speed recovery. The proposed method adds a time-varying constant to the power reference for the maximum power point tracking (MPPT) function and allows the rotor to recover its speed along with the MPPT curve. The proposed method was analysed and validated on a modified IEEE 14-bus test system however, the simulation environment was not disclosed. The simulation results indicated that the proposed method could provide a frequency nadir improvement with a lower kinetic energy cost for the DFIG in various scenarios and reduces the secondary frequency nadir. The performance of the proposed method is affected by wind speed, as the winds speed affects the levels of kinetic energy available. The proposed method was only tested against two wind speed conditions, 8 m/s and 10 m/s. The paper concludes by stating that due to the inherent variability and uncertainty of wind power, the frequency support capacity of DFIGs may be unable to meet the instantaneous frequency system requirements and may be required to operate with ESS systems.

In (Xu & Xu, 2017), the effect of different power curves to release kinetic energy for grid frequency support is considered and two solutions are proposed. The first of the two proposed solutions aim at reducing the rate of change of frequency (RoCoF) while the second method is aimed at improving the RoCoF and the frequency nadir. The amount of kinetic energy used for frequency support was considered and the minimum wind turbine rotor speeds at various wind conditions were defined to avoid a substantial reduction in mechanical power while the wind turbine is supporting the grid frequency. The proposed solutions were validated by simulations using MATLAB/Simulink and indicate that the proposed solutions can reduce the RoCoF and frequency nadir while minimising the power imbalance then the rotor is reaccelerated. Given that wind turbines can regulate their power quicker than conventional generators and only have a limited and temporary kinetic energy reserve that can be used to support the grid frequency that has to return to the wind turbine system after frequency control,

it might be beneficial to use wind turbines to improve the RoCoF while conventional generators are used to reduce the frequency nadir.

A power reference model that operates reliably during uncertain wind conditions while providing grid frequency support is proposed in (Kheshti et al., 2019). The proposed frequency support scheme provides an emulated inertial response to a disturbance by releasing a portion of the rotor's available kinetic energy and decreases linearly with rotor speed. To determine the effectiveness of the proposed scheme, the proposed scheme was studied – along with other methods – on large-scale integrated wind farms on IEEE 9-bus and New England 39-bus systems simulated DIgSILENT Power Factory and MATLAB.

In (Wang & Tomsovic, 2019), a dynamic demand control strategy that co-ordinates with the DFIG control is presented. This co-ordinated control strategy for DFIGs can provide an inertial response and primary frequency support. In addition, it can mitigate the secondary frequency dip following frequency support and improve the performance of the primary frequency support. For the demand control to work optimally, controllable loads with high power ratings that can accept a changing connection state and that will have minimal user impact are suggested. The proposed control strategy was simulated in MATLAB/Simulink while the DFIG unit model and aggregated controllable load model was developed in OpenModelica and linked to ePHASORsim, a real-time power system transient simulation software.

To improve the frequency nadir while ensuring a rapid frequency stabilisation for high wind power penetration levels, a temporary frequency support scheme of a DFIG is proposed in (Yang, Kim, et al., 2018). At the onset of a frequency disturbance, the power reference is incremented by the incremental power, which is a value that varies with rotor speed and wind power penetration level and maintained for a pre-set period. The reference will decrease during this deceleration phase with the reduction in speed and release less kinetic energy. This, however, will aid in the rapid recovery of the rotor speed and during the acceleration phase the scheme will decrease the output of the DFIG with both rotor speed and time until the reference intersects the MPPT curve again. The results are obtained by running various scenarios on an IEEE 14-bus system and indicate that the scheme arrest the frequency nadir at a higher level, except for scenario 2. The proposed control scheme was simulated using EMTP-RV.

The paper (De Paola et al., 2016) proposes a method to control variable speed wind turbines to provide a frequency response through temporary over production. The control method aims to determine the optimal power extraction profile between multiple generators to minimize the total loss of efficiency while allowing for an increase in generation. In case of frequency events, the cumulative generation is increased by a specified amount, while the power profile of individual turbines is determined by resolving an optimal control problem to minimise the loss of efficiency. The results of this method were evaluated through simulations and the concept

was also extended to recover the VSWTs to their initial state of maximum efficiency in minimum time.

In (Yang, Kang, et al., 2018), a stable stepwise short-term frequency support scheme based on a DFIG wind farm is proposed and aims to improve the frequency nadir while quickly recovering the rotor speed. When a frequency event occurs, the output power is raised by increasing the power reference prior to the event and sustaining it for some predetermined period determined by the frequency nadir. The power reference then linearly decreases with the rotor speed until it converges with rotor speed to some pre-set value. To then recovery the rotor speed, at the pre-set rotor speed, the power reference decreases with the rotor speed and time until it intersects with the MPPT reference. The proposed scheme was deployed on an IEEE 14-bus system with one DFIG-based wind farm and simulated on EMTP-RV. The simulation results of the four case studies showed that the proposed stepwise short-term frequency support scheme can raise the frequency nadir while recovering the rotor quicker than other conventional schemes in the case studies.

A summary of the papers classified as Emulated Inertial Control, grouped by research area is shown in Table 2.5.

Table 2.5: Publications in emulated inertial control for VSWTs

Research Area	Reference	Year of Publication
Droop Control	(Jiang et al., 2022)	2022
	(Chen et al., 2021)	2021
	(Lao et al., 2021)	2021
	(Yang et al., 2022)	2021
	(Mahish & Pradhan, 2020)	2020
	(Zhao et al., 2020)	2020
	(Azizipanah-Abarghooee et al., 2020)	2020
	(Peng et al., 2020)	2020
	(Guo et al., 2020)	2020
	(Garmroodi et al., 2018)	2018
	(Binbing et al., 2020)	2018
	(Adeuyi et al., 2017)	2017
	(Toulabi, Bahrami, et al., 2017)	2017
	(Li, Xu & Wong, 2017)	2017
	(Toulabi, Dobakhshari, et al., 2017)	2017
	(Li, Xu, Ostergaard, et al., 2017)	2017
	(Fang et al., 2018b)	2017
	(Zhang et al., 2017)	2017
	(Ashouri-Zadeh et al., 2016)	2016
	(Zhang et al., 2016)	2016
	(Ghosh et al., 2016)	2016
	(Lee et al., 2016)	2016

Research Area	Reference	Year of Publication
	(Wang et al., 2015)	2015
Hidden Inertia Control	(Xiong et al., 2021)	2021
	(Li & Ye, 2021)	2021
	(Kabsha & Rather, 2020)	2020
	(Zeng et al., 2019)	2019
	(Khajehoddin et al., 2019)	2018
	(Ma et al., 2018)	2018
	(Martinez Sanz et al., 2015)	2015
Fast Power Reserve	(Yang et al., 2020)	2020
	(Kheshti et al., 2019)	2019
	(Wang & Tomsovic, 2019)	2019
	(Yang, Kim, et al., 2018)	2018
	(Xu & Xu, 2017)	2017
	(Yang, Kang, et al., 2018)	2017
	(De Paola et al., 2016)	2016

2.6.2 RQ2: What are the limitations of VSWTs in supporting the grid frequency?

The rate of change of power of wind turbines could limit the effective implementation of frequency support methods. High rate of change of power in wind turbines leads to an increase in maintenance cost. Simply applying a rate limiter to the power function of the wind turbine generator may reduce the efficacy of frequency support strategies. In (Arani & Mohamed, 2016), a small-signal analysis is done to study the effects of frequency regulation methods on the rate of change of power of wind turbines. Both DFIG and PMSG wind turbine generators are considered. A detailed model of a wind turbine generator was developed in the paper. The model considered the double-mass nature of the mechanical system, active damping controller and frequency support mechanisms namely, droop and virtual inertia. The model in the paper allowed for a small-signal analysis of the frequency support dynamics in the wind turbine generator and the characterisation of the associated mechanical stresses imposed on the generator. The paper has shown that droop and virtual inertia frequency support methods subject the mechanical system to high rates of change of torque and power which accelerate the aging process. The paper has investigated the use of the DC-link capacitors to respond to the fast transient portion of the frequency support dynamics while the kinetic energy stored within the rotating mass of the turbine is still used in the slower but high-energy portion of the frequency support. Furthermore, the paper also studies the management of these two sources and verified all analytical results using time-domain simulations using MATLAB/Simulink based on detailed non-linear models.

The paper (Ruttledge & Flynn, 2016), considers the potential issues associated with system-wide integration of emulated inertia technologies and issues associated with implementing large scale frequency support controls, namely the potential delayed frequency recovery and

the variation in the optimal response with different frequency conditions, are identified in this paper. Two differently sized systems with wind integration and emulated inertial repose capabilities that represent simplified dynamic power system models are developed in MATLAB/Simulink to investigate the impact of varying system conditions. The findings of the paper show that there are implications for the development of ancillary services markets and grid code requirements for systems with a high penetration level of non-synchronous generation. The differences between the emulated inertial response from wind power plants and the inertial response from conventional synchronous generator-based plants should be considered if the integrity and stable operation of the grid is to be maintained. System planners and operators should ensure that the way in which energy is delivered and recovered from wind turbines is realised as a function of the system demand, wind penetration level, geographical wind distribution and reserve level. A failure to consider this may lead to an undesirable frequency response from wind generation and impact the grid stability.

In (Wang et al., 2017), the frequency support capabilities of VSWTs are studied. The impact of inertial control is analysed, and it has been determined that at a large scale may lead to a potential delayed grid frequency recovery and a variation in the optimal response under varying system conditions. In addition, the paper states that should inertial control or emulated inertia technology be adopted at scale, further development will be required. Two simplified dynamic power system models, one small and one medium-large sized system, were developed in MATLAB/Simulink with inertial control capabilities to investigate the impact of varying system conditions on the optimal tuning of the inertial control parameters. The results highlight the importance of resource tuning and issues relating to what is defined as an optimal response while implementation approaches for system operators considering the use of inertial control to emulate an inertial response is proposed.

2.7. Discussion and Future Work

With the relevance of VSWTs for frequency support owing to the increase in wind power penetration and concerns about the frequency of the grid (Fernández-Bustamante et al., 2021), research in this field can make a profound impact addressing practical concerns. The categories of VSWT frequency support are based on the prevailing methods used since each method has advantages and practical limitations.

The period of literature surveyed, showed a marked increase in publications from 2017 to 2019 followed by a period of consistent publications except for the current year seen in Figure 2.2, likely due to the time of conducting this study. The absence of an exponential growth but instead consistent rate of publication could be attributed to the well understood problem of increasing wind power penetration and grid frequency stability without ancillary support from

WTGs. Recent literature surveyed revealed that the focus is in improving the frequency support characteristics of VSWTs by modifying already understood frequency support methods, combining methods, or proposing novel methods.

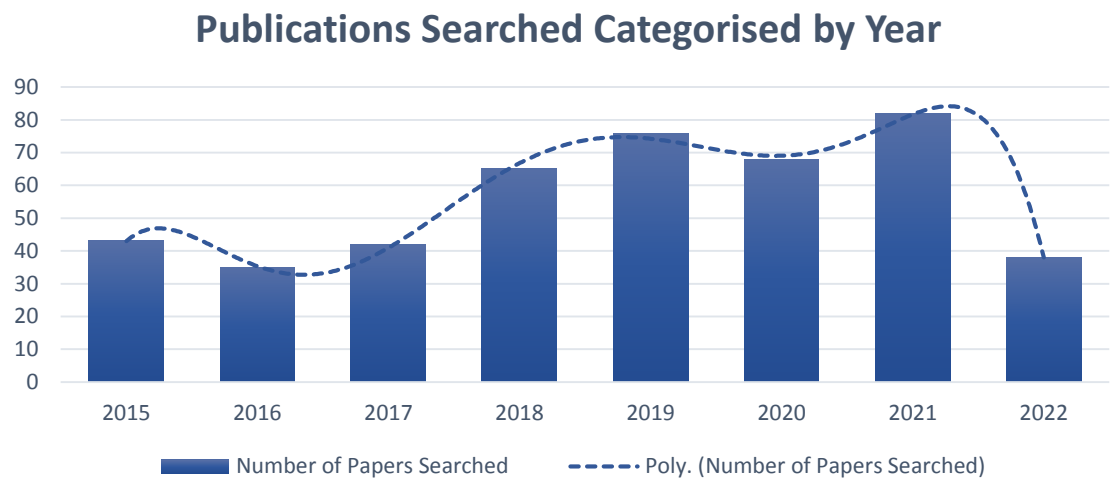

Figure 2.2: Cumulative Publications returned by search strings

Figure 2.3 shows a graph of the number of journal articles admitted to this study, based on the inclusion and exclusion criteria, grouped by the year of publication. From this graph, it can be noted that there is a persistent interest in this field with a peak in publications in 2017 and a reduction in publications in 2019 but recovering in 2020. 2022 is excluded from comment as this is present year, and some journals may not have published papers at the time of conducting this study. This indicates a consistent interest in this research area. This may be attributed to the periodic publishing of journals and the extensive review process resulting in a more even distribution of published papers. Nevertheless, this does indicate relevance in this area of study. Furthermore, the trend of the graph in Figure 2.3, likely deviates from the general trend Figure 2.2, due to the exclusion of conference papers and not necessarily a decline in interest in this research area.

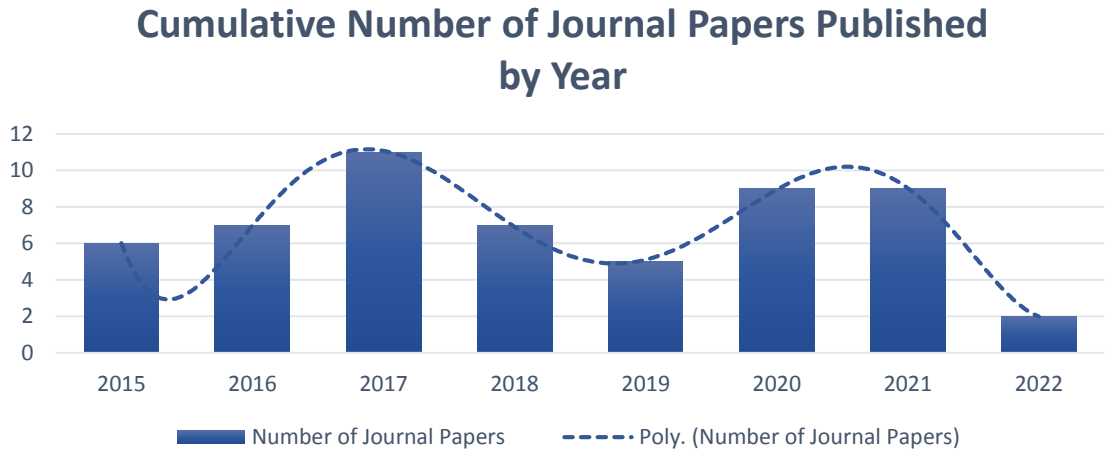

Figure 2.3: Cumulative number of journal papers grouped by year of publication

Of the journal papers studied in this systematic literature review, 11 papers were classified as those that used de-loading as a primary means of providing frequency support, 9 relied on ESS and 45 implemented an emulated inertial response. The research area that gained the most focus identified in this review, is droop control based with 23 journal publications. MATLAB/Simulink was identified as the most prevalent simulation environment used in the literature that was surveyed, with a total of 25 Papers stating the use of MATLAB/Simulink as the simulation environment. A graph of journal papers grouped by simulation environment is shown in Figure 2.4.

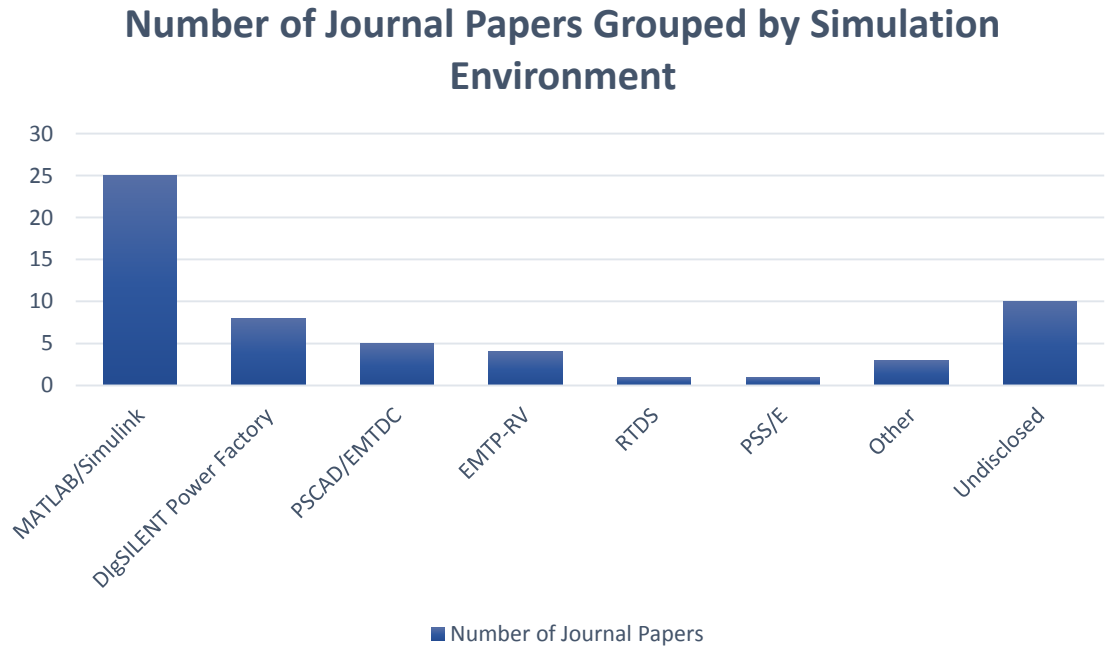

Figure 2.4: Number of journal papers grouped by simulation environment

When screening literature, it was observed that a limited number literature identified and studied the limitations of VSWTs providing grid frequency support. Since the impact of low inertia has been studied, this area of research will continue to be relevant as the prevalence of WTGs increase. However, better understanding the impacts of VSWTs providing grid frequency support on the VSWT structure and the small signal stability of the grid would greatly benefit this field of research.

2.8. Conclusion

VSWT for grid frequency support is research area that can provide solutions to grids with high wind power penetration in a world where grids seek to decarbonise their generating fleet. The main objective of this research is to present relevant information in a modern timeframe on the current implementations and limitations for VSWTs to provide grid frequency support to provide the reader with a comprehensive view on the topic. The study was conducted using the Systematic Literature Review methodology that facilitated the systematic process of searching, locating, assessing, analysing, and categorising existing papers in literature. An extensive review was conducted from various databases from 2015 to mid-2022. From the results, it is seen that there is a consistent interest in the research in present time.

The main limitation of this work is that number of papers selected for the study, and that it did not expand to include the other aspects of VSWT providing grid frequency support such as the economic and mechanical aspects. This will be looked at in future works.

CHAPTER 3: Mathematical Modelling

3.1. Introduction

A prevailing number of megawatt-class WTGs commissioned in the generation of electricity are Variable Speed Wind Turbine (VSWT) generators that allow some speed variation during operation (Walling et al., 2012). Grid connected VSWT generators use power electronic converters to interface with the grid and this allows for a greater deal of control over VSWT generators as opposed to Fixed Speed Wind Turbine (FSWT) generators (Kim et al., 2013). The industry has standardised on its classification of WTGs into types according to the technology used (Walling et al., 2012). This has been summarized in Table 3.1 below (although Type 1 and Type 2 WTGs are not VSWTs, they have been included for completeness):

Table 3.1: Summary of wind turbine generator types (Walling et al., 2012)

Type	Description	Typology
1	Fixed speed wind turbines that use induction generators	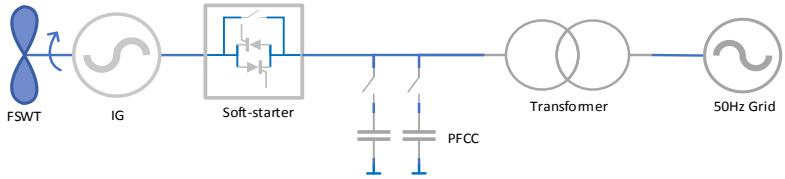
2	Fixed speed wind turbines that use induction generators with provision to dynamically adjust the rotor resistance	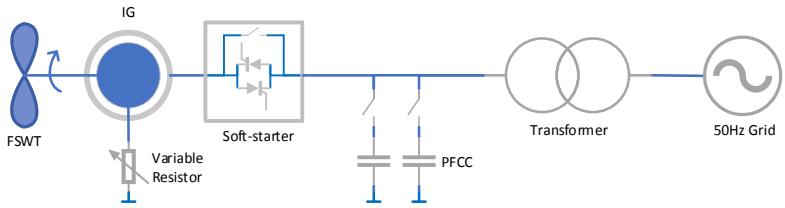
3	Variable speed wind turbines that are normally Doubly-Fed Induction Generators and use partially rated power electronic converters	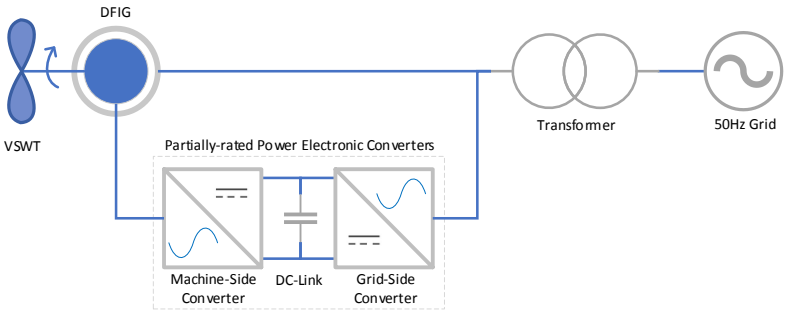
4	Variable speed wind turbines that use fully rated power electronic converters.	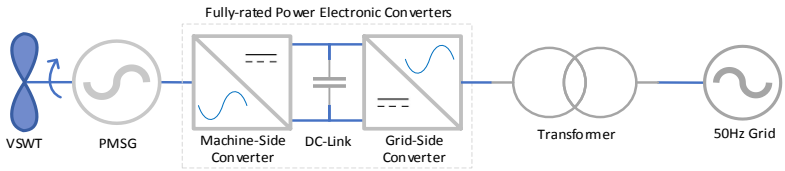

3.2. The Variable Speed Wind Turbine

3.2.1 Aerodynamic Model

The power that can be extracted from the wind, P_m, is found to be that is half the air density multiplied by the cube of wind velocity (Huleihil & Mazor, 2012) and can be expressed by Equation **(3.1)** where: ρ is the density of air; r the radius of the wind turbine; C_p the wind turbine power coefficient; v_{wind} the wind speed; λ the tip speed ratio and β the pitch angle.

$$P_m = \frac{1}{2}\rho\pi r^2 v_{wind}^3 C_p(\lambda, \beta) \tag{3.1}$$

The wind turbine power coefficient, C_P, has a maximum theoretical limit of 59.3% called the Betz limit (Khurshid et al., 2022). The wind turbine power coefficient, shows the effect of the rotor speed and pitch angle variation on the aerodynamic power (Yang et al., 2022), is a nonlinear function of tip-speed ration, λ, and pitch angle, β, is expressed by Equation **(3.2)** (Yang et al., 2020).

$$C_p(\boldsymbol{\lambda}, \beta) = C_1\left(C_2\lambda + \frac{C_3 - C_4(2.5+\beta) + C_5\lambda_i}{e^{C_6\lambda_i}}\right) \tag{3.2}$$

The coefficients of C_1 through to C_8 are listed below:

$C_1 = 0.645$

$C_2 = 0.00912$

$C_3 = -5$

$C_4 = 0.4$

$C_5 = 116$

$C_6 = 21$

$C_7 = 0.08$

$C_8 = 0.035$

With λ_i given by Equation **(3.3)** (Yang et al., 2020).

$$\lambda_i = \frac{1}{\lambda + C_7(2.5+\beta)} - \frac{C_8}{1 + (2.5+\beta)^3} \tag{3.3}$$

The Tip Speed ratio, λ, can be calculated by Equation **(3.4)** (Yang et al., 2020) where ω_r is the angular velocity of the wind turbine rotor:

$$\lambda = \frac{\omega_r r}{v_{wind}} \tag{3.4}$$

The maximum power of a given wind turbine occurs at the maximum performance coefficient of the turbine and for a given wind speed there is an optimum rotor speed which gives the optimum tip speed ratio that yield the maximum power from the rotor (Bubshait et al., 2017). VSWTs are able, and often do, implement an MPPT algorithm to extract the maximum amount of energy from the wind (Kim et al., 2013). The aim of the MPPT algorithm is to adjust the angular velocity of the rotor to an optimum speed for the current wind speed to attain the maximum active power output (Kim et al., 2013). The power reference for the MPPT is given by Equation **(3.5)**.

$$P_{MPPT} = \frac{1}{2}\rho\pi r^2 \left(\frac{\omega_r r}{\lambda_{opt}}\right)^3 C_{p,max} \tag{3.5}$$

The value of λ is defined as the optimal value, λ_{opt} when a maximum value of C_P, $C_{P,\,max}$ is attained when β = 0. Equation **(3.5)** can be rewritten such that the turbine and drive train attributes like blade length, blade profile and gear ratio can be represented by a constant k_g and given by Equation **(3.6)** (Yang et al., 2020).

$$P_{MPPT} = k_g {\omega_r}^3 \tag{3.6}$$

3.2.2 Drivetrain Model

The dynamics between the wind turbine and induction generator is represented by a two-mass shaft model. The two-mass shaft mechanical system is shown in Figure 3.1 (Boukhezzar & Siguerdidjane, 2011).

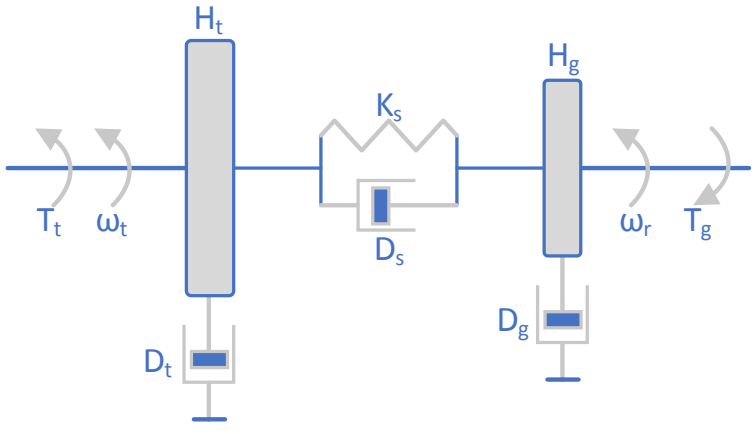

Figure 3.1: Two-mass Shaft Model (Boukhezzar & Siguerdidjane, 2011)

The two-mass shaft model shown in Figure 3.1 is characterised by Equations (3.7) to (3.9) (Yang et al., 2020).

$$2H_t \frac{d\omega_t}{dt} = T_t - K_s\theta_s - D_s(\omega_s - \omega_r) - D_t\omega_t \tag{3.7}$$

$$2H_g \frac{d\omega_r}{dt} = K_s\theta_s - D_s(\omega_t - \omega_r) - D_g\omega_r - T_g \tag{3.8}$$

$$\frac{d\theta_s}{dt} = \omega(\omega_t - \omega_r) \tag{3.9}$$

Where the inertia time constants of the wind turbine are given by H_t and generator by H_g; the angular speeds of the wind turbine and generator are given by ω_t and ω_r, respectively; the torque of the wind turbine is given by T_t and the torque of the generator is given by T_g. The damping constants of the wind turbine and generator are given by D_t and D_g respectively. Lastly, the shaft stiffness, damping constant and torsional twist are each given by K_s, D_s and θ_s, respectively.

3.2.3 Pitch Control Model

The pitch control is used to control the speed and the output power of the wind turbine by adjusting the pitch angle (Chang et al., 2010). When the generator rotor speed, ω_r, exceeds its reference speed, ω_{ref}, the pitch angle is controlled to track the rotor reference speed so that the wind turbine power coefficient, C_p, is equal to its maximum value (Chang et al., 2010). Additionally, the pitch angle is increased to limit the generator output power, P_{DFIG}, to its nominal value, P_{ref}, when the wind speed exceeds its rated value (Chang et al., 2010). The pitch control system is shown in Figure 3.2 (Chang et al., 2010).

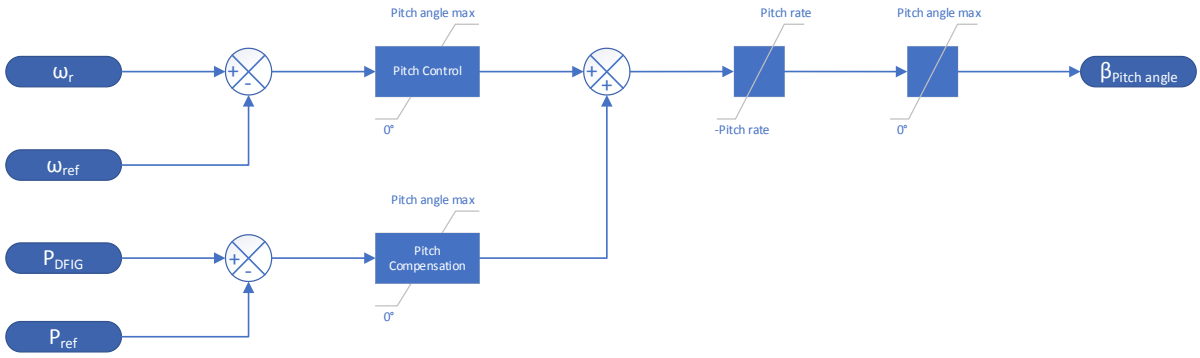

Figure 3.2: Pitch Control System (Chang et al., 2010)

The reference rotor speed, ω_{ref}, is 1.2 pu (with the synchronous rotational speed as the base value) while the output power of the wind turbine is not less than 0.75 pu (with a base value of the rated mechanical power of the wind turbine) (Chang et al., 2010). While the output power of the wind turbine is less than 0.75 pu, then the reference rotor speed, ω_{ref}, can be calculated by Equation (3.10) (Chang et al., 2010). However, the rotor reference speed, ω_{ref}, has a minimum value of 0.7 pu.

$$\omega_{ref} = -0.67(P_{DFIG})^2 + 1.42(P_{DFIG}) + 0.51 \tag{3.10}$$

3.2.4 Induction Machine Model

The doubly-fed induction generator (DFIG) is an asynchronous wind turbine generator, also known as a Type 3 WTG, where the rotor is connected via sliprings to a three-phase inverter and stator is connected directly to the grid via a transformer (Fletcher & Yang, 2010). The term 'doubly-fed' is attributed to the fact that both the rotor and stator are connected to electrical sources (Fletcher & Yang, 2010).

To assist in the analysis, modelling and control of electrical machines, transformations between abc and $dq0$ reference frames are used (O'Rourke et al., 2019). A set of $dq0$ axes rotating at a particular speed ω, is referred to as a reference frame. Park's transformation matrix can be applied to convert the abc quantities to $dq0$ (O'Rourke et al., 2019). Reference-frames using a different speed ω for the rotating $dq0$ axes, and not that of the rotor speed, can still be described by Park's transformation matrix (O'Rourke et al., 2019). The transformation matrix from abc to $dq0$ reference frame is given in Equation (3.11) (Opal-RT Technologies, 2018).

$$\begin{bmatrix} d \\ q \\ 0 \end{bmatrix} = \frac{2}{3} \begin{bmatrix} \cos(\omega t) & \cos\left(\omega t - \frac{2\pi}{3}\right) & \cos\left(\omega t + \frac{2\pi}{3}\right) \\ \sin(\omega t) & \sin\left(\omega t - \frac{2\pi}{3}\right) & \sin\left(\omega t + \frac{2\pi}{3}\right) \\ 0.5 & 0.5 & 0.5 \end{bmatrix} \cdot \begin{bmatrix} a \\ b \\ c \end{bmatrix} \tag{3.11}$$

The d-q axis stator and rotor voltage equations of an induction generator in the synchronous reference frame is expressed by Equations (3.12) and (3.13) for the d-axis and q-axis stator voltage, respectively and Equations (3.14) and (3.15) for the d-axis and q-axis rotor voltage respectively (Yang et al., 2020).

$$v_{ds} = r_s i_{ds} + \frac{d\psi_{ds}}{dt} - \omega_s \psi_{qs} \tag{3.12}$$

$$v_{qs} = r_s i_{qs} + \frac{d\psi_{qs}}{dt} + \omega_s \psi_{ds} \tag{3.13}$$

$$v_{dr} = r_r i_{dr} + \frac{d\psi_{dr}}{dt} - s\omega_s \psi_{qr} \tag{3.14}$$

$$v_{qr} = r_r i_{qr} + \frac{d\psi_{qr}}{dt} + s\omega_s \psi_{dr} \tag{3.15}$$

Where v_{ds} and v_{qs} are the d-axis and q-axis stator voltages respectively; v_{dr} and v_{qr} are the d-axis and q-axis rotor voltages respectively; i_{ds} and i_{qs} are the stator currents in the d-axis and q-axis, respectively and i_{dr} and i_{qr} are the rotor currents in the d-axis and q-axis, respectively. The stator flux linkages in the d-axis and q-axis are ψ_{ds} and ψ_{qs}, respectively; the rotor flux linkages in the d-axis and q-axis are ψ_{dr} and ψ_{qr}, respectively. The stator and rotor resistances are r_s and r_r, respectively.

The d-q axis flux linkages for the stator and rotor windings can be written as Equations (3.16) and (3.17) for the d-axis and q-axis stator flux linkages, respectively and Equations (3.18) and (3.19) for the d-axis and q-axis rotor flux linkages respectively (Yang et al., 2020).

$$\psi_{ds} = l_s i_{ds} + l_m i_{dr} \tag{3.16}$$

$$\psi_{qs} = l_s i_{qs} + l_m i_{qr} \tag{3.17}$$

$$\psi_{dr} = l_r i_{dr} + l_m i_{ds} \tag{3.18}$$

$$\psi_{qr} = l_r i_{qr} + l_m i_{qs} \tag{3.19}$$

The stator, rotor and magnetizing inductances are represented by l_s, l_r, and l_m, respectively.

3.2.5 DFIG Power Flow Model

Figure 3.3 shows a generic circuit of a DFIG and the inclusion of the back-to-back power convertors that form part of the rotor circuit (Fletcher & Yang, 2010) and a control system block. The power electronic converters in the rotor circuit are typically referred to as partially-rated – normally at 30% of the nominal generator power – as they only need to handle the rotor power and not that of the entire machine, like fully rated converters found in Type 4 WTGs (Fletcher & Yang, 2010). Due to this attribute [of partially rated converters] the system cost and losses of the power electronics is lower (Fletcher & Yang, 2010).

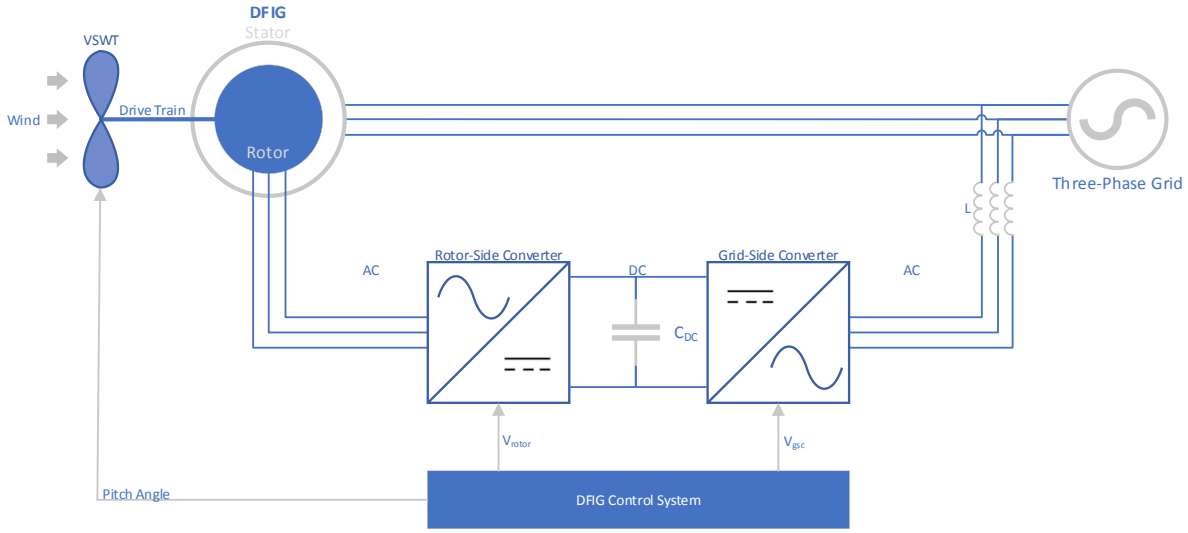

Figure 3.3: Generic Topology of a Type 3 WTG (DFIG) (The MathWorks Inc, 2019)

The back-to-back converter topology in the rotor circuit provides a means to convert the variable voltage and frequency (wild AC) of the VSWT into a fixed voltage and frequency output that may interface with the grid. In this back-to-back topology the Rotor-Side Converter (RSC) can control the 3-Phase AC excitation of the machine so that it may interface with the grid. This 3-Phase AC excitation causes an apparent rotation of the rotor's magnetic field relative to the rotor (Walling et al., 2012). When the excitation is applied in a positive phase sequence the apparent rotation of the rotor's field is in the same direction as the rotor. Conversely, if the excitation current is supplied with a negative phase sequence, then the apparent rotation of the rotor's field will rotate against the direction of the rotor (Walling et al., 2012). Looking at the rotor from a stationary reference point, the rotor's magnetic field rotates at the speed which is the sum of the rotor's mechanical speed plus the apparent rotational speed due to the applied AC excitation (Walling et al., 2012). This is described by Equation (3.20).

$$f_{grid} = f_{mechanical} \pm f_{excitation} \tag{3.20}$$

The Grid-Side Converter (GSC) aims to maintain a constant DC-link voltage regardless of the magnitude and direction of the rotor power. The direction of the flow of real power dependents on if the DFIG is operating above or below synchronous speed. Above synchronous speed, power is generated in both rotor and stator and will flow out of the rotor through the back-to-back converter and add to that of the stator (Walling et al., 2012). It follows that operation below synchronous speed will cause real power to flow into the rotor while at synchronous speed the excitation will be DC and the only power consumed is because of the ohmic losses in the winding resistance of the rotor (Walling et al., 2012). The operating principle of the DFIG wind turbine is shown by the power flow diagram in Figure 3.4.

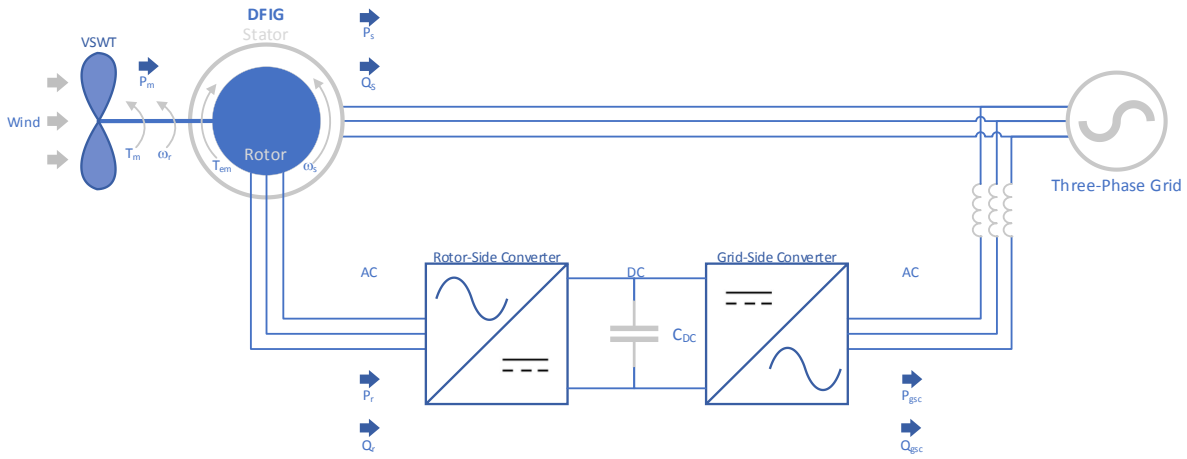

Figure 3.4: DFIG Power Flow Diagram (The MathWorks Inc, 2019)

The mechanical power and the electrical output power of the stator is computed by Equation (3.21) (The MathWorks Inc, 2019), where: P_m is the power transmitted to the rotor that has been captured by the wind turbine, ω_r is the rotational speed of the rotor and P_s is the electrical output power of the stator (The MathWorks Inc, 2019).

$$P_m = T_m \omega_r P_s \tag{3.21}$$

From Equation (3.21), it follows that the mechanical power transmitted to the rotor, P_m, can be expressed in terms of the electromagnetic torque applied to the rotor by the generator, T_{em}, and the rotational speed of the magnetic flux in the air-gap of the generator, known as the synchronous speed of the generator, ω_s (The MathWorks Inc, 2019). This expression is shown in Equation (3.22) (The MathWorks Inc, 2019).

$$P_m = T_{em} \omega_s \tag{3.22}$$

For a lossless generator, the mechanical equation which describes the dynamic behaviour of the rotor mechanical speed in terms of the mechanical torque, T_m, and the electromagnetic torque, T_{em}, is given by (3.23) (The MathWorks Inc, 2019).

$$J \frac{d\omega_r}{dt} = T_m - T_{em} \tag{3.23}$$

At a fixed speed for a lossless generator during steady state it follows that the mechanical torque applied to the rotor, T_m, is equal to the electromagnetic torque, T_{em} (3.24) and that the mechanical power transmitted to the rotor, P_m, is equal to the sum of the electrical output power of the stator, P_s, and the rotor, P_r (3.25) (The MathWorks Inc, 2019).

$$T_m = T_{em} \tag{3.24}$$

$$P_m = P_s + P_r \tag{3.25}$$

By making P_r the subject of the formula, the electrical output of the rotor can be expressed in Equation (3.26) as:

$$P_r = P_m - P_s \tag{3.26}$$

It follows that:

$$P_r = T_m \omega_r - T_{em} \omega_s \tag{3.27}$$

$$P_r = -T_m \frac{\omega_s - \omega_r}{\omega_s} \omega_s \tag{3.28}$$

The slip of the generator, s, is defined by Equation (3.29) (The MathWorks Inc, 2019).

$$s = \frac{\omega_s - \omega_r}{\omega_s} \tag{3.29}$$

It follows from Equation (3.29) (The MathWorks Inc, 2019), that Equation (3.28) (The MathWorks Inc, 2019) can be expressed as:

$$P_r = -sT_m \omega_s \tag{3.30}$$

$$P_r = -sP_s \tag{3.31}$$

The value of the generator slip, s, is substantially lower than 1 and as a result P_r is only fraction of P_s (The MathWorks Inc, 2019). The sign of P_r is a function of the slip sign, s, since T_m is positive for power generation and ω_s is positive and constant for a constant frequency grid voltage (The MathWorks Inc, 2019). At sub-synchronous speed, a positive phase-sequence AC voltage, with a frequency proportional to the product of the grid frequency and slip, is generated by the rotor-side converter (The MathWorks Inc, 2019). At sub-synchronous speed, P_r is negative for positive slip and power to the rotor, P_r, is absorbed from the DC link capacitor and tends to decrease the DC voltage (The MathWorks Inc, 2019). Conversely, at super-synchronous speed a negative phase-sequence AC voltage, with a frequency proportional to the product of the grid frequency and slip, is generated by the rotor-side converter (The MathWorks Inc, 2019). Furthermore, at super-synchronous speed, P_r, is positive for negative slip and power from the rotor, P_r, is transmitted to the DC link capacitor and tends to raise the DC voltage (The MathWorks Inc, 2019)**.** The grid-side converter can both generate or absorb power, P_{gsc} , to maintain a constant DC voltage (The MathWorks Inc, 2019).

3.2.6 Power Electronics Model

Centred around the range of frequencies to be represented, there are three simulation methods that are currently available in Simulink's Specialised Power Systems to model the voltage-sourced converter (VSC) based energy conversion systems of the DFIG that is connected to the grid (The MathWorks Inc, 2022i). Namely, the detailed model, the average model, and the phasor model. The differences of each model and the intended use are explained below.

The detailed model includes a detailed representation of the power electronic IGBT converters to achieve an acceptable accuracy with the switching frequencies used and is well suited for observing harmonics and studying the control system dynamic performance over relatively short periods time, ranging from hundreds of milliseconds to one second (The MathWorks Inc, 2022i).

Unlike the detailed model which includes a detailed representation of the power electronic IGBT converters, the average model represents the IGBT converters by equivalent voltage sources generating the AC voltage averaged over one cycle of the switching frequency (The MathWorks Inc, 2022i). This model is suited for observing control system and power system interaction but does not represent harmonics (The MathWorks Inc, 2022i). The use of this model allows for larger time steps, typically 50 µs, and simulations of several seconds (The MathWorks Inc, 2022i).

Lastly, the phasor model is best suited to simulate the low frequency electromechanical oscillations over longer periods of time ranging from tens of seconds to minutes (The MathWorks Inc, 2022i). The sinusoidal voltages and currents are replaced by their phasor quantities at the nominal system frequency in the phasor simulation method (The MathWorks Inc, 2022i).

This study will be using the average model since as the focus of this study is the interaction between the DFIG control system and the power system. The equivalent controlled ac voltage sources that represent the output line-to-line voltages of the RSC and GSC respectively, are shown in Figure 3.5 (Chang et al., 2010). The RSC is represented by V_{ab_RSC} and V_{bc_RSC} while V_{ab_GSC} and V_{bc_GSC} represent the GSC.

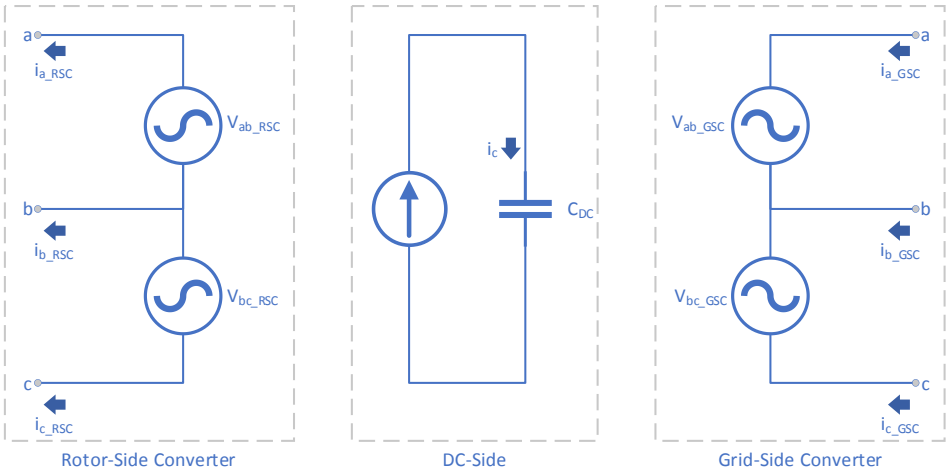

Figure 3.5: Average model power electronic converters (Chang et al., 2010)

3.2.7 Rotor-Side Converter Control Model

The RSC control system is shown in Figure 3.6 and consists of a stator flux estimator, a speed regulator, torque controller, reactive power regulator and current regulator. The RSC can control the active and reactive power of the DFIG by regulating the *dq* components of the rotor voltage and current (Ontiveros et al., 2011). In this instance, the d-axis current component affects the torque and subsequently the active power, while the q-axis current component sets the reactive power flow of the DFIG (Ontiveros et al., 2011).

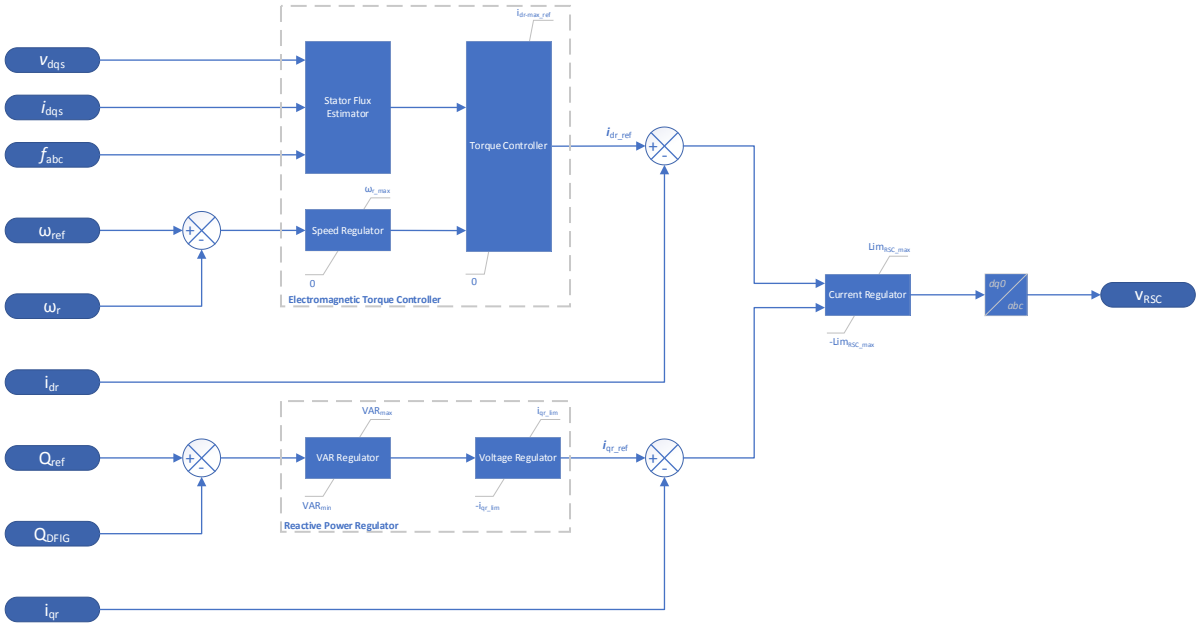

Figure 3.6: Rotor-Side Converter Control System

The Electromagnetic Torque Controller comprises of the stator flux estimator, speed regulator and torque controller. The Stator Flux Estimator estimates the magnetic flux of the stator by

using the frequency, dq-axis voltage and current of the stator as inputs. The output of the Stator Flux Estimator is passed to the Torque Controller. The error between the rotor reference speed, ω_{ref} and the rotor speed ω_r, is passed to the Speed Regulator which consists of a Proportional-Integral (PI) type controller. The output of the Speed Regulator is also passed to the Torque Controller and the output of the Torque Controller is the d-axis reference current, i_{dr_ref}.

The Reactive Power Regulator, which comprises of the VAR and Voltage regulators, keeps the reactive power at the grid terminals constant. The reference reactive power, Q_{ref}, is compared to the actual reactive power measured at the grid terminals, Q_{DFIG}, and passed to the VAR Regulator which consists of an integrator element. The output of the VAR Regulator is the reference voltage for the Voltage Regulator and the output of the of the Voltage Regulator is the q-axis current reference, i_{qr_ref}.

The d-axis rotor current, i_{dr}, is compared to the reference rotor current, i_{dr_ref}, from the Electromagnetic Torque Controller and error is passed to the Current Regulator. Similarly, the q-axis rotor current, i_{qr} is compared to the reference rotor current, i_{qr_ref}, from the Reactive Power Regulator and the error is also passed to the Current Regulator. The error is reduced by the Current Regulator which is a PI controller. The Current Regulator assisted by the feedforward terms given in Equations (3.32) and (3.33).

$$v_{dRSC\_ff} = R_r i_{dr} - s\omega_s L_m i_{qs} - s\omega_s (L_r + L_m) i_{qr} \tag{3.32}$$

$$v_{qRSC\_ff} = R_r i_{qr} + s\omega_s L_m i_{ds} + s\omega_s (L_r + L_m) i_{dr} \tag{3.33}$$

The output of the Current Regulator is the *dq* components of the rotor-side converter, $V_{RSC\text{-}dq}$. This is transformed back to the *abc* reference frame to produce the output voltage control signal of the grid-side converter, V_{RSC}.

3.2.8 Grid-Side Converter Control Model

The grid-side converter regulates the voltage of the DC bus capacitor and can be used to control the amount of reactive power that is either generated or absorbed (Chang et al., 2010). The grid-side converter control system is shown in Figure 3.7 and comprises of a DC link voltage regulator, and a current regulator.

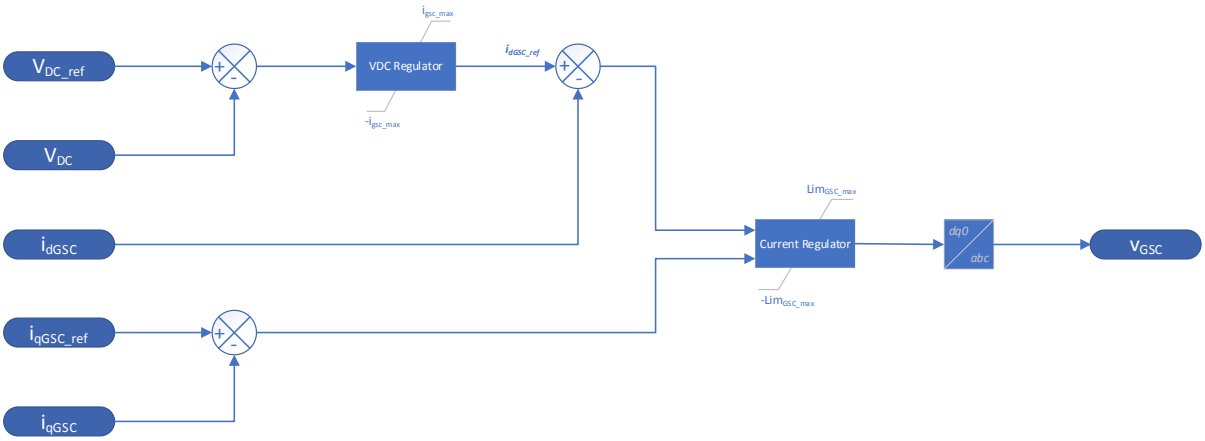

Figure 3.7: Grid-Side Converter Control System

The error between the reference DC-side voltage, V_{DC_ref} and the measured DC-side voltage, V_{DC} is passed to the VDC Regulator which consists of a PI controller. The output of the PI controller is the d-axis reference current i_{dGSC_ref}. The reactive current reference, i_{qGSC_ref}, is set to zero as the grid-side converter in this study operates at unity power factor.

The magnitude and phase of the voltage generated by the grid-side converter is controlled by the current regulator. The current regulator assisted by feedforward terms given in Equations (3.34) and (3.35), where L_{ci} and R_{ci} are the inductance and resistance, respectively of the grid-side converter coupling inductance (Chang et al., 2010).

$$v_{dGSC\_ff} = v_{ds} - R_{ci}i_{dGSC\_ref} + \omega_s L_{ci} i_{qGSC\_ref} \tag{3.34}$$

$$v_{qGSC\_ff} = v_{qs} - R_{ci}i_{qGSC_{ref}} - \omega_s L_{ci} i_{dGSC\_ref} \tag{3.35}$$

The output of the Current Regulator is the *dq* components of the grid-side converter, $V_{GSC\text{-}dq}$. This is transformed back to the *abc* reference frame to produce the output voltage control signal of the grid-side converter, V_{GSC}.

3.2.9 Frequency Support Model

The rotor-side converter will follow a MPPT algorithm to extract the maximum power from the WTG (Bubshait et al., 2017). Supplementary frequency control loops can be added to the existing controller to establish a link between the WTGs output power and the system frequency (Guoyi Xu et al., 2016). Such a controller that couples the WTG output power and the system frequency is shown in Figure 3.8 (Yang et al., 2022).

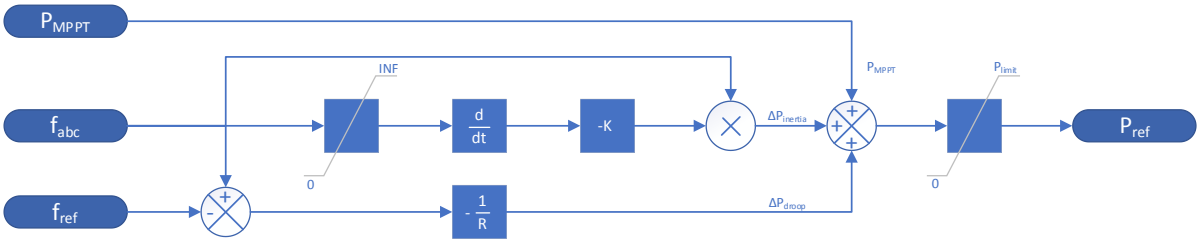

Figure 3.8: Frequency Support Control System Overview (Yang et al., 2022)

The frequency support controller, shown in Figure 3.8 (Yang et al., 2022), uses the kinetic energy of a DFIG VSWT to provide temporary frequency support. The controller aims to recover kinetic energy from the VSWT for short term frequency support. During a frequency event, the rotor will decelerate, until it reaches the minimum allowed speed, as the kinetic energy is recovered to support the grid frequency after which it will return to optimal operating speed (Xu et al., 2016). WTGs only have limited and temporary kinetic energy that can be released for frequency support. Kinetic energy used for frequency response control must be restored once used (Boyle et al., 2018).

The frequency support controller in Figure 3.8 (Yang et al., 2022) consists of droop control and an emulated or hidden inertia control. The attributes of the droop control are that its output is small during the initial period of a frequency disturbance and becomes larger with an increase in frequency deviation. The output of the droop control, ΔP_{droop}, is expressed by Equation (3.36) (Yang et al., 2022) where f_{abc} is the measured grid frequency, f_{ref} is the nominal frequency and R is the droop gain.

$$\Delta P_{droop} = -\frac{f_{abc} - f_{ref}}{R} \tag{3.36}$$

The attributes of the emulated inertial response of the DFIG are that the emulated inertial response is dominant during the initial period of a frequency disturbance and continues to become less with an increase in frequency deviation as the frequency nadir is approached and the RoCoF decreases. The output of the emulated inertial response control, $\Delta P_{inertia}$, is expressed by Equation (3.37) (Yang et al., 2022), where K is the gain of the emulated inertia response control.

$$\Delta P_{inertia} = -K \cdot f_{abc} \cdot \frac{df_{abc}}{dt} \tag{3.37}$$

The frequency support model shown in Figure 3.9, adapted from Figure 3.8 (Yang et al., 2022), to emulate an inertial response by injecting additional power during a frequency disturbance by increasing the d-axis rotor reference current. This causes the rotor speed to decrease due to the additional temporary loading due to an increase in the rotor-side converter current

reference. The d-axis rotor reference current term is comprised of the output from the torque regulator, i_{dr_MPPT}, and the sum of the supplementary frequency support controller terms $i_{dr\_inertia}$.

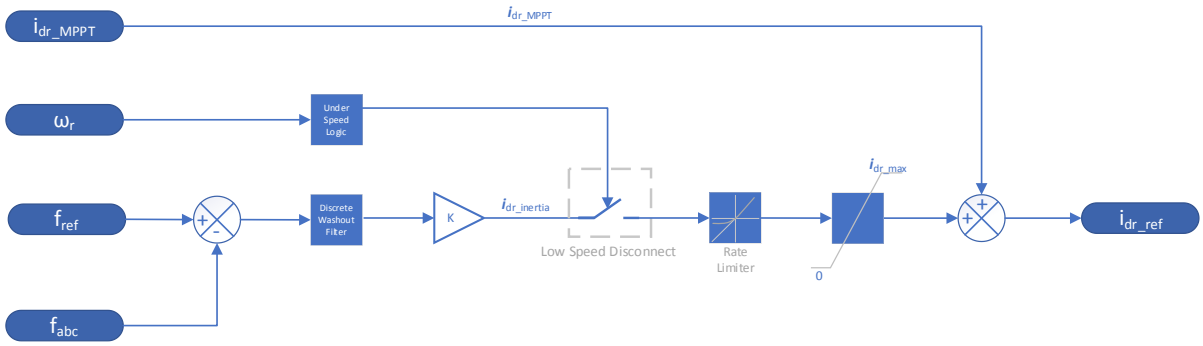

Figure 3.9: Adapted Frequency Support Controller

The error that is produced by the difference between the reference grid frequency, f_{ref}, and the measured grid frequency, f_{abc}, is passed through a washout filter. A washout filter is a high-pass filter that rejects steady state inputs but passes transient inputs (Hassouneh et al., 2004). Subsequently, washout filters facilitate automatic following of a desired setpoint as the output of the washout filter diminishes at steady state (Hassouneh et al., 2004). The washout filter rejects steady state input and prevents the frequency support controller from contributing during normal operation when the grid is at its nominal frequency or once the frequency has stabilised following a frequency disturbance.

The output of the high-pass filter is passed to a gain term, K, to produce an emulated inertial response, $i_{dr\_inertia}$, to changes in grid frequency. It can be shown that a high-pass filter and gain term can produce the equivalent response to explicitly differentiating a signal. To illustrate this, consider a first-order low-pass filter transfer function shown in Equation (3.38).

$$G(s) = \frac{\omega_c}{(s + \omega_c)} \tag{3.38}$$

Recall that that differentiating a signal is equivalent to multiplying it by s in the Laplace domain. Differentiating the signal from the low-pass filter yields Equation (3.39).

$$G(s) = \frac{s\omega_c}{s + \omega_c} \tag{3.39}$$

The transfer function of a high-pass filter is shown in Equation (3.40)

$$G(s) = \frac{s}{s + \omega_c} \tag{3.40}$$

It can then be concluded that taking the derivative of a low-pass filtered signal is comparable to applying a high-pass filter to the input signal and then multiplying it by a gain term that is

equal to the cut-off frequency. The continuous-time system can be transformed to a discrete-time system such that Figure 3.9 is modelled as a time-discrete system. The discrete representation of the washout filter is given by the transfer function of (3.41) (The MathWorks Inc, 2022c), where T is the filter time constant and T_s is the filter sample time.

$$G(z) = \frac{z - 1}{z + \frac{T_s}{T} - 1} \tag{3.41}$$

While providing frequency support, it is possible to stall the DFIG WT or operate it outside its stable operating rage. To prevent this, an under-speed logic is introduced to inhibit the frequency support when the rotor speed is below a minimum threshold. The under-speed logic disconnects the inertial response term. To provide additional context, the frequency support controller integrated to the RSC controller is shown in Figure 3.10.

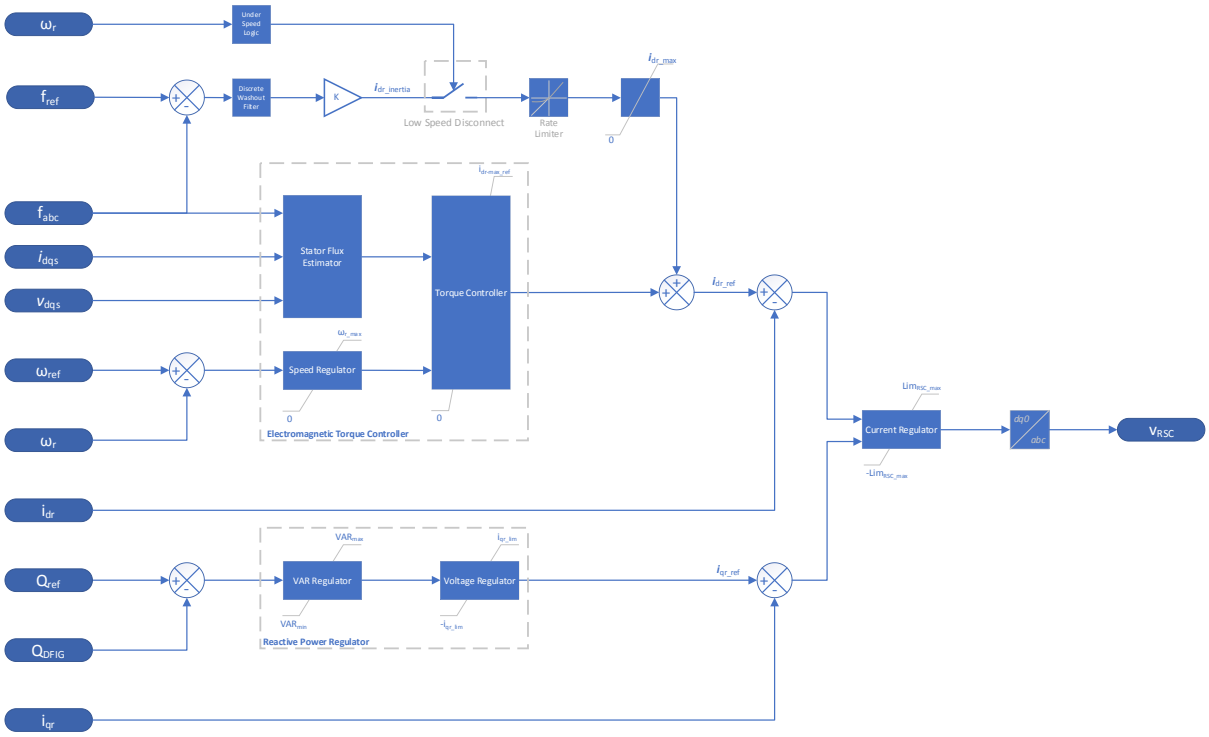

Figure 3.10: Rotor-Side Converter Control with Frequency Support Controller

3.3. Conclusion

The mathematical modelling for a DFIG with a supplementary controller to provide frequency support has been presented in this chapter. To verify the accuracy DFIG model (without the supplementary frequency support control) presented in this chapter, the simulation results of the DFIG under normal operating conditions presented in (Yang et al., 2020) will be compared to the results of the DFIG modelled presented in this chapter.

CHAPTER 4: Simulations and Results

4.1. Introduction

The computer modelling of the model presented in the previous chapter and simulation results is presented in this chapter. The normal operation of the model presented in the previous chapter, without frequency support, is benchmarked against various case studies of the MPPT operation of the DFIG presented in (Yang et al., 2020). The benchmarking is conducted on a representative network of the one presented in (Yang et al., 2020). The simulation results obtained through the benchmarking process are compared and analysed to validate the model presented. Following the validation of the model presented in the previous chapter, a frequency support controller is introduced. The performance of the frequency support method is evaluated as through the same case studies as the benchmark. In the Systematic Literature Review, Chapter 2, MATLAB/Simulink was identified as the most prevalent simulation environment in the literature surveyed. Following on this, MATLAB/Simulink has been chosen to be the simulation environment for this study.

4.2. System Layout

The IEEE 14-bus system represents a simple approximation of the American Electric Power system, in Midwestern US, as of February 1962 (University of Washington, 1993). For reference, the parameters of the IEEE 14-bus system are given in Appendix B. In (Yang et al., 2020), a modified IEEE 14-bus system is used as the test system and is shown in Figure 4.1 (Yang et al., 2020). The modified IEEE 14-bus system presented in (Yang et al., 2020) consists of two voltage zones, connected by T1, T2 and T3. Busses 1 through to 5 form part of the 132 kV zone while busses 6 through to 14 form part of the 33 kV zone. The 14-bus system presented in (Yang et al., 2020) also includes five synchronous generators, 11 static loads, and an aggregated wind farm model.

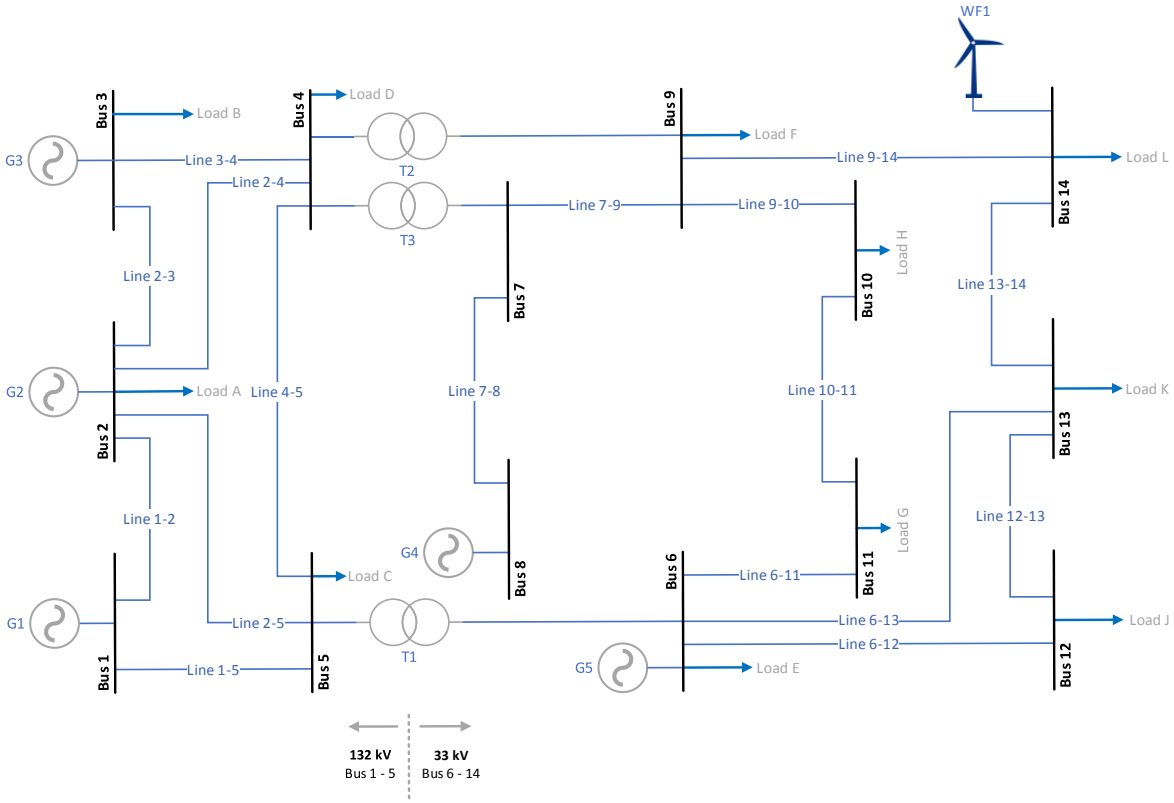

Figure 4.1: Single Line Diagram of a modified IEEE 14-Bus System (Yang et al., 2020)

All synchronous generators in the modified IEEE 14-bus system presented in (Yang et al., 2020) are assumed to be steam turbine synchronous generators. An aggregated windfarm model, WF1, is connected to Bus 14 (Yang et al., 2020). In an aggregated model, the total number of units is an equivalent unit whose rated power is equal to the sum of the rated powers of the individual unit (Saadatmand et al., 2021) and follows that the output power of the wind farm can be expressed by Equation (4.1).

$$\sum_{n=1}^{nWTG} WTG_{Power}\ MW \tag{4.1}$$

Where $nWTG$ is the number of WTGs and WTG_{Power} is the output power of an individual wind turbine.

4.3. Simulations

4.3.1 Simulink Model

The simulation methods and the various major subsystems for the Simulink model are discussed in this section, beginning with the aggregated wind farm subsystem. The aggregated wind farm subsystem consists of 80, 1.5 MW class DFIG WTs. The DFIG subsystem is an

average model type where the power electronic interfaces are replaced with controlled voltage sources. The parameters of an individual WT are shown in Table 4.1. The wind farm connects to the 33 kV voltage zone by a 575 V/33 kV transformer.

Table 4.1: DFIG Parameters

Parameter	Value
Nominal Apparent Power	1.667 MVA
Nominal Active Power	1.5 MW
Stator Resistance, $\boldsymbol{r_s}$	0.023 pu
Stator Leakage Inductance, $\boldsymbol{l_s}$	0.171 pu
Magnetizing Inductance, $\boldsymbol{l_m}$	2.9 pu
Rotor Resistance, $\boldsymbol{r_r}$	0.016 pu
Rotor Leakage Inductance, $\boldsymbol{l_r}$	0.156 pu
Operating Range of ω_r	0.75 – 1.2 pu

Based on the IEEE 14-bus system load parameters shown in Table B.2, the electrical loads on the network are modelled as Wye-Grounded RLC 3-Phase load in Simulink. Since the 3-Phase RLC load accepts active power and reactive power in actual units (watts and volt-ampere reactive respectively), the per-unit values of the IEEE 14-bus system were converted to actual values using a 100 MVA base and placed in their respective voltage zones. The loads on the network are detailed in Table 4.2 and the detailed calculations are shown in Appendix C

Table 4.2: Load Parameters

Parameter	Power (MW)	Reactive Power (MVAR)
Load A	21.7	12.7
Load B	94.2	19
Load C	7.6	1.6
Load D	47.8	0
Load E	11.2	7.5
Load F	29.5	16.6
Load G	3.5	1.8
Load H	9	5.8
Load J	6.1	1.6
Load K	13.5	5.8
Load L	14.9	5

The synchronous generator subsystem is modelled with a steam turbine and governor connected to a synchronous machine. The steam turbine and governor model comprise of a

steam prime mover, including a speed governing system, a four-stage steam turbine and a shaft with up to four masses. The complete steam turbine and governor model is shown in Figure 4.2 (The MathWorks Inc, 2022f).

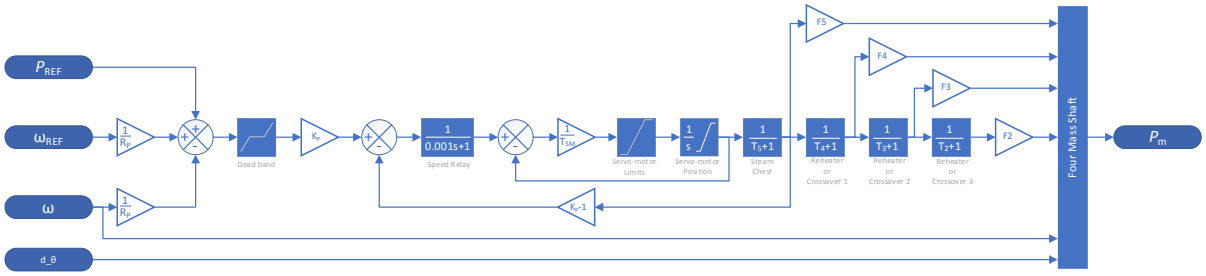

Figure 4.2: Steam Turbine and Governor Model (The MathWorks Inc, 2022f)

The four stages of the steam turbine are each modelled by a first-order transfer function (The MathWorks Inc, 2022f). The first stage represents the steam chest while the remaining three stages represent either reheaters or crossover piping (The MathWorks Inc, 2022f). The boiler is not modelled, instead the boiler pressure is a constant at 1 pu (The MathWorks Inc, 2022f). The four mass shaft system couples to the mass of the synchronous machine for a total of five masses and is characterised by mass inertias H, damping factors D and rigidity coefficients K (The MathWorks Inc, 2022f). The steam turbine and governor model parameters are given in Table 4.3. The output of the Steam Turbine and Governor Model is the mechanical power which is the input to a round rotor synchronous machine.

Table 4.3: Steam Turbine and Governor Parameters

Parameter		Value
Nominal speed of synchronous machine		3000 RPM
Regulator gain, K_p		3
Permanent droop, R_p		0.085 pu
Speed relay, T_{sr}		0.001 s
Servo-motor time constant, T_{sm}		0.15 s
Steam turbine time constants	T_2	14.05 s
	T_3	5.0 s
	T_4	1.0 s
	T_5	0.1 s
Turbine torque fractions	F_2	0.5
	F_3	0.5
	F_4	0
	F_5	0

To solve electrical systems using Simscape Electrical Specialised Power Systems, three simulation methods are available through the Simulink Powergui block (The MathWorks Inc, 2022a). For small sized systems, the continuous method using Simulink variable-step is more normally accurate. For large systems however, such as those with either many states or non-linear blocks, the accuracy of continuous simulation method slows down the simulation (The MathWorks Inc, 2022a). For large systems, it is advantageous to instead discretize the system and use the fixed time step discrete simulation method for improved simulation speed (The MathWorks Inc, 2022a). To further improve simulation speed, the variable-step discrete solver was used. The variable-step discrete solver maintains accuracy by computing the required step size based on model dynamics and the specified level of required accuracy. Despite the increase in computational overhead due to computing the required step size, the potential reduction in the number of steps can reduce the simulation time. However, for real-time simulations, a fixed-step solver should be used as the variable-step size cannot be mapped to a real-time clock (The MathWorks Inc, 2022b). The last simulation method is the phasor method. It is typically used when only the change in magnitude and phase of the voltages and currents of a system are of interest such as studying the electromechanical oscillations resulting from the interaction of the machine inertias and regulators (The MathWorks Inc, 2022a). The phasor simulation drastically reduces the simulation speed as the set of differential equations are replaced by algebraic equations (The MathWorks Inc, 2022a).

The interaction between the electrical system and the control system dynamics are studied over a period of 120 s to 160 s. To improve simulation time while maintaining acceptable accuracy and accounting for the continuous states of various subsystems, the discrete simulation method was used. Electrical systems are discretised using the Tustin/Backward Euler method. This method combines the numerical accuracy of the Tustin method and the numerical oscillation damping characteristics of the Backward-Euler method (The MathWorks Inc, 2022h). The precision of the simulation is controlled by the time step used for discretisation, and normally 20 µs to 50 µs provides good simulation results for switching transients on 50 Hz or 60 Hz power systems (The MathWorks Inc, 2022h).

Discretised electrical machines are non-linear elements that are simulated as current sources (The MathWorks Inc, 2022h). Until MATLAB R2019a electrical machines required a parasitic resistive or capacitive element at the machine terminals when connecting to an inductive network to avoid numerical oscillations (The MathWorks Inc, 2022h). The magnitude of the parasitic load depends on the sample time and integration method used to discretise the model (The MathWorks Inc, 2022h). In MATLAB R2019a two additional methods, the Trapezoidal robust and Backward Euler robust, were introduced as part of a robust solver that allows for more accurate and faster simulation of machines without the need for a parasitic element (The MathWorks Inc, 2022h). In addition, the robust solver can simulate a machine at no load or

with a circuit breaker connected in series (The MathWorks Inc, 2022h). The Trapezoidal robust method is marginally more accurate than the Backward Euler method, especially for larger sample times (The MathWorks Inc, 2022h).

To start the simulation at steady state, the Load Flow Tool was used to initialise the three-phase machines. The Load Flow Tool uses the Newton-Raphson method to provide a robust and quicker convergence solution when compared to the Machine Initialization Tool (The MathWorks Inc, 2022d). It is worth noting however, that in MATLAB R2022b, wound rotor asynchronous machines are not supported in the Load Flow Tool and the Machine Initialisation Tool is no longer supported. As a result, the wound rotor induction generator used in modelling the DFIG aggregated wind farm, could not be initialised using this method. Instead, the simulation is run for an additional 60 s to afford the system sufficient time to be well established before subjecting it to disturbances. The results presented are therefore referenced from when steady state has been detected. An alternative method to start the simulation from steady state based on generating initial conditions by simulating the model until it reaches steady state and storing those values, in conjunction with the initialisation method already employed will be explored in future work.

4.3.2 Results: Benchmarking

The results of three benchmark case studies, as presented in (Yang et al., 2020), are compared to the results of (Yang et al., 2020) to validate the accuracy model developed in this study are presented. The case studies in (Yang et al., 2020), cover a disturbance under two different wind speed conditions and a consecutive disturbance. The MPPT results of (Yang et al., 2020) is compared to the DFIG model presented in this study without the supplementary frequency support controller enabled to establish an accurate baseline.

The data obtained from simulations was processed using a Hampel filter, to preserve the system dynamics which is in the order of seconds and present those dynamics clearly but reject any noise (which could be caused by numerical oscillations) which is in the order of milliseconds to microseconds and is not of interest to this study. The Hampel filter detects and removes outliers and is a variation of the Three-Sigma rule of statistics (The MathWorks Inc, 2022g). For a given sample, a median of a window that is comprised of the sample and its neighbouring samples centred about the sample point is calculated. In addition, the standard deviation of each sample about its window median using the median absolute deviation is estimated (The MathWorks Inc, 2022e). If difference between the sample and the median is greater than three standard deviations, the sample is replaced by the median. With increased window length the Hampel filter is preferred over the median filter (The MathWorks Inc, 2022e). In (The MathWorks Inc, 2022e), it is shown how the Hampel filter removes high-frequency

noise while preserving the shape of a sine wave even with large window lengths. The conditions of each case study and an analysis of the results are discussed under the respective case studies.

4.3.2.1 Case 1: Wind speed condition of 10 m.s^{-1}

The first case study investigates the effect of a generator generating 130 MW tripping at 10 s with wind speed conditions of 10 m.s^{-1}. Figure 4.3 shows the plotted simulation results of the system frequency response of the model in this study. Figure 4.4 shows the system frequency response of the power system in (Yang et al., 2020) to a disturbance with a connected DFIG-based windfarm. When Figure 4.3 is compared to the MPPT trace of Figure 4.4, it can be seen that the model presented in this study has a similar frequency response when subjected to the same disturbance under the same wind speed conditions. The frequency nadir of Figure 4.4 is stated in (Yang et al., 2020) to be 49.125 Hz, while the frequency nadir of Figure 4.3 has been measured to be 49.125 Hz.

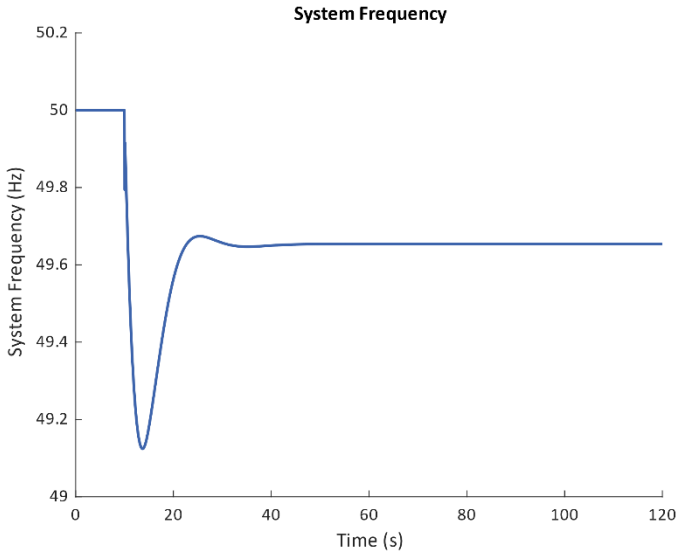

Figure 4.3: Case 1 system frequency benchmark results

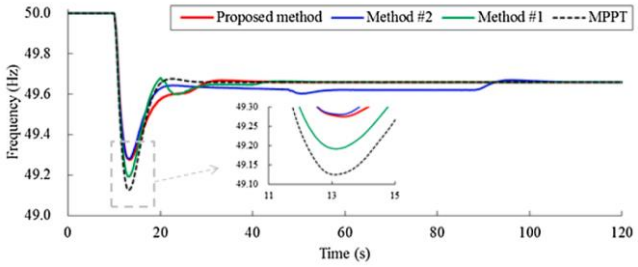

Figure 4.4: Case 1 benchmark system frequency (Yang et al., 2020)

Figure 4.5 shows the plotted simulation results of the WPP output of the model in this study. When compared to the MPPT WPP output of (Yang et al., 2020) in Figure 4.6, the model presented in this study exhibits a slight perturbation in the WPP output power at 10 s when the system is subjected to a 130 MW loss of generation (an effective increase in load of 130 MW to the system).

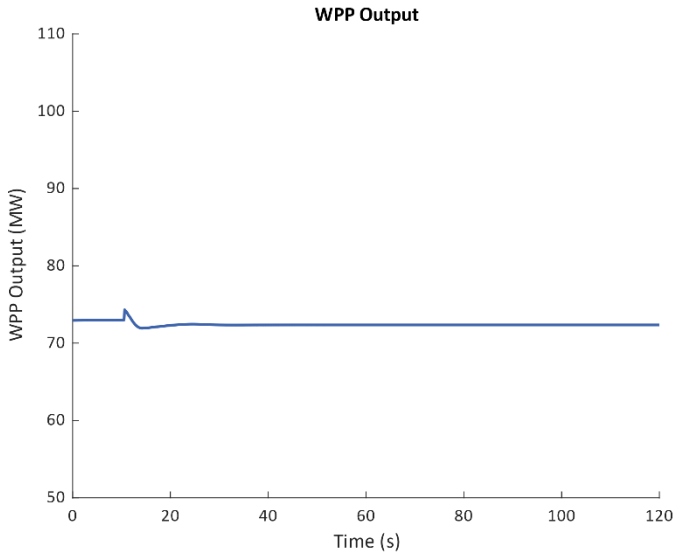

Figure 4.5: Case 1 WPP output benchmark results

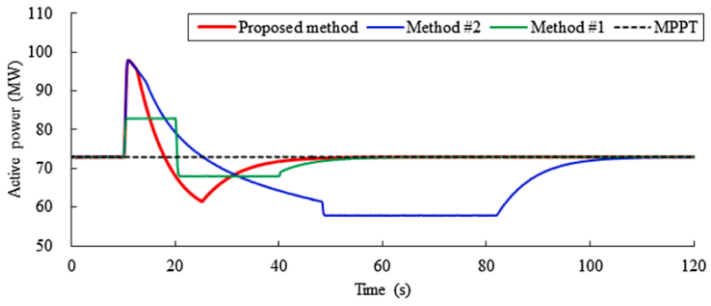

Figure 4.6: Case 1 benchmark WPP output (Yang et al., 2020)

When the disturbance occurs at 10 s, the WPP output power at peaks at 74.32 MW and declines to a trough of 71.94 MW before settling at 72.35 MW. The perturbation is 1.97 % above the average output and the trough is 0.41 % below the average WPP output for the simulation period. In Figure 4.7, at 10 s when the perturbation occurs in the WPP output, there is no deviation in rotor speed of the WTG.

The rotor speed shown in Figure 4.7 remains consistent throughout the disturbance induced at 10 s. This behaviour is identical to the MPPT operation of the WTG Rotor speed shown in Figure 4.8. The simulation model therefore exhibits acceptable accuracy for the analysis of WT kinetic energy recovery for frequency support.

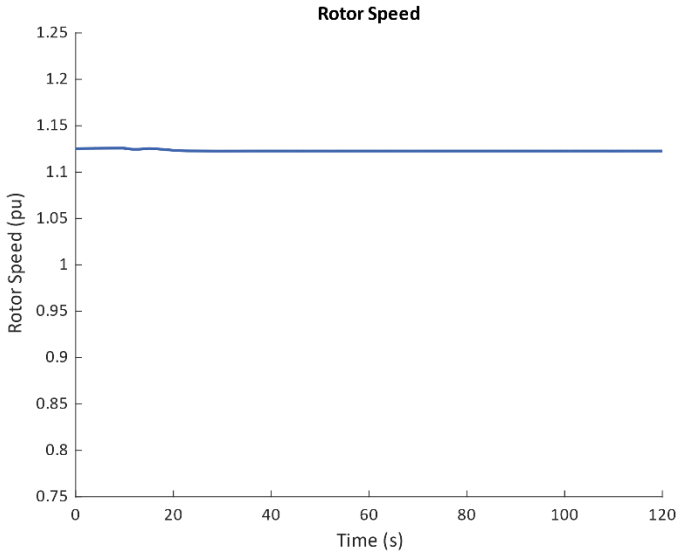

Figure 4.7: Case 1 WTG rotor speed benchmark results

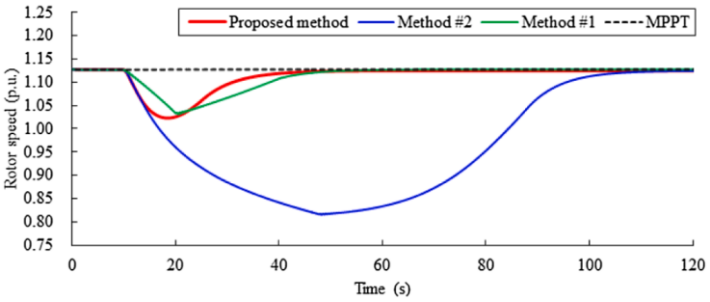

Figure 4.8: Case 1 benchmark WTG rotor speed (Yang et al., 2020)

4.3.2.2 Case 2: Wind speed condition of 8 m.s^{-1}

The second case study investigates the effect of a generator generating 130 MW tripping at 10 s with wind speed conditions of 8 m.s^{-1}. Figure 4.9 shows the plotted simulation results of the system frequency response of the model in this study. Figure 4.10 shows the system frequency response of the power system in (Yang et al., 2020) to a disturbance with a connected DFIG-based windfarm. When Figure 4.9 is compared to the MPPT trace of Figure 4.10, it can be seen that the model presented in this study has a comparable frequency response when subjected to the same disturbance under the same wind speed conditions with an exception of a raised frequency nadir in Figure 4.9. The frequency nadir of Figure 4.10 is stated in (Yang et al., 2020) to be 49.125 Hz, while the frequency nadir of Figure 4.9 has been measured to be 49.15 Hz, an increase of 0.025 Hz.

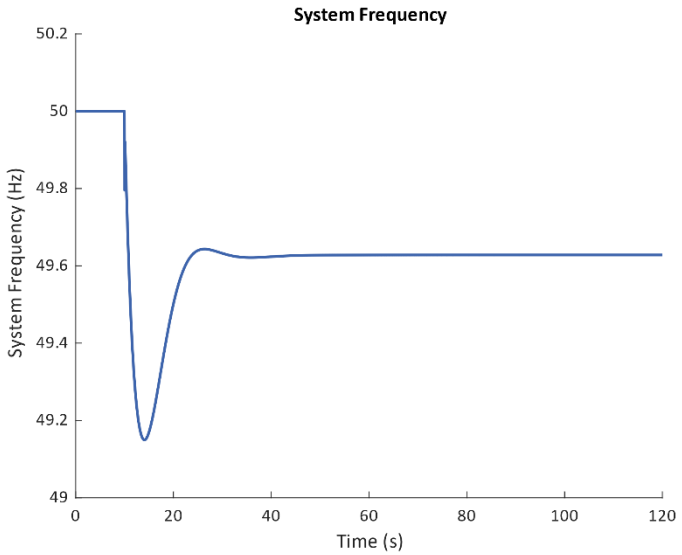

Figure 4.9: Case 2 system frequency benchmark results

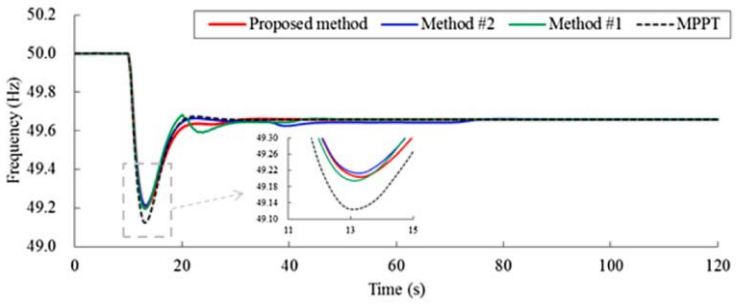

Figure 4.10: Case 2 benchmark system frequency (Yang et al., 2020)

The lower wind speed of 8 $m.s^{-1}$ results in a reduced average WPP output when compared to Case 1. This necessitates a larger contribution from the synchronous generators in the system to maintain the nominal system frequency of 50 Hz (recalling that the nominal frequency of a transmission network is maintained by the balance of generation and consumption of electricity). The increase in synchronous generator contribution due to the reduction in WPP output, from an average of 72.35 MW in case 1 to 35.86 MW, effectively reduces the wind power penetration. The 0.025 Hz raise in frequency nadir is a consequence of the effective decline in wind power penetration.

Figure 4.11 shows the plotted simulation results of the WPP output of the model in this study. When compared to the MPPT WPP output of (Yang et al., 2020) in Figure 4.12, the model presented in this study exhibits a slight perturbation in the WPP output power at 10 s when the system is subjected to a 130 MW loss of generation (an effective increase in load of 130 MW to the system).

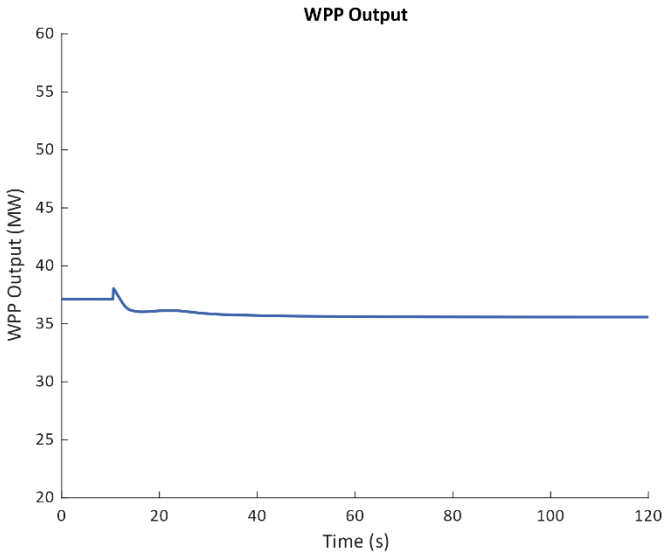

Figure 4.11: Case 2 benchmark WPP output results

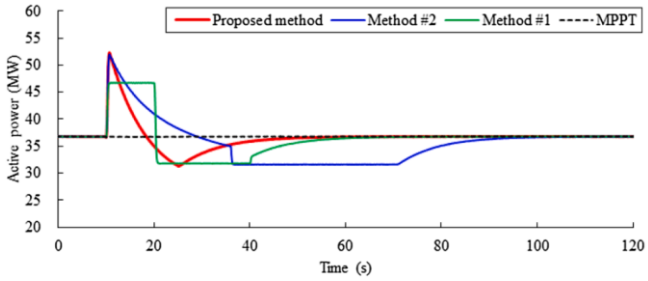

Figure 4.12: Case 2 benchmark WPP output (Yang et al., 2020)

When the circuit breaker switches at 10 s resulting in a 130 MW loss of generation, the WPP output power at peaks at 38.06 MW and settles at an average output of at 35.86 MW. The perturbation is 6 % above the average WPP output for the simulation period. In Figure 4.13, at 10 s when the perturbation occurs in the WPP output, there is gradual decline rotor speed of the WTG.

The rotor speed shown in Figure 4.13 gradually reduces following the disturbance induced at 10 s and remains constant from 40 s to 120 s. This behaviour approximates the MPPT operation of the WTG Rotor speed shown in Figure 4.14, by the rotor speed following the WPP output. The decline in rotor speed does not result in an increase in WPP output and the simulation model exhibits a degree of accuracy that is acceptable accuracy for the analysis of WT kinetic energy recovery for frequency support.

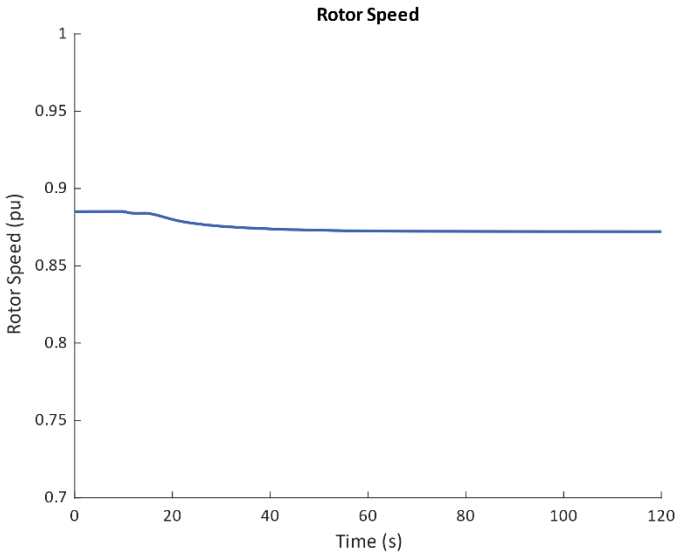

Figure 4.13: Case 2 WTG rotor speed benchmark results

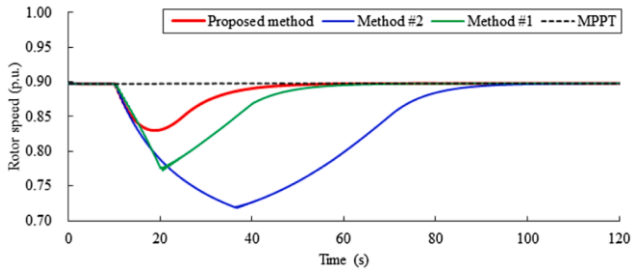

Figure 4.14: Case 2 benchmark rotor speed (Yang et al., 2020)

4.3.2.3 Case 3: Wind speed condition of 10 m.s^{-1} with a consecutive disturbance

The third case study investigates the effect of a consecutive disturbance. A generator generating 130 MW, is tripped at 10 s and an additional generator, is tripped at 50 s with wind speed conditions of 10 m.s^{-1}. Figure 4.15 shows the plotted simulation results of the system frequency response of the model in this study. Figure 4.16 shows the system frequency response of the power system in (Yang et al., 2020) to a consecutive disturbance with a connected DFIG-based windfarm. When Figure 4.15 is compared to the MPPT trace of Figure 4.16, it can be seen that the model presented in this study has a comparable frequency response when subjected to the same disturbances under the same wind speed conditions. The frequency nadir of Figure 4.16 is stated in (Yang et al., 2020) to be 49.125 Hz, while the frequency nadir of Figure 4.15 is 49.125 Hz. The frequency nadir of Figure 4.15 caused by the second disturbance is 49.288 Hz.

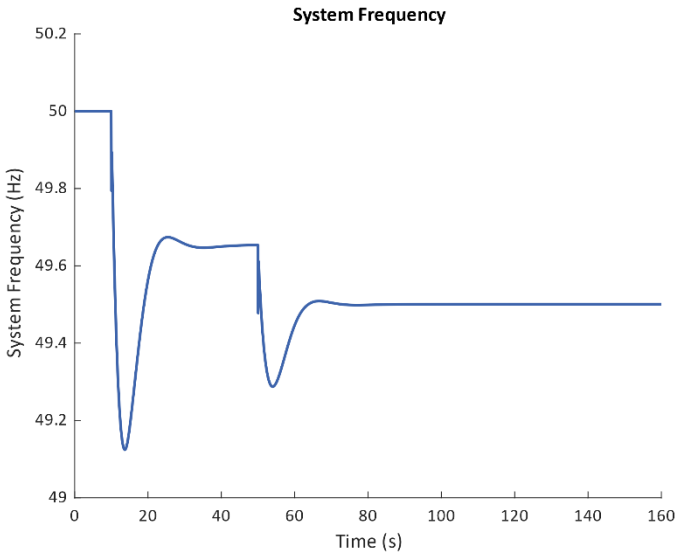

Figure 4.15: Case 3 system frequency benchmark results

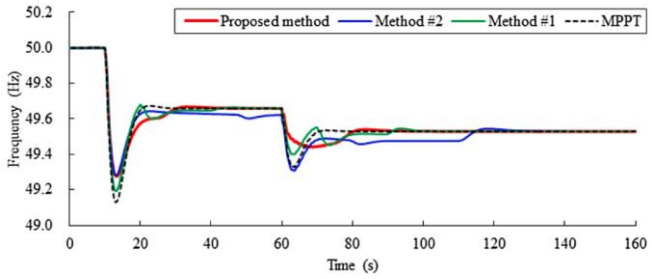

Figure 4.16: Case 3 benchmark system frequency (Yang et al., 2020)

Figure 4.17 shows the plotted simulation results of the WPP output of the model in this study. When compared to the MPPT WPP output of (Yang et al., 2020) in Figure 4.18, the model presented in this study exhibits a slight perturbation in the WPP output power at 10 s and at 50 s when the system is subjected to a loss of generation (an effective increase in load).

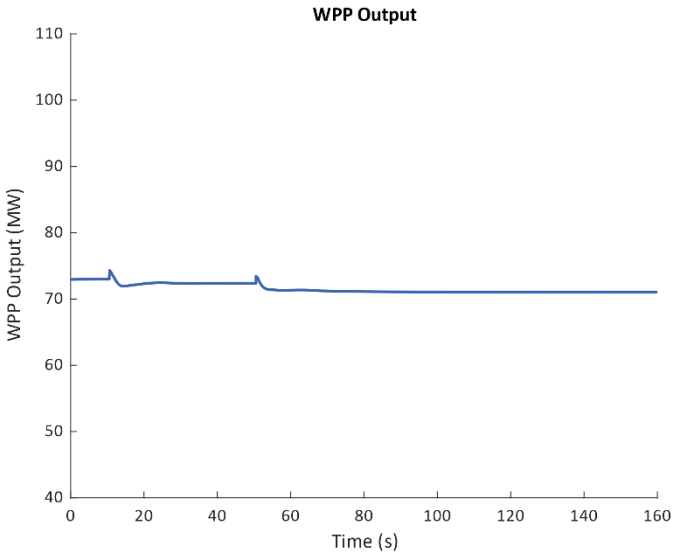

Figure 4.17: Case 3 benchmark WPP output results

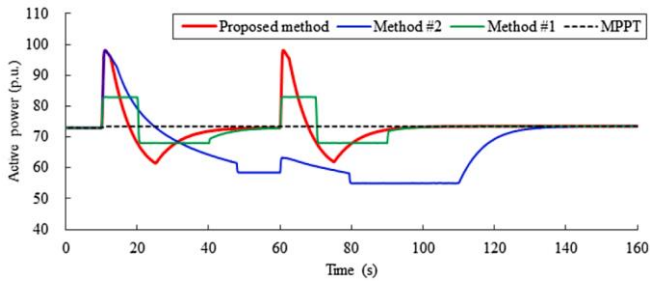

Figure 4.18: Case 3 benchmark WPP output (Yang et al., 2020)

When the circuit breaker switches at 10 s resulting in a loss of generation, the WPP output power at peaks at 74.32 MW and declines to a trough of 71.94 MW before settling at 72.35 MW. At 50 s, when a second loss of generation occurs, the WPP output power peaks at 73.44 MW before settling at 71.05 MW. There is a decline from 73 MW in average WPP output from the start of the simulation before the first disturbance to 71.05 MW average WPP output following the last disturbance to the system during the simulation period.

In Figure 4.19, at 10 s and 50 s when the perturbations occur in the WPP output, there is no significant deviation in rotor speed of the WTG. The rotor speed shown in Figure 4.19 remains consistent throughout the disturbances induced at 10 s and 50 s. This behaviour is comparable to the MPPT operation of the WTG Rotor speed shown in Figure 4.20 and the decline in rotor speed resulting from a disturbance does not result in an increase in WPP output. The simulation model therefore exhibits acceptable accuracy for the analysis of WT kinetic energy recovery for frequency support, but a more accurate model may be required for analysis at a smaller time scale or other areas of study such as power quality.

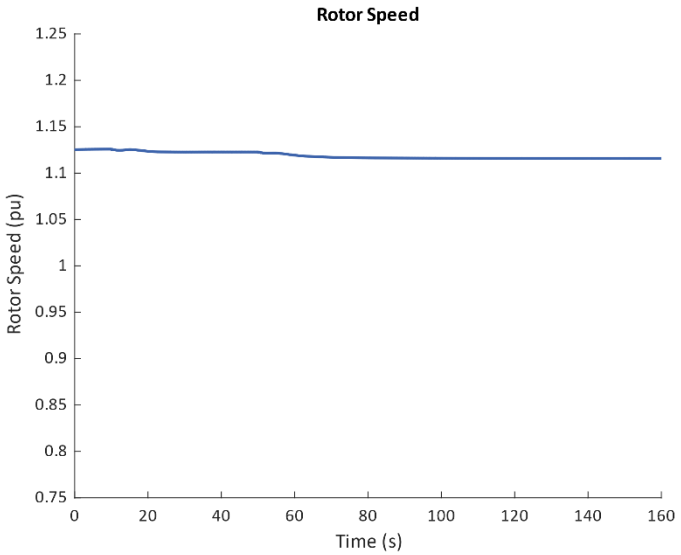

Figure 4.19: Case 3 WTG Rotor Speed Benchmark Results

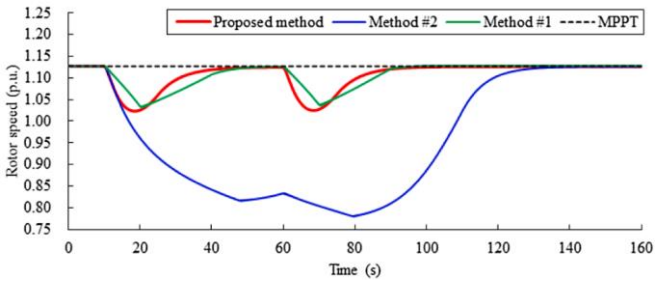

Figure 4.20: Case 3 benchmark rotor speed (Yang et al., 2020)

The benchmark results for the model presented in this study was benchmarked through three case studies presented in and compared to the results in (Yang et al., 2020). The Simulink based model presented in this section has been shown to have acceptable accuracy for the topic of this study.

4.3.3 Results: Proposed Frequency Support Controller

The DFIG model presented in this study has been validated against the published work presented in (Yang et al., 2020). The performance of the additional frequency support controller is studied under five scenarios. The first three case studies are identical two the benchmark results and provides a meaningful way to evaluate the performance and efficacy of the frequency support controller. An additional two case studies, a temporary wind speed deviation and a temporary disturbance, are introduced to study the robustness of the controller. The data obtained from simulations was processed using a Hampel filter, with the same parameters as the benchmark model, prior to graphing.

4.3.3.1 Case 1: Wind speed condition of 10 m.s^{-1}

Figure 4.21 shows the results of the system frequency response of the transmission network with a DFIG-based windfarm partaking in frequency support. When Figure 4.3 is compared to Figure 4.21, it can be seen that the frequency nadir of 49.125 Hz in Figure 4.3, has been raised by the DFIG-based windfarm partaking in frequency support to 49.41 Hz when subjected to the same disturbance under the same wind speed conditions of 10 m.s^{-1}.

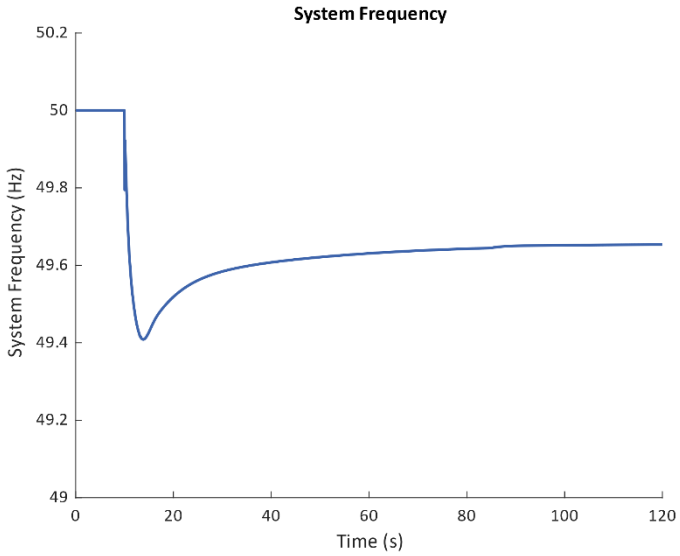

Figure 4.21: Case 1 system frequency with frequency support results

Figure 4.22 shows Figure 4.21 superimposed on Figure 4.3 (lower opacity trace) to provide a clear comparison of the system frequency. In Figure 4.22 it is shown that the DFIG-based WPP with frequency support raises the frequency nadir when compared to an MPPT operation of the DFIG-based WPP.

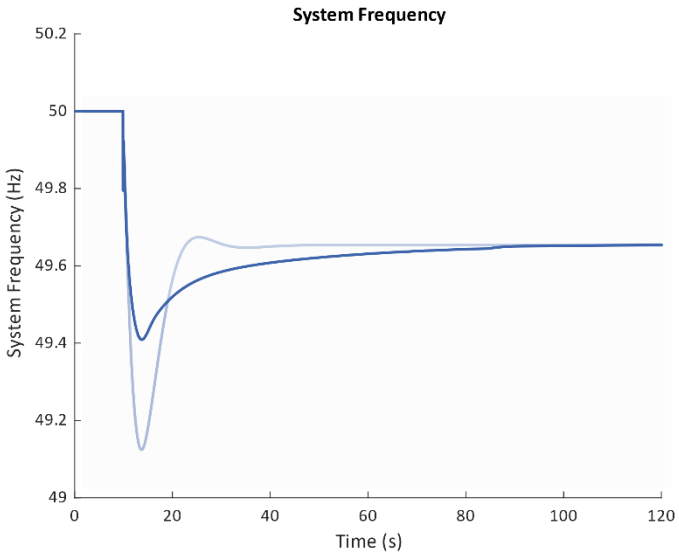

Figure 4.22: Case 1 frequency support results overlayed with case 1 benchmark results

The WPP output power is shown in Figure 4.23. When the disturbance occurs at 10 s, the WPP output power begins to rise rapidly and peaks at 114.6 MW. This temporary overproduction of power from the WPP acts to raise the system frequency nadir. Then after reaching the peak WPP output power, the WPP output begins to decline as the system frequency begins to rise to the new setpoint. However, the WPP output continues to decline below the pre-disturbance WPP output power of 72.55 MW to a trough of 61.25 MW at 39 s before gradually increasing to 71.78 MW by the end of the simulation. It was previously stated that the limited kinetic energy of the rotor needs to return to the rotor following the recovery of kinetic energy for frequency support. This behaviour can be seen by the reduced WPP output power following the rapid injection of active power.

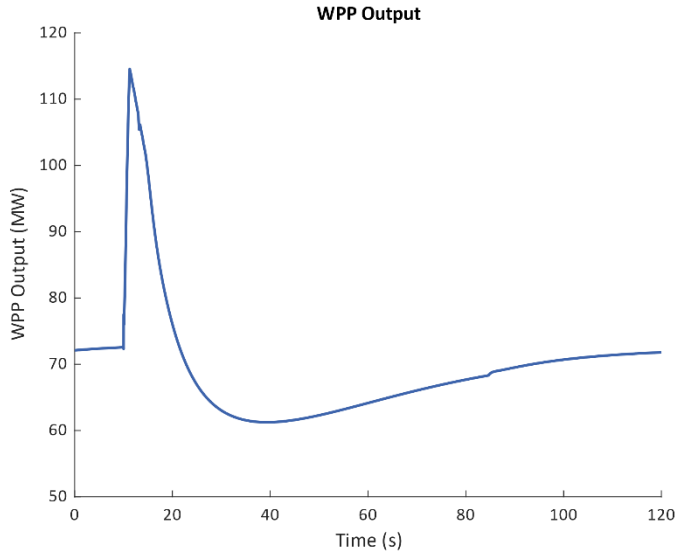

Figure 4.23: Case 1 WPP output with frequency support

The rotor speed shown in Figure 4.24 begins to decrease when the disturbance induced at 10 s. At the instance of the disturbance, the kinetic energy of the rotor is converted to electrical energy. The power electronic interface of the WTG enables a rapid increase output power to a disturbance. When comparing the rate of increase output power in Figure 4.23, to the rate of decrease in rotor speed in Figure 4.24, it can be seen that the rotor deceleration is more gradual when compared to the rate of increase in active power. This decoupling between WPP output and rotor speed indicates that the frequency response controller can tailor the emulated inertial response. The emulated inertial response can be tuned to make optimal use of the available kinetic energy of the rotating mass.

In Figure 4.24 the rotor speed reaches a minimum speed of 0.88 pu at 28 s, during the frequency support period, before beginning to accelerate back to 1.11 pu by the end of the simulation. The rotor speed is above the minimum speed of 0.75 pu and is shown to have a monotonic deceleration and acceleration. In this case study, no secondary deviations in the system frequency are noted in Figure 4.21 while the rotor recovers to pre-disturbance speed.

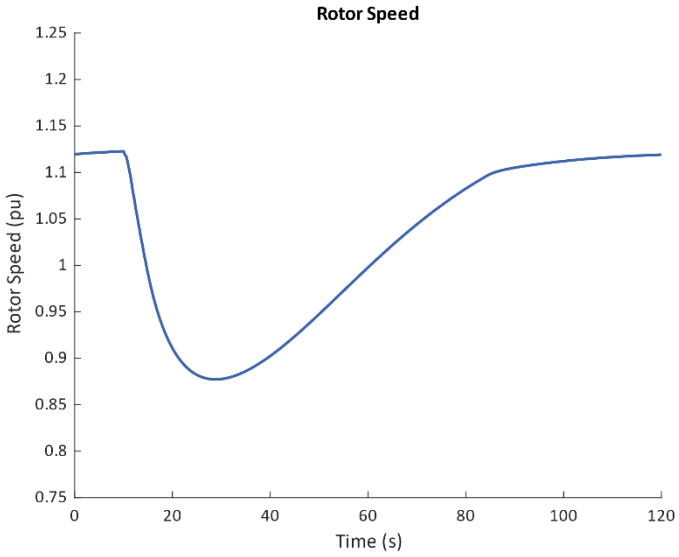

Figure 4.24: Case 1 rotor speed with frequency support

4.3.3.2 Case 2: Wind speed condition of 8 m.s^{-1}

Figure 4.25 shows the results of the system frequency response of the network with the DFIG-based windfarm partaking in frequency support. In Figure 4.25, it appears that the frequency decline would be arrested at 49.46 Hz at 13 s, but at 14.4 s the frequency begins to decline once more before reaching a frequency nadir of 49.28 Hz. This secondary frequency decline is attributed to frequency support controller's response to a disturbance with reduced available

kinetic energy because of the lower wind speed. When Figure 4.9 is compared to Figure 4.25, it can be seen that the frequency nadir of 49.15 Hz in Figure 4.9, has been raised when subjected to the same disturbance under the same wind speed conditions of 8 $m.s^{-1}$.

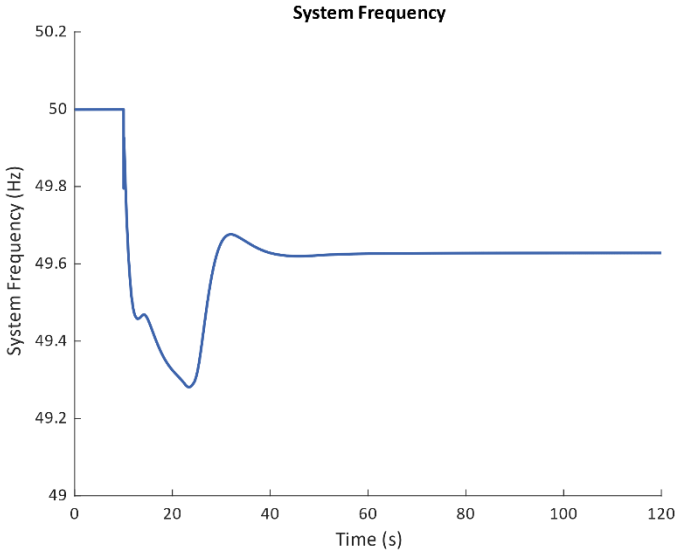

Figure 4.25: Case 2 system frequency with frequency support results

Figure 4.26 shows Figure 4.25 superimposed on Figure 4.9 (lower opacity trace) to provide a clear comparison of the system frequency. In Figure 4.26 it is shown that the DFIG-based WPP with frequency support raises the frequency nadir when compared to an MPPT operation of the DFIG-based WPP.

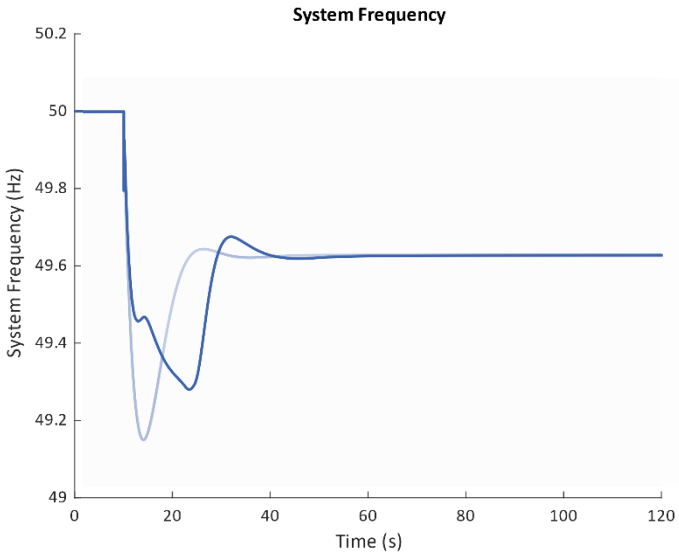

Figure 4.26: Case 2 frequency support results overlayed with case 2 benchmark results

The WPP output power is shown in Figure 4.27. When the disturbance occurs at 10 s, the WPP output power begins to rise rapidly and peaks at 79.74 MW. This temporary overproduction of power from the WPP acts to raise the system frequency nadir. Then after reaching the peak WPP output power, the WPP output begins declines as the Under Speed Logic reduces the output of the frequency support controller to zero. However, the WPP output continues to decline below the pre-disturbance WPP output power of 36.77 MW to 0 MW at 22.5 s before increasing the output from 0 MW at 24.8 s to 35.5 MW by the end of the simulation. The 2.3 s period of no output power from the WPP, is attributed to the rotor speed of the WTGs of the WPP falling below the minimum bound of their rotor speed operating range. Despite the discontinuous WPP output, the frequency support controller still raises the frequency nadir.

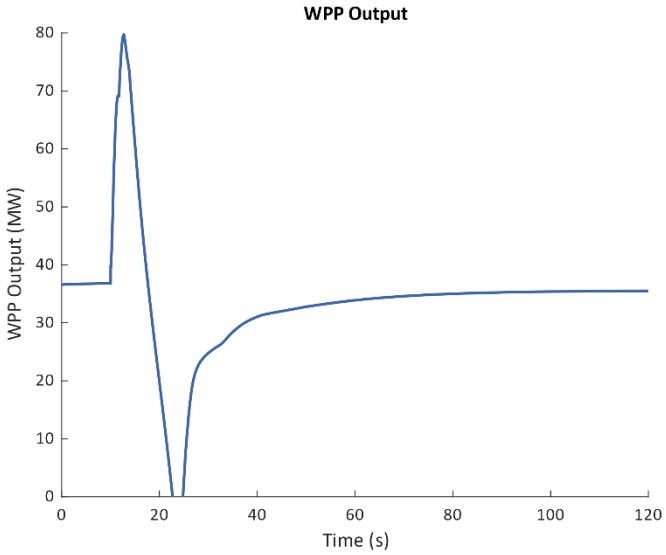

Figure 4.27: Case 2 WPP output with frequency support

The rotor speed shown in Figure 4.28 begins to decrease when the disturbance induced at 10 s. At the instance of the disturbance, the kinetic energy of the rotor is converted to electrical energy. When comparing the rate of increase output power in Figure 4.27, to the rate of decrease in rotor speed in Figure 4.28, it can be seen that the rotor deceleration is more comparable compared to the rate of increase in active power. This is attributed to less kinetic energy in the rotating mass available for frequency support. The frequency support controller, however, does not dynamically optimise its response to varying levels of kinetic energy available.

In Figure 4.28 the rotor speed reaches a minimum speed of 0.64 pu at 18.6 s, during the frequency support period and drops below the minimum speed of 0.75 pu. The time taken by the under-speed logic to negate the contribution of the frequency support controller causes the

rotor speed to reduce below the minimum rotor speed. The deceleration of the rotor is shown to be monotonic however, the recovery of the rotor is a non-monotonic acceleration back to 0.87 pu by the end of the simulation. In this case study, no secondary deviations in the system frequency are noted in Figure 4.25 while the rotor recovers to pre-disturbance speed.

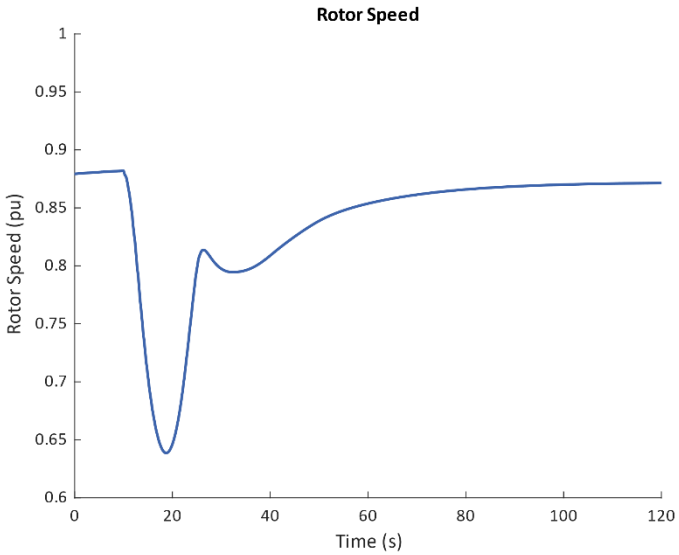

Figure 4.28: Case 2 rotor speed with frequency support

4.3.3.3 Case 3: Wind speed condition of 10 m.s^{-1} with a consecutive disturbance

Figure 4.29 shows the results of the system frequency response of transmission network to a consecutive disturbance of generators tripping at 10 s and at 50 s, with the DFIG-based windfarm partaking in frequency support. This scenario is identical to benchmarking Case 3. In Figure 4.29, the first frequency nadir of 49.4 Hz is reached at 13.8 s following the first disturbance at 10 s. The system frequency recovers to 49.62 Hz prior to the second disturbance occurring and following this second disturbance at 50 s, a frequency nadir of 49.44 Hz is reached at 51.6 s. The system frequency recovers 49.53 Hz at 79 s following the consecutive disturbances. However, at this point the system frequency succumbs to another frequency deviation as the rotor speed reaches its minimum speed and under speed logic reduces the frequency support controller contribution to zero.

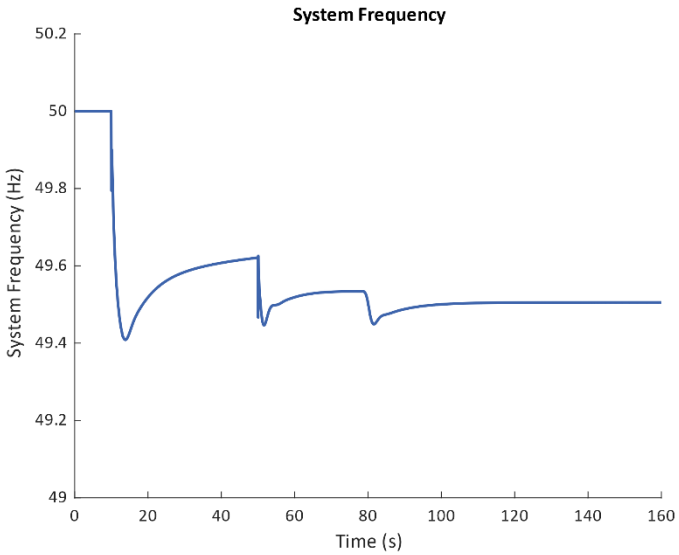

Figure 4.29: Case 3 system frequency with frequency support results

Figure 4.30 shows Figure 4.29 superimposed on Figure 4.15 (lower opacity trace) to provide a clear comparison of the system frequency. In Figure 4.30 it is shown that the DFIG-based WPP with frequency support raises the frequency nadir when compared to an MPPT operation of the DFIG-based WPP but introduces an additional frequency disturbance to the system before converging to the new steady state of 49.5 Hz.

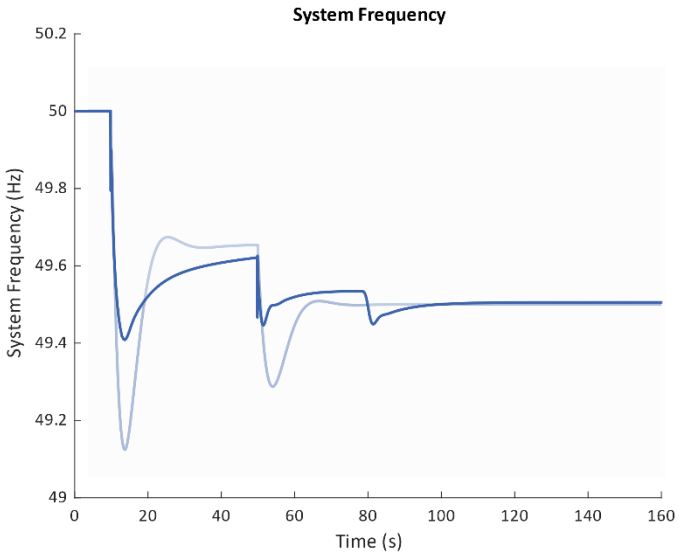

Figure 4.30: Case 3 frequency support results overlayed with case 3 benchmark results

The WPP output power is shown in Figure 4.31. When the disturbance occurs at 10 s, the WPP output power begins to rise rapidly and peaks at 114.6 MW. This temporary overproduction of power from the WPP acts to raise the system frequency nadir. After reaching the peak WPP output power, the WPP output begins to decline as the system frequency

approaches a new steady state but continues to decline below the pre-disturbance WPP output power of 72.55 MW to 61.2 MW at 39.2 s due to the rotor recovering its speed. When the second disturbance occurs at 50 s, the WPP output power rises to 84.8 MW at 51.8 s to overcome the frequency disturbance caused by the second generator tripping. The WPP output power begins to decline as the system frequency begins to recover and continues to decline below 61.2 MW as the rotor has deviated considerably from its MPPT operation. The WPP output power reaches a minimum output of 47.2 MW at 80.3 s as the under-speed logic negates the contribution frequency support controller. The WPP output power has a non-monotonic increase to 69.1 MW as the rotor speed recovers.

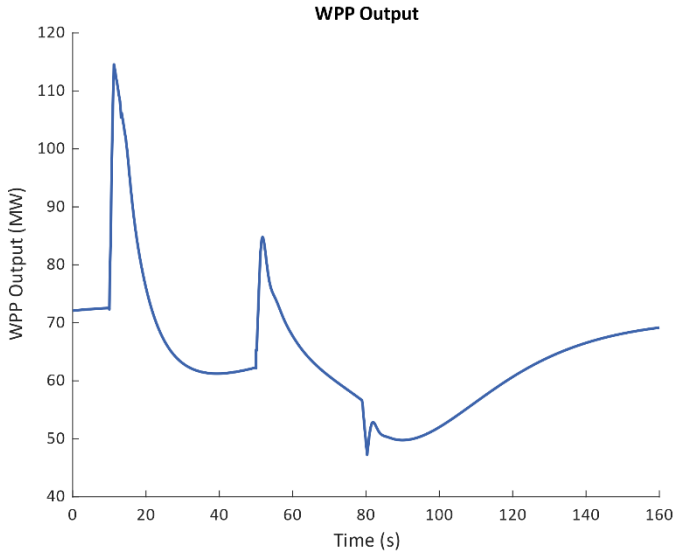

Figure 4.31: Case 3 WPP output with frequency support

The rotor speed during two consecutive disturbances at 10 s and at 50 s is shown in Figure 4.32. The rotor speed begins to decrease when the disturbance occurs at 10 s to a minimum speed of 0.87 pu at 28.9 s. The rotor speed recovers to a speed of 0.94 pu prior to the second disturbance at 50 s which occurs during the rotor recovery phase. The rotor speed begins to decline at the instance of the second as the kinetic energy is recovered to support the system frequency. The rotor speed following the second disturbance reaches a minimum speed of 0.75 pu at 79.6 s when the under-speed logic is triggered. This prevents any further exchange of kinetic energy from the rotor to electrical energy and leads to the third frequency drop to 49.45 Hz seen in Figure 4.29. The rotor recovers monotonically from its minimum speed to 1.05 pu by the end of the simulation.

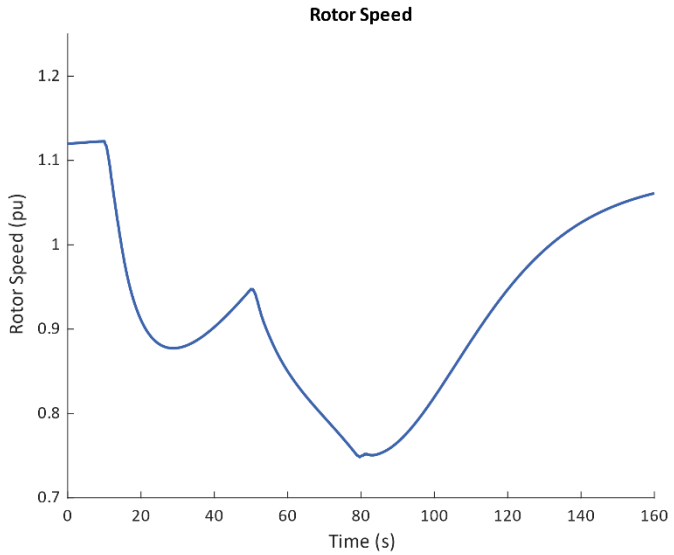

Figure 4.32: Case 3 Rotor Speed with Frequency Support

4.3.3.4 Case 4: Wind speed condition of 10 m.s^{-1} with fluctuating wind speed

The system frequency response to a disturbance of G2 tripping at 10 s with the DFIG-based windfarm partaking in frequency support with fluctuating wind speed is shown in Figure 4.33. The DFIG-based windfarm is subjected to a wind speed that momentary drops from 10 m.s^{-1} to 8 m.s^{-1} prior to the disturbance and recovers to 10 m.s^{-1} while the DFIG-based windfarm partakes in frequency support. The variations in the wind speed conditions persists for a duration of 10 s and leads to various levels of kinetic energy available for grid frequency support. The disturbance of G2 tipping at 10 s during a fluctuating windspeed results in a frequency nadir of 49.32 Hz at 13.46 s. A second frequency nadir of equal magnitude occurs at 22 s due to the rotor recovering, before the system frequency settles at 49.65 Hz.

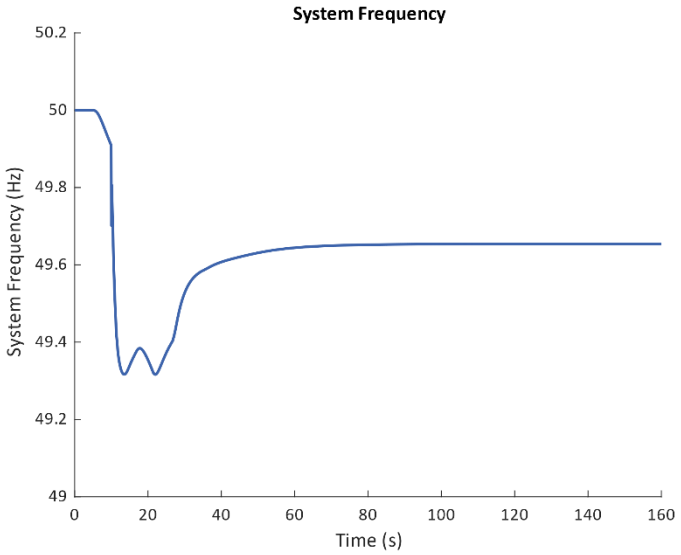

Figure 4.33: Case 4 System Frequency with Frequency Support Results

The WPP output power shown in Figure 4.34 declines from 72.55 MW to 58.19 MW prior to the disturbance at 10 s as the wind speed declines. When the disturbance occurs at 10 s, the WPP output power begins to rise from 58.19 MW rapidly and peaks at 101 MW. Following the peak WPP output power, the WPP output begins to decline as the system frequency approaches a new steady state but continues to decline below the pre-disturbance WPP output power of 27.26 MW at 26.74 s due to the rotor recovering its kinetic energy. The WPP output power has a monotonic increase from its minimum of 27.26 MW to 72.34 MW as the rotor speed recovers while the wind speed is 10 $m.s^{-1}$.

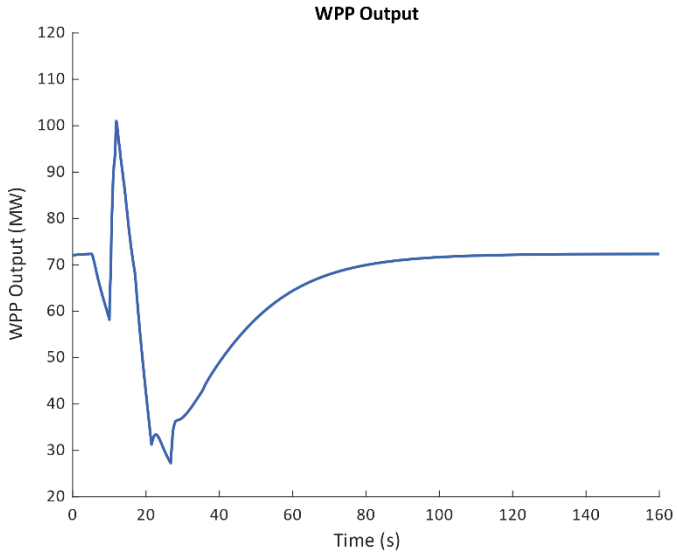

Figure 4.34: Case 4 WPP output with frequency support

The rotor speed response to the disturbances at 10 s during fluctuating wind is shown in Figure 4.35. The wind speed begins to drop from 10 $m.s^{-1}$ at 5 s, and can be seen by the rotor speed declining prior to the disturbance at 10 s. When the disturbance occurs at 10 s, the rotor speed decreases to a minimum speed of 0.72 pu at 19.54 s. The rotor recovers monotonically from its minimum speed to 1.12 pu by the end of the simulation. The rotor recovery phase coincides with an increase in windspeed from 8 $m.s^{-1}$ to 10 $m.s^{-1}$ and this accelerates the rotor recovery.

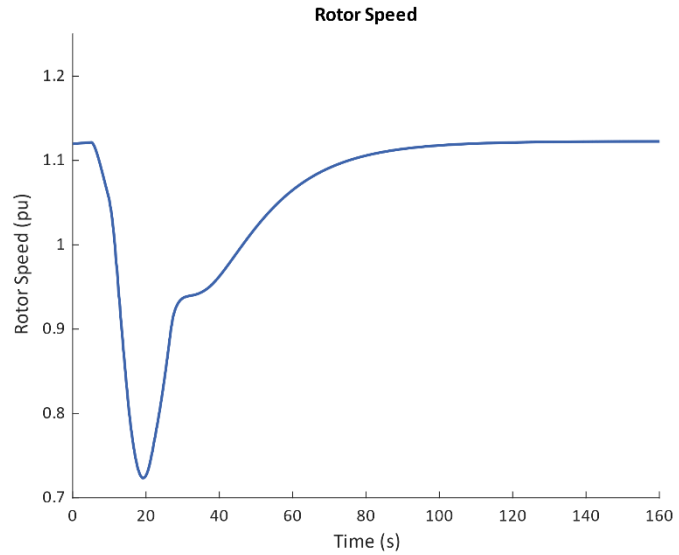

Figure 4.35: Case 4 rotor speed with frequency support

4.3.3.5 Case 5: Wind speed condition of 10 m.s^{-1} with a temporary disturbance

The system frequency response of the transmission network to a temporary 130 MW disturbance simulating generator G2 tripping at 10 s and reconnecting at 50 s with the DFIG-based windfarm partaking in frequency support is shown in Figure 4.36. The disturbance of G2 tipping at 10 s with windspeed conditions of 10 m.s^{-1} results in a frequency nadir of 49.41 Hz at 14.1 s. The system frequency recovers to 49.62 Hz prior to G2 reconnecting and the system frequency peaking at 50.23 Hz at 55.16 s. After the peak, the temporary disturbance, the system returns to its nominal frequency of 50 Hz.

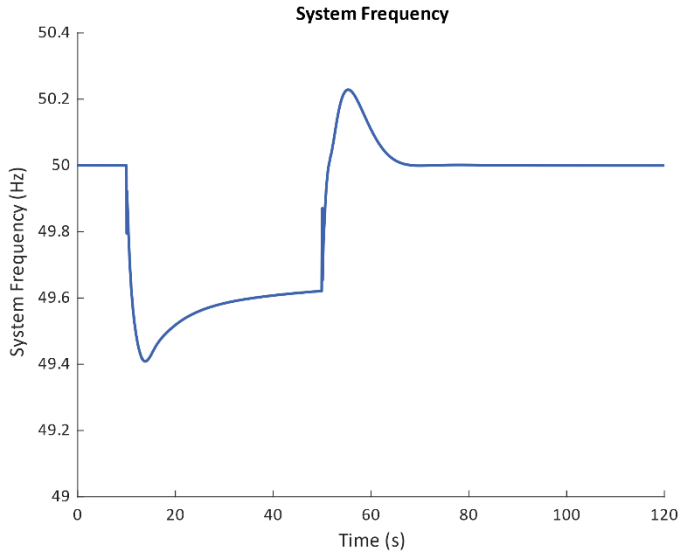

Figure 4.36: Case 5 system frequency with frequency support results

The WPP output power is shown in Figure 4.37. When the disturbance occurs at 10 s, the WPP output power begins to rise rapidly and peaks at 114.6 MW. After reaching the peak WPP output power, the WPP output begins to decline as the system frequency approaches a new steady state, but the WPP output continues to decline below the pre-disturbance WPP output power of 72.55 MW to 61.2 MW at 39.2 s due to the rotor recovering its speed. When G2 reconnects to the network at 50 s, the WPP output power rapidly declines to 7.9 MW at 51.6 s as the rapid rise in system frequency causes the frequency support controller contribution to rapidly reduce to zero. This behaviour of the frequency support controller is desirable as it works against both positive and negative frequency deviations from the nominal frequency. This behaviour can be expanded on in future work to even provide damping to the transmission network. The WPP output power rapidly recovers from the WPP output power nadir of 7.9 MW and settles at 72.47 MW.

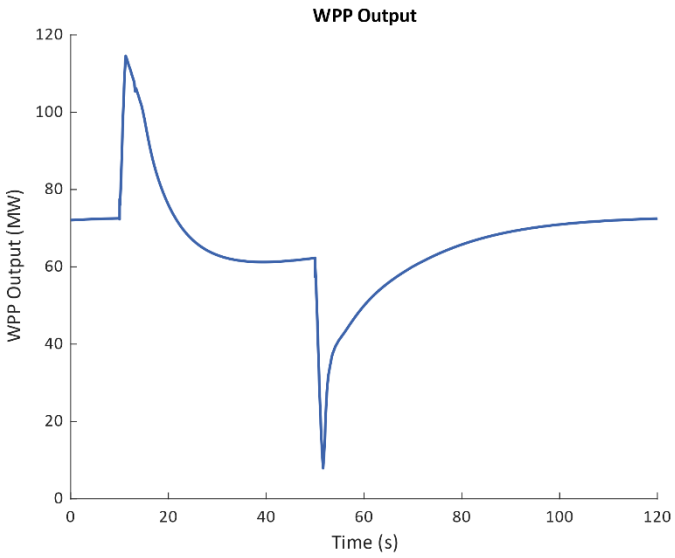

Figure 4.37: Case 5 WPP output with frequency support

In Figure 4.38 the rotor speed reaches a minimum speed of 0.88 pu at 28 s, during the frequency support period, before beginning to accelerate back to 1.11 pu by the end of the simulation. The rotor speed is shown to have a monotonic deceleration as the kinetic energy is recovered to support the system frequency when G2 trips. In Figure 4.38, the increase in rotor speed is shown to be non-monotonic during because of G2 reconnecting. In this case study, no secondary deviations in the system frequency are noted in Figure 4.36 while the rotor recovers to pre-disturbance speed.

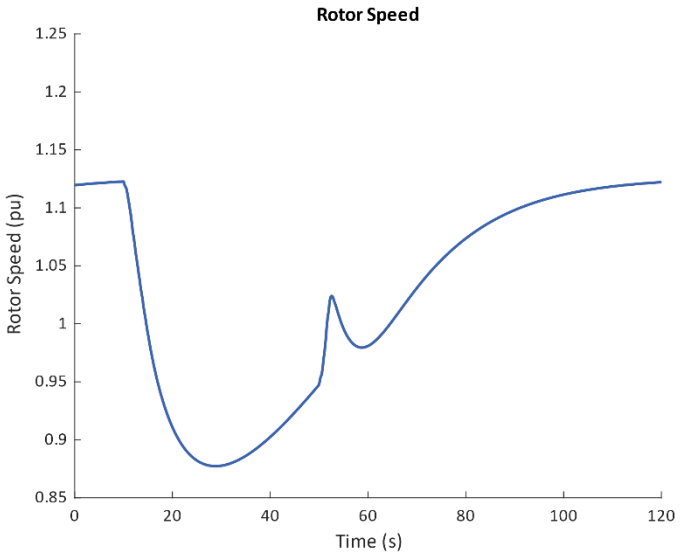

Figure 4.38: Case 5 rotor speed with frequency support

4.4. Discussion of Results

A software model of an aggregated DFIG-based WPP connected to a benchmark network has been presented in this chapter. The accuracy of the model has been conducted through benchmarking, by comparing the simulation results produced by this model to published work presented in (Yang et al., 2020). A numerical summary of the benchmark findings is shown in Table 4.4.

Table 4.4: Numerical Comparison of Benchmark Results

Case	Condition		Frequency nadir
1	Wind Speed: 10 $m.s^{-1}$	Benchmark	49.125 Hz
		Model	49.125 Hz
2	Wind Speed: 8 $m.s^{-1}$	Benchmark	49.125 Hz
		Model	49.15 Hz
3	Wind Speed: 10 $m.s^{-1}$ with a Consecutive Disturbance	Benchmark	49.125 Hz
		Model	49.125 Hz

After the benchmarking, a supplementary frequency support controller was added to the aggregated DFIG-based windfarm and the three initial case studies along with two additional case studies are evaluated. A numerical summary of the results is shown in Table 4.5.

Table 4.5: Numerical Comparison of Results

Case	Condition	Frequency nadir	Peak WPP output power	Minimum Rotor Speed
1	Wind Speed: 10 $m.s^{-1}$	49.41 Hz	114.6 MW	0.88 pu
2	Wind Speed: 8 $m.s^{-1}$	49.28 Hz	79.74 MW	0.64 pu
3	Wind Speed: 10 $m.s^{-1}$ with a Consecutive Disturbance	49.4 Hz	114.6 MW	0.75 pu
4	Wind Speed: 10 $m.s^{-1}$ with Fluctuating Wind Speed	49.32 Hz	101 MW	0.72 pu
5	Wind Speed: 10 $m.s^{-1}$ with a Temporary Disturbance	49.41 Hz	114.6 MW	0.88 pu

When comparing Case Study 1 through to Case Study 3 in Table 4.4 to Table 4.5, the DFIG-based WPP with frequency support has raised the frequency nadir across all three case studies when compared to the MPPT operation of a DFIG-based wind farm connected to the network.

4.5. Conclusion

The software model of an aggregated DFIG-based WPP has been presented in this chapter. The model has been benchmarked by comparing the simulation results produced by this model to published work presented in (Yang et al., 2020). By comparing the simulation results of the three case studies of model in this chapter to the work presented in (Yang et al., 2020), it is shown that the accuracy of the model developed in this chapter was shown to be acceptable for studying system frequency dynamics.

CHAPTER 5: Conclusion

5.1. Conclusions

The rotating mass of variable speed wind turbines are decoupled from the grid by their power converters and do not provide an inherent inertial response to frequency events on the grid. This reduces the effective system inertia of the grid which is of concern for frequency stability of the grid. To address this problem, this study introduces a supplementary frequency support controller to the rotor-side converter of a doubly-fed induction generator variable speed wind turbine. To overcome a frequency disturbance, the frequency support controller temporarily raises the active power output of the wind turbine generator by emulating an inertial response. The additional energy required for the temporary overproduction of active power during a frequency disturbance is obtained by recovering the kinetic energy of the spinning mass of the wind turbine generator. The results showed that the frequency support controller has provided frequency support by raising the frequency nadir following a disturbance when compared to the frequency nadir of identical scenarios without frequency support, even in the cases of consecutive disturbances. In a world where grids seek to decarbonise their generating fleet as climate change concerns become more prevalent, the need to shift to more sustainable forms of energy such as the adoption renewable energy has seen an increase. The development of grid frequency support strategies from renewable resources such as variable speed wind turbines will continue to be of importance to assist with the security of transmission grid's frequency stability.

5.2. Future Work

To further development and research on kinetic energy recovery for grid frequency support, some recommendations have been formulated. Future work should aim to extend the frequency support performance of the WTG in low wind conditions and varying wind speed conditions. A controlled de-load operation with the rotor speed higher than normal as presented in (Xu et al., 2016) could be a possible solution to address the performance of the frequency support controller operation in low levels and varying levels of kinetic energy in future work. With the method presented in (Xu et al., 2016), when a frequency event occurs, the decrease in rotor speed (caused by the recovery of kinetic energy) will cause the operating point of the WTG to shift toward that the MPPT curve. When the rotor speed reaches the optimal rotor speed, the deceleration stops, and the WTG settles with a higher mechanical power captured than before the frequency drop occurred (Xu et al., 2016).

Some frequency support implementations, such as the model presented in this study rely on a phase-locked-loop (PLL) to detect the grid's frequency and its derivative as well as the grid voltage phase angle. Such implementations are limited in their capabilities as they still

necessitate the presence of rotating inertia in the grid (D'Arco et al., 2015). This limits the deployment of such a system in weak grids or islanded operation and addressing this limitation is a topic for future work. Future work will also improve on the initialisation methods used in the computer modelling of the system. In addition to improving the modelling accuracy and further improving numerical robustness so that other fields of study such as power quality and rotor dynamics can be studied using the same model.

The utility of a supplementary controller for grid frequency support extends beyond VSWTs. Electric vehicles (EVs) can be used to provide grid frequency support through vehicle to grid (V2G) regulation services (Zhang & Leung, 2022). The authors of (Iqbal et al., 2020), present two controllers that provide bidirectional power flow which can provide frequency support during contingencies in an industrial microgrid. While in (Jan et al., 2021), it is proposed to use ESS alongside EVs to provide frequency support to a microgrid by presenting a control method to control the ESS and EVs during large-scale integration of RES or sudden change in load demand.

REFERENCES

Aberg, E. (International R.E.A.-I., Adib, R. (REN21), Appavou, F., Brown, A., Dwyer, S. (ISF-U., Epp, B. (solrico), Guerra, F. (REN21), Kondev, B., Murdock, H.E. (REN21), Musolino, E., Rutovitz, J. (ISF-U., Sawin, J.L. (Sunna R., Seyboth, K. (KMS R. and C., Skeen, J. (SOLA F.E., Sverrisson, F. (Sunna R., Teske, S. (ISF-U., Weckend, S. (IRENA) & Wuester, H. (IRENA). 2018. *RENEWABLES 2018 GLOBAL STATUS REPORT*.

Abouzeid, S.I., Guo, Y. & Zhang, H.C. 2021. Cooperative control framework of the wind turbine generators and the compressed air energy storage system for efficient frequency regulation support. *International Journal of Electrical Power and Energy Systems*, 130.

Adeuyi, O.D., Cheah-Mane, M., Liang, J. & Jenkins, N. 2017. Fast Frequency Response From Offshore Multiterminal VSC–HVDC Schemes. *IEEE Transactions on Power Delivery*, 32(6): 2442–2452.

Anaya-Lara, O., Jenkins, N., Ekanayake, J., Cartwright, P. & Hughes, M. 2009. *Wind energy generation : modelling and control*.

Arani, M.F.M. & Mohamed, Y.A.-R.I. 2016. Analysis and Mitigation of Undesirable Impacts of Implementing Frequency Support Controllers in Wind Power Generation. *IEEE Transactions on Energy Conversion*, 31(1): 174–186.

Ashouri-Zadeh, A., Toulabi, M. & Ranjbar, A.M. 2016. Coordinated design of fuzzy-based speed controller and auxiliary controllers in a variable speed wind turbine to enhance frequency control. *IET Renewable Power Generation*, 10(9): 1298–1308.

Attya, A.B.T. & Dominguez-Garcia, J.L. 2018. Insights on the Provision of Frequency Support by Wind Power and the Impact on Energy Systems. *IEEE Transactions on Sustainable Energy*, 9(2): 719–728.

Attya, A.B.T. & Hartkopf, T. 2015. Utilising stored wind energy by hydro-pumped storage to provide frequency support at high levels of wind energy penetration. *IET Generation, Transmission and Distribution*, 9(12): 1485–1497.

Azizipanah-Abarghooee, R., Malekpour, M., Dragicevic, T., Blaabjerg, F. & Terzija, V. 2020. A Linear Inertial Response Emulation for Variable Speed Wind Turbines. *IEEE Transactions on Power Systems*, 35(2): 1198–1208.

Bianchi, F.D. & Dominguez-Garcia, J.L. 2016. Coordinated Frequency Control Using MT-HVDC Grids With Wind Power Plants. *IEEE Transactions on Sustainable Energy*, 7(1): 213–220.

Binbing, W., Abuduwayiti, X., Yuxi, C. & Yizhi, T. 2020. RoCof droop control of PMSG-based wind turbines for system inertia response rapidly. *IEEE Access*, 8: 181154–181162.

Boukhezzar, B. & Siguerdidjane, H. 2011. Nonlinear Control of a Variable-Speed Wind Turbine Using a Two-Mass Model. *IEEE Transactions on Energy Conversion*, 26(1): 149–162. http://ieeexplore.ieee.org/document/5675666/.

Boyle, J., Littler, T. & Foley, A. 2018. Review of frequency stability services for grid balancing with wind generation. *The Journal of Engineering*, 2018(15): 1061–1065.

Boyle, J., Littler, T., Muyeen, S.M. & Foley, A.M. 2021. An alternative frequency-droop scheme for wind turbines that provide primary frequency regulation via rotor speed control. *International Journal of Electrical Power and Energy Systems*, 133.

Bubshait, A.S., Mortezaei, A., Simoes, M.G. & Busarello, T.D.C. 2017. Power Quality Enhancement for a Grid Connected Wind Turbine Energy System. *IEEE Transactions on Industry Applications*, 53(3): 2495–2505.

Chang, K., Xue, F., Fang, Y. & Yu, Y. 2010. Comparative simulation of dynamic characteristics of wind turbine doubly-fed induction generator based on RTDS and MATLAB. In *2010 International Conference on Power System Technology: Technological Innovations Making Power Grid Smarter, POWERCON2010*.

Chen, P., Qi, C. & Chen, X. 2021. Virtual Inertia Estimation Method of DFIG-based Wind Farm with Additional Frequency Control. *Journal of Modern Power Systems and Clean Energy*, 9(5): 1076–1087.

Choi, J.W., Heo, S.Y. & Kim, M.K. 2016. Hybrid operation strategy of wind energy storage system for power grid frequency regulation. *IET Generation, Transmission and Distribution*, 10(3): 736–749.

D'Arco, S., Suul, J.A. & Fosso, O.B. 2015. A Virtual Synchronous Machine implementation for distributed control of power converters in SmartGrids. *Electric Power Systems Research*, 122: 180–197.

DoE. 2018. State of Renewable Energy in South Africa - 2017. http://www.energy.gov.za/files/media/Pub/2017-State-of-Renewable-Energy-in-South-Africa.pdf 11 May 2019.

Dreidy, M., Mokhlis, H. & Mekhilef, S. 2017a. Inertia response and frequency control techniques for renewable energy sources: A review. *Renewable and Sustainable Energy Reviews*, 69(November 2015): 144–155.

Dreidy, M., Mokhlis, H. & Mekhilef, S. 2017b. Inertia response and frequency control techniques for renewable energy sources: A review. *Renewable and Sustainable Energy Reviews*, 69(July 2016): 144–155.

Eskom Transmission Division. 2014. Grid Connection Code for Renewable Power Plants (RPPs) Connected to the Electricity Transmission System (TS) or the Distrubution System(DS) in South Africa. , 2.8(July): 17.

Fang, J., Li, H., Tang, Y. & Blaabjerg, F. 2018a. Distributed Power System Virtual Inertia Implemented by Grid-Connected Power Converters. *IEEE Transactions on Power Electronics*, 33(10): 8488–8499.

Fang, J., Li, H., Tang, Y. & Blaabjerg, F. 2018b. Distributed Power System Virtual Inertia Implemented by Grid-Connected Power Converters. *IEEE Transactions on Power Electronics*, 33(10): 8488–8499.

Fernández-Bustamante, P., Barambones, O., Calvo, I., Napole, C. & Derbeli, M. 2021. Provision of frequency response from wind farms: A review. *Energies*, 14(20).

Fernández-Guillamón, A., Gómez-Lázaro, E., Muljadi, E. & Molina-Garcia, Á. 2021. A Review of Virtual Inertia Techniques for Renewable Energy-Based Generators. In *Renewable Energy - Technologies and Applications*. IntechOpen. https://www.intechopen.com/books/renewable-energy-technologies-and-applications/a-review-of-virtual-inertia-techniques-for-renewable-energy-based-generators.

Fletcher, J. & Yang, J. 2010. Introduction to the Doubly-Fed Induction Generator for Wind Power Applications, Paths to Sustainable Energy A. Ng, ed. http://www.intechopen.com/books/paths-to-sustainable-energy/introduction-to-the-doubly-fed-inductiongenerator-%0Afor-wind-power-applications.

Fu, Y., Wang, Y. & Zhang, X. 2017. Integrated wind turbine controller with virtual inertia and primary frequency responses for grid dynamic frequency support. *IET Renewable Power Generation*, 11(8): 1129–1137.

Garmroodi, M., Verbic, G. & Hill, D.J. 2018. Frequency Support from Wind Turbine Generators with a Time-Variable Droop Characteristic. *IEEE Transactions on Sustainable Energy*, 9(2): 676–684.

Ghosh, S., Kamalasadan, S., Senroy, N. & Enslin, J. 2016. Doubly Fed Induction Generator (DFIG)-Based Wind Farm Control Framework for Primary Frequency and Inertial Response Application. *IEEE Transactions on Power Systems*, 31(3): 1861–1871.

Guo, X., Yan, J., Xu, G., Hu, J. & Bi, T. 2020. Control of VSC-HVDC connected wind farms for system frequency support. *International Transactions on Electrical Energy Systems*, 30(5): 1–13.

Guoyi Xu, Dandan Ge & Tianzhi Cao. 2016. Combined deload and kinetic energy control of variable speed wind turbines for frequency support. In *2016 IEEE PES Asia-Pacific Power and Energy Engineering Conference (APPEEC)*. IEEE: 890–894.

Hassouneh, M.A., Hsien-Chiarn Lee & Abed, E.H. 2004. Washout filters in feedback control: benefits, limitations and extensions. In *Proceedings of the 2004 American Control Conference*. IEEE: 3950–3955 vol.5. https://ieeexplore.ieee.org/document/1383925/.

Huleihil, M. & Mazor, G. 2012. Wind Turbine Power: The Betz Limit and Beyond. In *Advances in Wind Power*. InTech: 13. http://www.intechopen.com/books/advances-in-wind-power/wind-turbine-power-the-betz-limit-and-beyond.

Iqbal, S., Xin, A., Jan, M.U., Abdelbaky, M.A., Rehman, H.U., Salman, S., Rizvi, S.A.A. & Aurangzeb, M. 2020. Aggregation of EVs for Primary Frequency Control of an Industrial Microgrid by Implementing Grid Regulation Charger Controller. *IEEE Access*, 8: 141977–141989.

Jan, M.U., Xin, A., Rehman, H.U., Abdelbaky, M.A., Iqbal, S. & Aurangzeb, M. 2021. Frequency Regulation of an Isolated Microgrid with Electric Vehicles and Energy Storage System Integration Using Adaptive and Model Predictive Controllers. *IEEE Access*, 9: 14958–14970.

Jiang, Q., Zeng, X., Li, B., Wang, S., Liu, T., Chen, Z., Wang, T. & Zhang, M. 2022. Time-Sharing Frequency Coordinated Control Strategy for PMSG-Based Wind Turbine. *IEEE Journal on Emerging and Selected Topics in Circuits and Systems*, 12(1): 268–278.

Kabsha, M.M. & Rather, Z.H. 2020. A New Control Scheme for Fast Frequency Support From HVDC Connected Offshore Wind Farm in Low-Inertia System. *IEEE Transactions on Sustainable Energy*, 11(3): 1829–1837.

Kamel, S., Kodsi, M. & Cañizares, C.A. *MODELING AND SIMULATION OF IEEE 14 BUS SYSTEM WITH FACTS CONTROLLERS*.

Khajehoddin, S.A., Karimi-Ghartemani, M. & Ebrahimi, M. 2019. Grid-Supporting Inverters With Improved Dynamics. *IEEE Transactions on Industrial Electronics*, 66(5): 3655–3667.

Kheshti, M., Ding, L., Nayeripour, M., Wang, X. & Terzija, V. 2019. Active power support of wind turbines for grid frequency events using a reliable power reference scheme. *Renewable Energy*, 139: 1241–1254.

Khurshid, A., Mughal, M.A., Othman, A., Al-Hadhrami, T., Kumar, H., Khurshid, I., Arshad & Ahmad, J. 2022. Optimal Pitch Angle Controller for DFIG-Based Wind Turbine System Using Computational Optimization Techniques. *Electronics (Switzerland)*, 11(8).

Kim, Y.-S., Chung, I.-Y. & Moon, S.-I. 2013. An Analysis of Variable-Speed Wind Turbine Power-Control Methods with Fluctuating Wind Speed. *Energies*, 6(7): 3323–3338. http://www.mdpi.com/1996-1073/6/7/3323.

Kitchenham, B., Pretorius, R., Budgen, D., Pearl Brereton, O., Turner, M., Niazi, M. & Linkman, S. 2010. Systematic literature reviews in software engineering – A tertiary study. *Information and Software Technology*, 52(8): 792–805.

Lao, H., Zhang, L., Zhao, T. & Zou, L. 2021. Novel insight on temporary frequency support of variable speed wind energy conversion system. *Wind Energy*, 24(12): 1353–1367.

Lee, J., Jang, G., Muljadi, E., Blaabjerg, F., Chen, Z. & Cheol Kang, Y. 2016. Stable Short-Term Frequency Support Using Adaptive Gains for a DFIG-Based Wind Power Plant. *IEEE Transactions on Energy Conversion*, 31(3): 1068–1079.

Li, G. & Ye, H. 2021. Hierarchical nonlinear model predictive control for frequency support of wind farm. *International Journal of Electrical Power and Energy Systems*, 129.

Li, Y., Xu, Z., Ostergaard, J. & Hill, D.J. 2017. Coordinated Control Strategies for Offshore Wind Farm Integration via VSC-HVDC for System Frequency Support. *IEEE Transactions on Energy Conversion*, 32(3): 843–856.

Li, Y., Xu, Z. & Wong, K.P. 2017. Advanced Control Strategies of PMSG-Based Wind Turbines for System Inertia Support. *IEEE Transactions on Power Systems*, 32(4): 3027–3037.

Lin, C.H. & Wu, Y.K. 2021. Overview of Frequency-Control Technologies for a VSC-HVDC-Integrated Wind Farm. *IEEE Access*, 9: 112893–112921.

Ma, H. & Li, H. 2013. Analysis of frequency dynamics in power grid: A Bayesian structure learning approach. *IEEE Transactions on Smart Grid*, 4(1): 457–466.

Ma, S., Geng, H., Yang, G. & Pal, B.C. 2018. Clustering-Based Coordinated Control of Large-Scale Wind Farm for Power System Frequency Support. *IEEE Transactions on Sustainable Energy*, 9(4): 1555–1564.

Mahish, P. & Pradhan, A.K. 2020. Distributed Synchronized Control in Grid Integrated Wind Farms to Improve Primary Frequency Regulation. *IEEE Transactions on Power Systems*, 35(1): 362–373.

Martinez Sanz, I., Chaudhuri, B. & Strbac, G. 2015. Inertial Response From Offshore Wind Farms Connected Through DC Grids. *IEEE Transactions on Power Systems*, 30(3): 1518–1527.

Miao, L., Wen, J., Xie, H., Yue, C. & Lee, W.-J. 2015. Coordinated Control Strategy of Wind Turbine Generator and Energy Storage Equipment for Frequency Support. *IEEE Transactions on Industry Applications*, 51(4): 2732–2742.

National Energy Regulator of South Africa. 2010. The South African grid code: The Network Code. , (July): 1–59. http://www.nersa.org.za/.

Okedu, K.E. 2017. Improving grid frequency dynamics of synchronous generators considering wind energy penetration grid dynamics and operation. In *2017 IEEE International Electric Machines and Drives Conference, IEMDC 2017*. IEEE: 1–6.

Ontiveros, L.J., Mercado, P.E. & Suvire, G.O. 2011. A new model of the double-feed induction generator wind turbine. In *2010 IEEE/PES Transmission and Distribution Conference and Exposition: Latin America, T and D-LA 2010*. 263–269.

Opal-RT Technologies. 2018. *Application note Park or DQ Transform variants Opal-RT Technologies Park/DQ transform variants 2 / 6*.

O'Rourke, C.J., Qasim, M.M., Overlin, M.R. & Kirtley, J.L. 2019. A Geometric Interpretation of Reference Frames and Transformations: dq0, Clarke, and Park. *IEEE Transactions on Energy Conversion*, 34(4): 2070–2083. https://ieeexplore.ieee.org/document/8836094/.

Oshnoei, A., Khezri, R., Muyeen, S. & Blaabjerg, F. 2018. On the Contribution of Wind Farms in Automatic Generation Control: Review and New Control Approach. *Applied Sciences*, 8(10): 1848.

Ouyang, J., Pang, M., Li, M., Zheng, D., Tang, T. & Wang, W. 2021. Frequency control method based on the dynamic deloading of DFIGs for power systems with high-proportion wind energy. *International Journal of Electrical Power and Energy Systems*, 128.

De Paola, A., Angeli, D. & Strbac, G. 2016. Scheduling of Wind Farms for Optimal Frequency Response and Energy Recovery. *IEEE Transactions on Control Systems Technology*, 24(5): 1764–1778.

Peng, X., Yao, W., Yan, C., Wen, J. & Cheng, S. 2020. Two-Stage Variable Proportion Coefficient Based Frequency Support of Grid-Connected DFIG-WTs. *IEEE Transactions on Power Systems*, 35(2): 962–974.

Pradhan, C., Bhende, C.N. & Samanta, A.K. 2018. Adaptive virtual inertia-based frequency regulation in wind power systems. *Renewable Energy*, 115: 558–574.

Ruttledge, L. & Flynn, D. 2016. Emulated Inertial Response From Wind Turbines: Gain Scheduling and Resource Coordination. *IEEE Transactions on Power Systems*, 31(5): 3747–3755.

Saadatmand, M., Gharehpetian, G.B., Siano, P. & Alhelou, H.H. 2021. PMU-Based FOPID Controller of Large-Scale Wind-PV Farms for LFO Damping in Smart Grid. *IEEE Access*, 9: 94953–94969. https://ieeexplore.ieee.org/document/9471802/.

Sáez, D., Cipriano, A., Andrzej, W., Xiros, N., Simani, S., Fantuzzi, C., Ron, J., Garces, F., Becerra, V.M., Warwick, K., Isidori, A., Marconi, L., Wertz, V. & Perez, T. 2008. *Optimal Control of Wind Energy Systems*. London: Springer London.

Tan, Y., Muttaqi, K.M., Ciufo, P., Meegahapola, L., Guo, X., Chen, B. & Chen, H. 2019. Enhanced Frequency Regulation Using Multilevel Energy Storage in Remote Area Power Supply Systems. *IEEE Transactions on Power Systems*, 34(1): 163–170.

Tessaro, H.J. & de Oliveira, R.V. 2020. Operating point optimization of wind turbine generators for provision of inertial response and frequency control. *International Transactions on Electrical Energy Systems*, 30(6): 1–17.

The MathWorks Inc. 2022a. Choosing an Integration Method - MATLAB & Simulink - MathWorks United Kingdom. https://uk.mathworks.com/help/sps/powersys/ug/choosing-an-integration-method.html 12 October 2022.

The MathWorks Inc. 2022b. Compare Solvers - MATLAB & Simulink - MathWorks United Kingdom. https://uk.mathworks.com/help/simulink/ug/compare-solvers.html 21 October 2022.

The MathWorks Inc. 2022c. Discrete-time or continuous-time washout or high-pass filter - Simulink - MathWorks United Kingdom. *The MathWorks Inc*. https://uk.mathworks.com/help/sps/ref/washoutdiscreteorcontinuous.html 23 October 2022.

The MathWorks Inc. 2022d. Environment block for Simscape Electrical Specialized Power Systems models - Simulink - MathWorks United Kingdom. https://uk.mathworks.com/help/sps/powersys/ref/powergui.html 13 October 2022.

The MathWorks Inc. 2022e. Filter outliers using Hampel identifier - MATLAB - MathWorks United Kingdom. https://uk.mathworks.com/help/dsp/ref/dsp.hampelfilter-system-object.html 21 October 2022.

The MathWorks Inc. 2019. Implement phasor model of variable speed doubly-fed induction generator driven by wind turbine - Simulink - MathWorks United Kingdom. *The MathWorks Inc*. https://uk.mathworks.com/help/physmod/sps/powersys/ref/windturbinedoublyfedinductiongeneratorphasortype.html 19 October 2019.

The MathWorks Inc. 2022f. Model the dynamics of speed governing system, steam turbine, and multimass shaft - Simulink - MathWorks United Kingdom. https://uk.mathworks.com/help/sps/powersys/ref/steamturbineandgovernor.html 12 October 2022.

The MathWorks Inc. 2022g. Outlier removal using Hampel identifier - MATLAB hampel - MathWorks United Kingdom. https://uk.mathworks.com/help/signal/ref/hampel.html#description 21 October 2022.

The MathWorks Inc. 2022h. Simulating Discretized Electrical Systems - MATLAB & Simulink - MathWorks United Kingdom. https://uk.mathworks.com/help/sps/powersys/ug/simulating-discretized-electrical-systems.html 12 October 2022.

The MathWorks Inc. 2022i. Wind Farm - DFIG Average Model - MATLAB & Simulink - MathWorks United Kingdom. *The MathWorks Inc*. https://uk.mathworks.com/help/physmod/sps/ug/wind-farm-dfig-average-model.html 10 August 2022.

Torreglosa, J.P., García-Triviño, P., Fernández-Ramirez, L.M. & Jurado, F. 2016. Control strategies for DC networks: A systematic literature review. *Renewable and Sustainable Energy Reviews*, 58: 319–330.

Toulabi, M., Bahrami, S. & Ranjbar, A.M. 2017. An Input-to-State Stability Approach to Inertial Frequency Response Analysis of Doubly-Fed Induction Generator-Based Wind Turbines. *IEEE Transactions on Energy Conversion*, 32(4): 1418–1431.

Toulabi, M., Dobakhshari, A.S. & Ranjbar, A.M. 2017. An Adaptive Feedback Linearization Approach to Inertial Frequency Response of Wind Turbines. *IEEE Transactions on Sustainable Energy*, 8(3): 916–926.

Ulbig, A., Borsche, T.S. & Andersson, G. 2014. *Impact of low rotational inertia on power system stability and operation*. IFAC.

University of the Witwatersrand. 2022. Research Methodology - Research Support - LibGuides at University of the Witwatersrand. https://libguides.wits.ac.za/c.php?g=693518&p=4914913 1 May 2022.

University of Washington. 1993. pg_tca14bus. http://labs.ece.uw.edu/pstca/pf14/pg_tca14bus.htm 1 September 2022.

Walling, R.A., Gursoy, E. & English, B. 2012. Current contributions from Type 3 and Type 4 wind turbine generators during faults. In *PES T&D 2012*. IEEE: 1–6. http://ieeexplore.ieee.org/document/6281623/.

Wang, S. & Tomsovic, K. 2018. A Novel Active Power Control Framework for Wind Turbine Generators to Improve Frequency Response. *IEEE Transactions on Power Systems*, 33(6): 6579–6589.

Wang, S. & Tomsovic, K. 2019. Fast frequency support from wind turbine generators with auxiliary dynamic demand control. *IEEE Transactions on Power Systems*, 34(5): 3340–3348.

Wang, X., Gao, W., Scholbrock, A., Muljadi, E., Gevorgian, V., Wang, J., Yan, W. & Zhang, H. 2017. Evaluation of different inertial control methods for variable-speed wind turbines simulated by fatigue, aerodynamic, structures and turbulence (FAST). *IET Renewable Power Generation*, 11(12): 1534–1544.

Wang, Y., Meng, J., Zhang, X. & Xu, L. 2015. Control of PMSG-Based Wind Turbines for System Inertial Response and Power Oscillation Damping. *IEEE Transactions on Sustainable Energy*, 6(2): 565–574.

Xiong, L., Yang, S., He, Y., Li, P., Huang, S., Wang, Z. & Wang, J. 2022. Specified time consensus control of ESSs for frequency support with DFIG wind turbines. *International Journal of Electrical Power and Energy Systems*, 135.

Xiong, L., Yang, S., Huang, S., He, D., Li, P., Khan, M.W. & Wang, J. 2022. Optimal Allocation of Energy Storage System in DFIG Wind Farms for Frequency Support Considering Wake Effect. *IEEE Transactions on Power Systems*, 37(3): 2097–2112.

Xiong, Y., Yao, W., Wen, Jianfeng, Lin, S., Ai, X., Fang, J., Wen, Jinyu & Cheng, S. 2021. Two-Level Combined Control Scheme of VSC-MTDC Integrated Offshore Wind Farms for Onshore System Frequency Support. *IEEE Transactions on Power Systems*, 36(1): 781–792.

Xu, G., Ge, D. & Cao, T. 2016. Variable Speed Wind Turbines for Frequency Support 1. : 890–894.

Xu, G. & Xu, L. 2017. Improved use of WT kinetic energy for system frequency support. *IET Renewable Power Generation*, 11(8): 1094–1100.

Yan, R. & Saha, T.K. 2015. Frequency response estimation method for high wind penetration considering wind turbine frequency support functions. *IET Renewable Power Generation*, 9(7): 775–782.

Yan, W., Wang, X., Gao, W. & Gevorgian, V. 2020. Electro-mechanical modeling of wind turbine and energy storage systems with enhanced inertial response. *Journal of Modern Power Systems and Clean Energy*, 8(5): 820–830.

Yang, D., Gao, H.-C., Zhang, L., Zheng, T., Hua, L. & Zhang, X. 2020. Short-term frequency support of a doubly-fed induction generator based on an adaptive power reference

function. *International Journal of Electrical Power & Energy Systems*, 119(9): 105955. https://doi.org/10.1016/j.ijepes.2020.105955.

Yang, D., Jin, Z., Zheng, T. & Jin, E. 2022. An adaptive droop control strategy with smooth rotor speed recovery capability for type III wind turbine generators. *International Journal of Electrical Power and Energy Systems*, 135.

Yang, D., Kang, M., Kim, J., Hong, J. & Kang, Y.C. 2018. Stable stepwise short-term frequency support of a DFIG-based wind farm. *International Transactions on Electrical Energy Systems*, 28(3): e2495.

Yang, D., Kim, J., Kang, Y.C., Muljadi, E., Zhang, N., Hong, J., Song, S.-H. & Zheng, T. 2018. Temporary Frequency Support of a DFIG for High Wind Power Penetration. *IEEE Transactions on Power Systems*, 33(3): 3428–3437.

Ye, H., Pei, W. & Qi, Z. 2016. Analytical modeling of inertial and droop responses from a wind farm for short-term frequency regulation in power systems. *IEEE Transactions on Power Systems*, 31(5): 3414–3423.

Zeng, X., Liu, T., Wang, S., Dong, Y. & Chen, Z. 2019. Comprehensive Coordinated Control Strategy of PMSG-Based Wind Turbine for Providing Frequency Regulation Services. *IEEE Access*, 7: 63944–63953.

Zhang, S. & Leung, K.C. 2022. A Smart Cross-System Framework for Joint Allocation and Scheduling With Vehicle-to-Grid Regulation Service. *IEEE Transactions on Vehicular Technology*, 71(6): 6019–6031.

Zhang, X., Wang, Y., Fu, Y. & Xu, L. 2016. A novel method for obtaining virtual inertial response of DFIG-based wind turbines. *Wind Energy*, 19(2): 313–328.

Zhang, Y., Tomsovic, K., Djouadi, S.M. & Pulgar-Painemal, H. 2017. Hybrid Controller for Wind Turbine Generators to Ensure Adequate Frequency Response in Power Networks. *IEEE Journal on Emerging and Selected Topics in Circuits and Systems*, 7(3): 359–370.

Zhao, X., Xue, Y. & Zhang, X.-P. 2020. Fast Frequency Support From Wind Turbine Systems by Arresting Frequency Nadir Close to Settling Frequency. *IEEE Open Access Journal of Power and Energy*, 7(February): 191–202.

Zhao-xia, X., Mingke, Z., Yu, H., Guerrero, J.M. & Vasquez, J.C. 2019. Coordinated Primary and Secondary Frequency Support Between Microgrid and Weak Grid. *IEEE Transactions on Sustainable Energy*, 10(4): 1718–1730.

APPENDICES

APPENDIX A: Selection of publications

Paper A.1

Bhowon, A., Abo-Al-Ez, K.M., Adonis, M., 2022. Variable-Speed Wind Turbines for Grid Frequency Support: A Systematic Literature Review. Mathematics 10, 3586. https://doi.org/10.3390/math10193586

Abstract — As the finite nature of non-renewable energy resources is realised and climate change concerns become more prevalent, the need to shift to more sustainable forms of energy such as the adoption of renewable energy has seen an increase. More specifically, wind energy conversion systems (WECS) have become increasingly important as a contribution to grid frequency support, to maintain power at the nominal frequency and mitigate power failures or supply shortages against demand. Therefore, limiting deviations in frequency is imperative and, thus, the control methods of WECS are called to be investigated. The systematic literature review methodology was used and aimed at investigating these control methods used by WECS, more specifically variable-speed wind turbines (VSWT), in supporting grid frequency as well as the limitations of such methods. The paper identifies these to be de-loading, energy storage systems and emulated inertial response. Further classification of these is presented regarding these control methods, which are supported by literature within period of 2015–2022. The literature indicated a persistent interest in this field; however, a few limitations of VSWTS were identified. The emulated inertial response, specifically using a droop control-based frequency support scheme, was the primary means of providing frequency support. This systematic literature review may be limited by the number of papers selected for the study. Results and conclusions will not only be useful for WECS development but also in assisting with the security of the transmission grid's frequency stability. Future work will focus on further studying the limitations of WECS providing frequency support.

Keywords — variable-speed wind turbine (VSWT); frequency support; frequency regulation; systematic literature review (SLR); wind energy conversion system (WECS); renewable energy

Paper A.2

Bhowon, A., Abo-Al-Ez, K.M., Adonis, M. **Under review**. Kinetic Energy Recovery of a Doubly-Fed Induction Generator for Frequency Support.

Abstract — Large synchronous generators provide an inherent inertial response to frequency deviations due to their large rotating mass that is coupled to the grid via an electro-mechanical interaction be-tween the rotor and stator. Conversely, the rotating mass of variable speed wind turbines are decoupled from the grid by their power converters and do not provide an inherent inertial response to frequency events on the grid. This reduces the effective system inertia of the grid which is of concern for frequency stability of the grid. To address this problem, this study introduces a supplementary frequency support controller to the rotor-side converter of a doubly-fed induction generator variable speed wind turbine. The frequency support controller temporarily raises the active power output of the wind turbine generator in response to a frequency disturbance. The additional energy required for the temporary overproduction of active power during a frequency disturbance is obtained by recovering the kinetic energy of the spinning mass of the wind turbine generator. The simulation results obtained using MATLAB/Simulink, showed that the frequency support controller has provided frequency support by raising the frequency nadir following a disturbance when compared to the frequency nadir to of identical scenarios without frequency support, even in the cases of consecutive disturbances. In a world where grids seek to decarbonise their generating fleet as climate change concerns become more prevalent, the need to shift to more sustainable forms of energy such as the adoption renewable energy has seen an increase.

Keywords — variable-speed wind turbine (VSWT); frequency support; frequency regulation; doubly-fed induction generator (DFIG); kinetic energy recovery; renewable energy

APPENDIX B: IEEE 14-bus system parameters

The parameters of the IEEE 14-bus system, on a 100 MVA base is given in the following tables below. The generator parameters are given in Table B.1, the load parameters are given in Table B.2, the transformer parameters are given in Table B.3 and the transmission line parameters are given in Table B.4.

Table B.1: Generator Parameters (Kamel et al., n.d.)

Parameter	Description	G1	G2	G3	G4	G5
MVA	Rated power	615	60	60	25	25
x_l	Leakage reactance	0.2396	0.00	0.00	0.134	0.134
r_a	Armature resistance	0.00	0.0031	0.0031	0.0014	0.0041
x_d	d-axis Synchronous leakage reactance	0.8979	1.05	1.05	1.25	1.25
x'_d	d-axis Transient synchronous leakage reactance	0.2995	0.1850	0.1850	0.232	0.232
x''_d	d-axis Sub-transient synchronous leakage reactance	0.23	0.13	0.13	0.12	0.12
T'_{do}	d-axis Open-circuit transient time constant	7.4	6.1	6.1	4.75	4.75
T''_{do}	d-axis Open-circuit sub-transient time constant	0.03	0.04	0.04	0.06	0.06
x_q	q-axis Synchronous leakage reactance	0.646	0.98	0.98	1.22	1.22
x'_q	q-axis Transient synchronous leakage reactance	0.646	0.36	0.36	0.715	0.715
x''_q	q-axis Sub-transient synchronous leakage reactance	0.4	0.13	0.13	0.12	0.12
T'_{qo}	q-axis Open-circuit transient time constant	0.00	0.3	0.3	1.5	1.5
T''_{qo}	q-axis Open-circuit sub-transient time constant	0.033	0.099	0.099	0.21	0.21
H	Inertia constant	5.148	6.54	6.54	5.06	5.06
D	Damping constant	2	2	2	2	2

Table B.2: Load Parameters (Kamel et al., n.d.) (University of Washington, 1993)

Parameter	Power (pu)	Reactive Power (pu)
Load A	0.2170	0.1270
Load B	0.9420	0.1900
Load C	0.0760	0.0160
Load D	0.4780	0.00
Load E	0.1120	0.0750
Load F	0.2950	0.1660
Load G	0.0350	0.0180
Load H	0.0900	0.0580
Load J	0.0610	0.0160
Load K	0.1350	0.0580
Load L	0.1490	0.0500

Table B.3: Transformer Parameters (Kamel et al., n.d.) (University of Washington, 1993)

Parameter	Resistance (pu)	Reactance (pu)	Tap ratio
T1	0.00	0.25202	0.932
T2	0.00	0.55618	0.969
T3	0.00	0.20912	0.978

Table B.4: Transmission Line Parameters (Kamel et al., n.d.) (University of Washington, 1993)

Parameter	Resistance (pu)	Reactance (pu)	Line Charging (pu)
Line 1-2	0.01938	0.05917	0.0528
Line 1-5	0.05403	0.22304	0.0492
Line 2-3	0.04699	0.19797	0.0438
Line 2-4	0.05811	0.17632	0.0374
Line 2-5	0.05695	0.17388	0.034
Line 3-4	0.06701	0.17103	0.0346
Line 4-5	0.01335	0.04211	0.0128
Line 6-11	0.09498	0.1989	0.00
Line 6-12	0.12291	0.25581	0.00
Line 6-13	0.06615	0.13027	0.00
Line 7-8	0.00	0.17615	0.00
Line 7-9	0.00	0.11001	0.00
Line 9-10	0.03181	0.08450	0.00
Line 9-14	0.12711	0.27038	0.00
Line 10-11	0.08205	0.19207	0.00
Line 12-13	0.22092	0.19988	0.00
Line 13-14	0.17093	0.34802	0.00

APPENDIX C: Detailed load calculations

The detailed calculations for the various loads shown in Table B.2 are shown below. A base value, S_{Base}, of 100 MVA was used.

Load A

$$S_{A(pu)} = 0.2170 + j0.1270$$
$$S_A = S_{A(pu)} \cdot S_{Base}$$
$$S_A = 21.7 + j12.7\ MW$$

Load B

$$S_{B(pu)} = 0.9420 + j0.1900$$
$$S_B = S_{B(pu)} \cdot S_{Base}$$
$$S_B = 94.2 + j19\ MW$$

Load C

$$S_{C(pu)} = 0.0760 + j0.0160$$
$$S_C = S_{C(pu)} \cdot S_{Base}$$
$$S_C = 7.6 + j1.6\ MW$$

Load D

$$S_{D(pu)} = 0.4780 + j0.0000$$
$$S_D = S_{D(pu)} \cdot S_{Base}$$
$$S_D = 47.8\ MW$$

Load E

$$S_{E(pu)} = 0.1120 + j0.0750$$
$$S_E = S_{E(pu)} \cdot S_{Base}$$
$$S_E = 11.2 + j7.5\ MW$$

Load F

$$S_{F(pu)} = 0.2950 + j0.1660$$
$$S_F = S_{F(pu)} \cdot S_{Base}$$
$$S_F = 29.5 + j16.6\ MW$$

Load G

$$S_{G(pu)} = 0.0350 + j0.0180$$
$$S_G = S_{G(pu)} \cdot S_{Base}$$
$$S_G = 3.5 + j1.8\ MW$$

Load H

$$S_{H(pu)} = 0.0900 + j0.0580$$
$$S_H = S_{H(pu)} \cdot S_{Base}$$
$$S_H = 9 + j5.8\ MW$$

Load J

$$S_{J(pu)} = 0.0610 + j0.0160$$
$$S_J = S_{J(pu)} \cdot S_{Base}$$
$$S_J = 6.1 + j1.6\ MW$$

Load K

$$S_{K(pu)} = 0.1350 + j0.0580$$
$$S_K = S_{K(pu)} \cdot S_{Base}$$
$$S_K = 13.5 + j5.8\ MW$$

Load L

$$S_{L(pu)} = 0.1490 + j0.0500$$
$$S_L = S_{L(pu)} \cdot S_{Base}$$
$$S_L = 14.9 + j5\ MW$$

APPENDIX D: Plotting script code

The code of the plotting script used to plot the data in MATLAB is shown below:

```
load("<FileName>.mat")
%% Loading
ValuesRotor=data{1}.Values;
ValuesSysF=data{2}.Values;
ValuesWPP=data{3}.Values;
%% Data Truncation
startRotor=find(ValuesRotor.Time==60);
Timeseries=ValuesRotor.Time(startRotor:end);
timenewRotor=Timeseries-60;
startSysF=find(ValuesSysF.Time==60);
TimeseriesSysF=ValuesSysF.Time(startSysF:end);
timenewSysF=TimeseriesSysF-60;
startWPP=find(ValuesWPP.Time==60);
TimeseriesWPP=ValuesWPP.Time(startWPP:end);
timenewWPP=TimeseriesWPP-60;
%% Data Processing
window=50000;
RotorSpeed=ValuesRotor.Data(startRotor:end);
RotorSpeed=hampel(RotorSpeed,window);
SysF=ValuesSysF.Data(startSysF:end);
SysF=hampel(SysF,window);
WPP=ValuesWPP.Data(startWPP:end);
WPP=hampel(WPP,window);

%% Plotting
f1=figure;
plot(timenewRotor,RotorSpeed,'-','LineWidth',1.5,'Color','#3D64AC');
title('Rotor Speed');
xlabel('Time (s)');
ylabel('Rotor Speed (pu)');
box off;
% Axis Range
ylim([min_y1 max_ y1]);
xlim([min_x1 max_y1]);
% Set Fonts
fontname(f1,"Calibri");
fontsize(f1,"default");
% Save File
saveas(f1,'RotorSpeedGraph.svg')

f2=figure;
plot(timenewSysF,SysF,'-','LineWidth',1.5,'Color','#3D64AC');
title('System Frequency');
xlabel('Time (s)');
ylabel('System Frequency (Hz)');
box off;
```

```
% Axis Range
ylim([min_y2 max_ y2]);
xlim([min_x2 max_y2]);
% Set Fonts
fontname(f2,"Calibri");
fontsize(f2,"default");
% Save File
saveas(f2,'SystemFrequencyGraph.svg')

f3=figure;
plot(timenewWPP,WPP,'-','LineWidth',1.5,'Color','#3D64AC');
title('WPP Output');
xlabel('Time (s)');
ylabel('WPP Output (MW)');
box off;
% Axis Range
ylim([min_y3 max_ y3]);
xlim([min_x3 max_y3]);
% Set Fonts
fontname(f3,"Calibri");
fontsize(f3,"default");
% Save File
saveas(f3,'WPPOutputGraph.svg')
```